

NONLINEAR CONTROL FOR SYSTEMS CONTAINING INPUT UNCERTAINTY VIA
A LYAPUNOV-BASED APPROACH

By

WILLIAM MACKUNIS

A DISSERTATION PRESENTED TO THE GRADUATE SCHOOL
OF THE UNIVERSITY OF FLORIDA IN PARTIAL FULFILLMENT
OF THE REQUIREMENTS FOR THE DEGREE OF
DOCTOR OF PHILOSOPHY

UNIVERSITY OF FLORIDA

2009

© 2009 William MacKunis

This work is dedicated to my parents, whose confidence in me never waivers.

ACKNOWLEDGMENTS

I would like to express sincere gratitude to my advisor, Dr. Warren E. Dixon, whose experience and motivation were instrumental in my recent academic success. As an advisor, he provided guidance in my research and encouragement in developing my own ideas. As a mentor, he helped me understand the intricacies of working in a professional environment and helped develop my professional skills. I feel fortunate to have had the opportunity to work with him.

I would also like to extend my gratitude to Dr. Norman Fitz-Coy for his technical assistance in the aerospace aspects of my research. I also appreciate my committee members Dr. Carl D. Crane III and Dr. J. Hammer for any time and help they provided.

I would like to thank my coworkers, family, and friends for their support and encouragement.

TABLE OF CONTENTS

	<u>page</u>
ACKNOWLEDGMENTS	4
LIST OF TABLES	8
LIST OF FIGURES	9
ABSTRACT	11
CHAPTER	
1 INTRODUCTION AND MOTIVATION	12
1.1 Satellite Attitude Control	12
1.2 Aircraft Control	15
1.3 Research Plan	19
1.3.1 Contributions of Completed Research	19
1.3.2 Limitations of Completed Research	20
1.3.3 Future Research Plans	20
1.3.4 Research Schedule	20
2 ADAPTIVE SATELLITE ATTITUDE CONTROL IN THE PRESENCE OF INERTIA AND CMG GIMBAL FRICTION UNCERTAINTIES	22
2.1 Introduction	22
2.2 Dynamic Model	22
2.3 Kinematic Model	25
2.4 Control Objective	26
2.5 Adaptive Control Development	27
2.5.1 Tracking Error Dynamics	27
2.5.2 Stability Analysis	31
2.6 Asymptotic Tracking Extension	33
2.6.1 Closed-Loop Error System	33
2.6.2 Stability Analysis Ignoring Static Friction	33
2.7 Simulation Results	34
2.8 Conclusions and Future Work	37
3 ADAPTIVE NEURAL NETWORK SATELLITE ATTITUDE CONTROL IN THE PRESENCE OF INERTIA AND CMG ACTUATOR UNCERTAINTIES	39
3.1 Introduction	39
3.2 Dynamic Model and Properties	39
3.3 Kinematic Model	42
3.4 Control Objective	43
3.5 Feedforward NN Estimation	45
3.6 Control Development	46

3.6.1	Open-Loop Error System	47
3.6.2	Closed-Loop Error System	49
3.6.3	Stability Analysis	52
3.7	Simulation Results	54
3.8	Conclusion	57
4	ASYMPTOTIC TRACKING FOR AIRCRAFT VIA AN UNCERTAIN DYNAMIC INVERSION METHOD	59
4.1	Introduction	59
4.2	Aircraft Model and Properties	59
4.3	Control Development	63
4.3.1	Open-loop Error System	64
4.3.2	Closed-loop Error System	66
4.4	Stability Analysis	67
4.5	Simulation Results	70
4.6	Conclusion	75
5	ADAPTIVE DYNAMIC INVERSION FOR ASYMPTOTIC TRACKING OF AN AIRCRAFT REFERENCE MODEL	79
5.1	Introduction	79
5.2	Aircraft Model	79
5.3	Control Development	81
5.4	Stability Analysis	85
5.5	Simulation Results	88
5.6	Conclusion	94
6	GLOBAL ADAPTIVE OUTPUT FEEDBACK MRAC	98
6.1	Introduction	98
6.2	System Model	98
6.3	Control Development	99
6.3.1	Control Objective	99
6.3.2	Open-Loop Error System	100
6.3.3	Closed-Loop Error System	101
6.4	Stability Analysis	106
6.5	Simulation Results	109
6.6	Conclusion	114
7	CONTRIBUTIONS AND FUTURE RESEARCH PLANS	116
7.1	Contributions of Previous Research	116
7.2	Limitations of Previous Research	116
7.3	Proposed Research Plans	117
	APPENDIX: PROOF OF LEMMAS 4-1 AND 6-1	118

REFERENCES 122
BIOGRAPHICAL SKETCH 129

LIST OF TABLES

<u>Table</u>		<u>page</u>
4-1	Parameters used in the DI controller simulation.	74
5-1	Parameters used in the ADI controller simulation.	90
6-1	Parameters Used in the Controller Simulations.	113

LIST OF FIGURES

<u>Figure</u>	<u>page</u>
1-1 Research Schedule	21
2-1 The University of Florida control moment gyroscope experimental test bed.	24
2-2 Quaternion tracking error.	36
2-3 Control input gimbal angular rate response.	37
2-4 $\dot{J}(\delta)$ vs. time.	38
3-1 Quaternion tracking error of closed-loop system.	57
3-2 Control input gimbal angular rates.	58
3-3 Time variation of the inertia matrix (i.e., $\dot{J}(\delta)$) during closed-loop operation.	58
4-1 Photograph of the Osprey aircraft testbed.	60
4-2 Plot of the discrete vertical (upward) wind gust used in the controller simulation.	72
4-3 Pitch rate response achieved during closed-loop longitudinal controller operation.	75
4-4 Forward velocity response achieved during closed-loop longitudinal controller operation.	76
4-5 Roll rate response achieved during closed-loop lateral controller operation.	77
4-6 Yaw rate response achieved during closed-loop lateral controller operation.	77
4-7 Control actuation away from trim used during closed-loop robust dynamic inversion controller operation for the lateral subsystem (top) and the longitudinal subsystem (bottom)	78
5-1 Pitch rate response achieved during closed-loop longitudinal controller operation.	91
5-2 Forward velocity response achieved during closed-loop longitudinal controller operation.	92
5-3 Roll rate response achieved during closed-loop lateral controller operation.	93
5-4 Yaw rate response achieved during closed-loop lateral controller operation.	94
5-5 Control actuation away from trim used during closed-loop adaptive dynamic inversion controller operation for the lateral subsystem (top) and the longitudinal subsystem (bottom).	95

5-6	Angle of attack (top) and forward velocity away from trim (bottom) responses for the closed-loop adaptive longitudinal system.	96
5-7	Control actuation away from trim used during closed-loop adaptive controller operation for the angle of attack tracking objective. Elevator deflection angle (top) and thrust (bottom).	97
6-1	Reference and actual forward velocity (top left), pitch rate (top right), roll rate (bottom left), and yaw rate (bottom right) responses during closed-loop longitudinal and lateral controller operation.	114
6-2	Control input elevator deflection (top left), thrust (top right), aileron deflection (bottom left), and rudder deflection (bottom right) used during closed-loop longitudinal and lateral controller operation.	115

Abstract of Dissertation Presented to the Graduate School
of the University of Florida in Partial Fulfillment of the
Requirements for the Degree of Doctor of Philosophy

NONLINEAR CONTROL FOR SYSTEMS CONTAINING INPUT UNCERTAINTY VIA
A LYAPUNOV-BASED APPROACH

By

William MacKunis

May 2009

Chair: Dr. Warren E. Dixon
Major: Aerospace Engineering

Controllers are often designed based on the assumption that a control actuation can be directly applied to the system. This assumption may not be valid, however, for systems containing parametric input uncertainty or unmodeled actuator dynamics.

In this dissertation, a tracking control methodology is proposed for aircraft and aerospace systems for which the corresponding dynamic models contain uncertainty in the control actuation. The dissertation will focus on five problems of interest: 1) adaptive CMG-actuated satellite attitude control in the presence of inertia uncertainty and uncertain CMG gimbal friction; 2) adaptive neural network (NN)-based satellite attitude control for CMG-actuated small-sats in the presence of uncertain satellite inertia, nonlinear disturbance torques, uncertain CMG gimbal friction, and nonlinear electromechanical CMG actuator disturbances; 3) dynamic inversion (DI) control for aircraft systems containing parametric input uncertainty and additive, nonlinearly parameterizable (non-LP) disturbances; 4) adaptive dynamic inversion (ADI) control for aircraft systems as described in 3); and 5) adaptive output feedback control for aircraft systems as described in 3) and 4).

CHAPTER 1

INTRODUCTION AND MOTIVATION

1.1 Satellite Attitude Control

Through ventures such as NASA’s New Millennium Program and DoD’s Operational Responsive Space [1], the space industry is moving toward smaller satellites and the buses that support them. Some proposed uses of these small satellites (small-sats) include astrophysics research, surveillance, and autonomous servicing, all of which require precision attitude motion. However, due to their smaller sizes, the attitude motion of these small-sats is more susceptible to external disturbances than their larger counterparts. Furthermore, the smaller sizes of these new small-sats limit the mass, power and size budgets allocated to their attitude control systems (ACS). These contradictory requirements necessitate novel solutions for the ACS.

Controllers that are based on the assumption that a torque can be directly applied about the body-fixed satellite axes (e.g., [2–5]) may not be well suited for applications that require high-precision attitude control, because the satellite torques are generated by actuators with additional dynamics. For example, (especially in small rigid-body satellites), the desired torques are typically generated by a cluster (e.g., [6, 7]) of single gimbal control moment gyroscopes (CMGs) due to their low mass and low power consumption properties. Unfortunately, the torque producing capacity of CMGs can deteriorate over time due to changes in the dynamics such as bearing degradation and increased friction in the gimbals. The ramifications of CMG friction build-up include increased power consumption due to energy dissipation. Examples of actual satellite failures resulting from CMG problems are the Hipparcos satellite and Magellan satellite [8]. Hipparcos failed and “spun down” due to numerous gyroscope failures. One of these failures was due to high and variable drag torque in gyro number 4, which led to premature degradation. The Magellan satellite was in transit to Venus for five months before it began exhibiting erratic motor current shifts in one of its gyros [8]. The cause of

this failure was found to be friction buildup due to a manufacturing process error in which the bearing lubricant was contaminated by a solvent.

The design of ACS for satellites is complicated due to parametric uncertainties, disturbances, and nonlinearities, which usually exist in the corresponding plant dynamics. To cope with these challenges, attitude controllers based on NNs are often utilized [9–17]. In [14], an attitude control approach based on the radial basis function neural network (RBFNN) is developed. The satellite dynamic model utilized in [14] includes no friction effects or disturbances in the reaction wheel actuators. Another NN attitude controller is presented in [17], which utilizes NNs to approximate the parametric uncertainties and nonlinearities present in the system dynamics. An online NN is used in [17] to re-optimize a Single Network Adaptive Critic, or SNAC-based optimal controller, which has been designed a priori for the nominal system. In [9], a NN attitude controller is developed based on a simplified nonlinear model of the Space Station Freedom. The dynamic model for the space station considered in [9] is simplified by assuming small roll/yaw attitude errors and small products of inertia. The attitude controller in [9] demonstrates the capability of the NN to adaptively compensate for varying inertia characteristics. The NN controllers presented in [9] and [17] are tested in attitude control problems under the assumption that a control torque can be directly applied about the spacecraft body-fixed axes.

Adaptive satellite attitude control is often utilized to cope with systems containing constant parametric uncertainty. In [18], an output feedback structured model reference adaptive controller (MRAC) is developed for spacecraft rendezvous and docking problems. The adaptive controller in [18] accommodates inertia uncertainty in the momentum wheel actuator dynamics; however, no frictional effects were assumed to be present in the actuator model. A quaternion-based, full-state feedback attitude tracking controller was designed in [2] for a rigid satellite in the presence of an unknown satellite inertia matrix. A model-error control synthesis (MECS) approach was used in [3] to cancel the effects

of modelling errors and external disturbances on the system. The control law proposed in [3] requires a model-error term to cancel the effects of a time delay, which is inherent to the MECS design. An adaptive control law is designed in [19], which incorporates a velocity-generating filter from attitude measurements. The controller in [19] is shown to achieve asymptotic convergence of the attitude and angular velocity tracking errors despite uncertainty in the satellite inertia, but it assumes no dynamic uncertainty in the control torque. While the aforementioned controllers perform well for applications involving large satellites, they may not be well suited for attitude control of CMG-actuated small-sats. In Chapter 2, a more suitable control design for such small-sats is developed.

A nonlinear adaptive controller is developed in Chapter 2 that compensates for inertia uncertainties and uncertain CMG gimbal friction. Instead of developing a control torque to solve the attitude tracking problem, the attitude tracking controller in Chapter 2 is developed in terms of the CMG gimbal angular velocity. The development is complicated by the fact that the control input is multiplied by a time-varying, nonlinear uncertain matrix. Additional complications arise because the gimbal velocity control term is embedded inside of a discontinuous nonlinearity (i.e., the standard signum function) resulting from the CMG static friction effects. A robust control method is used to mitigate the disturbance resulting from the static friction. In addition, potential singularities may exist in the Jacobian that transforms the torque produced by each CMG to desired torques about the satellite coordinate frame [20]. The singularity problem is circumvented by the use of a particular Jacobian pseudoinverse, coined the singularity robust steering law, which was introduced in [21], and has been implemented in several aerospace vehicles (e.g., see [20] and [22]). A uniformly ultimately bounded (UUB) stability result is proven via Lyapunov analysis for the case in which both static and dynamic friction effects are included in the CMG dynamic model. An asymptotic tracking extension is then formulated for the case where static friction effects are ignored.

An adaptive NN attitude tracking controller is developed in Chapter 3 for CMG-actuated small-sats, which compensates for uncertain satellite inertia, nonlinear disturbance torques, uncertain CMG gimbal friction, and CMG actuator disturbances. The NN weights and thresholds are adjusted on-line, with no off-line learning phase required. In addition to the unknown CMG gimbal friction assumed present in the CMG torque model (e.g., see [23]), unknown electromechanical disturbances are assumed to be present in the CMG actuators. Some of the challenges encountered in the control design are that the control input (i.e., CMG gimbal angular rate) is: premultiplied by a non-square, time-varying, nonlinear uncertain matrix due to dynamic gimbal friction and electromechanical disturbances; and is embedded in a hard nonlinearity due to static gimbal friction. Furthermore, due to the small size of the satellite considered in this development, the motion of the CMGs causes significant time-variation in the satellite inertia characteristics. The time-variation of the satellite inertia manifests itself as a nonlinear disturbance torque in the satellite dynamic model, which is handled via online NN approximation. Simulation results are provided to illustrate the efficacy of the proposed control design.

1.2 Aircraft Control

Feedback linearization is a general control method where the nonlinear dynamics of a system are canceled by state feedback yielding a residual linear system. Dynamic inversion is a similar concept as feedback linearization that is commonly used within the aerospace community to replace linear aircraft dynamics with a reference model [24–34]. For example, a general dynamic inversion approach is presented in [27] for a reference tracking problem for a minimum-phase and left-invertible linear system. A dynamic inversion controller is designed for a nonminimum-phase hypersonic aircraft system in [25], which utilizes an additional controller to stabilize the zero dynamics. A finite-time stabilization design is proposed in [26], which utilizes dynamic inversion. The technique in [26] required the input matrix to be full rank. Typically, dynamic inversion methods (e.g.,

[24, 25]) assume the corresponding plant models are exactly known. However, parametric uncertainty, additive disturbances, and unmodeled plant dynamics are always present in practical systems. Additional difficulties exist in designing ADI controllers for systems containing uncertainty in the input matrix. While robust control methods are often utilized to compensate for the inversion error in such cases [35–38], the required control effort can be large due to the high gain or high frequency feedback typically required in the robust control design. There remains a need for an ADI controller, which is capable of achieving asymptotic tracking for systems containing parametric uncertainty and unknown nonlinear disturbances while minimizing the required control effort.

Robust design methods are often utilized in DI controllers to compensate for parametric uncertainty and inversion error (e.g., see [35–38]). In Chapter 4 [35], a best-guess feedforward estimate for the parameteric uncertainty is used in conjunction with a robust control term to compensate for the corresponding inversion error. In [36], a stochastic robust dynamic inversion technique is applied to a nonlinear aircraft model at high angle of attack. The controller in [36] is designed to compensate for uncertainties in the aerodynamic parameters, and is applicable to systems for which the nominal model is feedback linearizeable. In [37], a robust trajectory tracking controller is designed for an unmanned aerial vehicle (UAV) using a two-time-scaled dynamic inversion method. The controllers in [36] and [37] are based on the assumption that one subset of the state components evolves much faster than the other subset. A sliding-mode controller is designed in [39] for an agile missile model containing aerodynamic uncertainty. The scalar input uncertainty in [39] was bounded and damped out through a discontinuous sliding-mode control element. A discontinuous sliding mode controller was also developed in [38] for attitude tracking of an unpowered flying vehicle with an uncertain column deficient non-symmetric input matrix. In our previous work in [35], a continuous robust controller was used to achieve semi-global asymptotic tracking of an aircraft reference model where the aircraft dynamics contained column deficient input

uncertainty. Robust control methods can be utilized to compensate for both structured and unstructured bounded uncertainty; however, robust control methods are based on worst-case uncertainty and disturbances and typically exploit high gain or high frequency components to achieve stability. Moreover, for a broad class of disturbances (e.g., an additive bounded nonvanishing disturbance) the steady state error is only proven to converge to a neighborhood, rather than an asymptotic stability result.

Motivated by the desire to improve the robustness to uncertainty over traditional methods, adaptive dynamic inversion (ADI) was developed as a method to compensate for parametric uncertainty (cf. [27, 29, 30, 33]). Typically, ADI methods MRAC techniques where the desired input-output behavior of the closed-loop system is given via the corresponding dynamics of a reference model [28, 30, 40]. Therefore, the basic task is to design a controller which will ensure the minimal error between the reference model and the plant outputs despite uncertainties in the plant parameters and working conditions. In [41], a full-state feedback adaptive control design was presented for a general class of fully-actuated nonlinear systems containing state-varying input uncertainty and a nonlinear disturbance that is linear in the uncertainty. The ADI design in [41] utilizes a matrix decomposition technique [42, 43] to yield a global asymptotic tracking result when the input uncertainty is assumed to be square and positive definite. A semi-global MIMO extension is also provided in [41] using a robust controller for the case when the input matrix uncertainty is square, positive definite, and symmetric. A full-state feedback adaptive controller is developed in [44], which compensates for parametric uncertainty in a linearly parametrizable nonlinearity and a square input gain matrix. The approach in [44] applies a matrix decomposition technique to avoid singularities in the control law. The technique in [44] is extended to an adaptive output feedback controller in [45] via the use of state estimators. An adaptive tracking controller is developed in [46] for nonlinear robot systems with kinematic, dynamic and actuator uncertainties where the input uncertainty is a constant diagonal matrix. In our previous work in [47], an ADI controller

is developed to achieve semi-global asymptotic tracking of an aircraft reference model where the aircraft dynamics contain column deficient non-symmetric input uncertainty. However, the controller in [47] depends on the output states and the respective time derivatives. Several efforts (e.g., [31–33, 48–51]) have been developed for the more general problem where the uncertain parameters or the inversion mismatch terms do not satisfy the linear-in-the-parameters assumption (i.e., non-LP). One method to compensate for non-LP uncertainty is to exploit a neural network as an on-line function approximation method as in [48–50]; however, all of these results yield uniformly ultimately bounded stability due to the inherent function reconstruction error.

In contrast to neural network-based methods to compensate for the non-LP uncertainty, a robust control approach was recently developed in [52] that exploits a unique integral of the sign of the error (coined RISE control in [53]) to yield an asymptotic stability result. The RISE-based control structure has been used for a variety of fully actuated systems in [52–60]. The contribution in Chapter 4 is the use of the RISE control structure to achieve asymptotic tracking control of a model reference system, where the plant dynamics contain a bounded additive disturbance (e.g., potential disturbances include: gravity, inertial coupling, nonlinear gust modeling, etc.). This result represents the first ever application of the RISE method where the controller is multiplied by a non-square matrix containing parametric uncertainty. To achieve the result, the typical RISE control structure is modified by adding a robust control term, which is designed to compensate for the uncertainty in the input matrix. The result is proven via Lyapunov-based stability analysis and demonstrated through numerical simulation.

Motivated by the desire to develop an adaptive method, neural network (NN)-based controllers have been typically used to compensate for unstructured uncertainty (e.g., see [61]). One drawback of NN-based control is that asymptotic stability is difficult to prove due to the inherent functional reconstruction error. A contribution in Chapter 5 is that a new robust control technique is used along with an adaptive control law to achieve an

asymptotic tracking result in the presence of parametric uncertainty in the input and state matrices and an additive nonvanishing nonlinear disturbance. An asymptotic tracking result is proven via a Lyapunov stability analysis, and a high fidelity numerical simulation is provided to show the performance of the proposed control design.

The contribution in Chapter 6 is the development of a continuous output feedback controller that achieves global asymptotic tracking of the outputs of a reference model, where the plant model contains a non-square, column deficient, uncertain input matrix and a non-vanishing disturbance that cannot be linearly parameterized. In comparison with the results presented in Chapters 4 and 5, the current development exploits the matrix decomposition technique in [42, 43] so that the controller depends only on the output states, and not the respective time derivatives. Global asymptotic tracking is proven via a Lyapunov stability analysis, and a high fidelity numerical simulation is provided to show the performance of the developed controller.

1.3 Research Plan

1.3.1 Contributions of Completed Research

- A singularity-robust attitude tracking controller for a rigid body satellite is developed, which adapts for parametric uncertainty in the satellite inertia matrix in addition to uncertainties in the input torque caused by static and dynamic CMG gimbal friction.
- A NN-based adaptive attitude tracking controller for a rigid body satellite is designed, which achieves UUB attitude tracking for a rigid-body satellite in the presence of general (i.e., non-LP) exogenous disturbances, parametric uncertainty in the satellite inertia matrix, and uncertainties in the input torque caused by static and dynamic CMG gimbal friction and electromechanical disturbances in the gimbal servo loops.
- The attitude controllers presented here are suitable for small-sats, for which significant disturbances resulting from the motion of the CMGs exist.
- An aircraft controller is presented, which achieves asymptotic tracking control of a model reference system where the plant dynamics contain input uncertainty and a non-LP disturbance. This result represents the first ever application of a continuous control strategy in a DI and MRAC framework to a nonlinear system with additive,

non-LP disturbances, where the control input is multiplied by a non-square matrix containing parametric uncertainty.

- An aircraft controller is developed, which achieves asymptotic tracking control of a model reference system where the plant dynamics contain input uncertainty and a non-LP disturbance. This result represents application of a continuous control strategy in an ADI framework to a nonlinear system with additive, non-LP disturbances, where the control input is multiplied by a non-square matrix containing parametric uncertainty.
- A robust adaptive output feedback (OFB) dynamic inversion control strategy is presented that achieves global asymptotic tracking of a reference model. The considered system contains linearly parameterizable uncertainty in the state and input matrices in addition to a non-LP disturbance. This result represents application of a continuous output feedback control strategy in an ADI framework to a nonlinear system with additive, non-LP disturbances, where the control input is multiplied by a non-square matrix containing parametric uncertainty.

1.3.2 Limitations of Completed Research

- Attitude controller designs developed in Chapters 2 and 3 are only able to achieve uniformly ultimately bounded tracking result (i.e., not asymptotic).
- All controllers proposed are designed to handle systems which are affine in the control input.

1.3.3 Future Research Plans

- Improve the CMG attitude control design to achieve an asymptotic tracking result (e.g., using RISE or a single network adaptive critic (SNAC) neural network).
- Design a controller capable of achieving asymptotic tracking for nonaffine-in-control dynamic systems (e.g., building on research by N. Hovakimyan).
- Experimentally validate the NN-based adaptive attitude controller using the UF Space Systems Group CMG test bed.

1.3.4 Research Schedule

The research schedule is illustrated in Figure [1-1](#)

	Fall '05	Spr '05	Sum '05	Fall '06	Spr '07	Sum '07	Fall '07	Spr '08	Sum '08	Fall '08	Spr '09	Sum '09
Adaptive CMG Attitude Control		████████████████████										
DI control for Aircraft			████████████████████									
Adaptive NN CMG Attitude Control				████████████████████								
ADI control with accel. measmts					████████████████████							
ADI control without accel. measurements							████████████████████					
General Class of Systems									████████████████████			
Asymptotic tracking for non-LP systems										████████████████████		
Dissertation Writing											████████████████████	

Figure 1-1. Research Schedule

CHAPTER 2
ADAPTIVE SATELLITE ATTITUDE CONTROL IN THE PRESENCE OF INERTIA
AND CMG GIMBAL FRICTION UNCERTAINTIES

2.1 Introduction

A nonlinear adaptive controller is developed in this dissertation that compensates for inertia uncertainties and uncertain CMG gimbal friction. Instead of developing a control torque to solve the attitude tracking problem, the attitude tracking controller in this dissertation is developed in terms of the CMG gimbal angular velocity. The development is complicated by the fact that the control input is multiplied by a time-varying, nonlinear uncertain matrix. Additional complications arise because the gimbal velocity control term is embedded inside of a discontinuous nonlinearity (i.e., the standard signum function) resulting from the CMG static friction effects. A robust control method is used to mitigate the disturbance resulting from the static friction. In addition, potential singularities may exist in the Jacobian that transforms the torque produced by each CMG to desired torques about the satellite coordinate frame [20]. The singularity problem is circumvented by the use of a particular Jacobian pseudoinverse, coined the singularity robust steering law, which was introduced in [21], and has been implemented in several aerospace vehicles (e.g., see [20] and [22]). A uniformly ultimately bounded (UUB) stability result is proven via Lyapunov analysis for the case in which both static and dynamic friction effects are included in the CMG dynamic model. An asymptotic tracking extension is then formulated for the case where static friction effects are ignored.

2.2 Dynamic Model

The dynamic model for a rigid body CMG actuated satellite can be expressed as [62, 63]

$$J\dot{\omega} = -\omega^\times J\omega + \tau_{cmg} - \dot{J}\omega. \quad (2-1)$$

In (2-1), $J(\delta) \in \mathbb{R}^{3 \times 3}$ represents the positive definite, symmetric satellite inertia matrix that is a function of the CMG gimbal angular position vector $\delta(t) \in \mathbb{R}^4$, $\omega(t) \in \mathbb{R}^3$ denotes the angular velocity of the satellite body-fixed frame \mathcal{F} with respect to \mathcal{I} expressed in

$\mathcal{F}, \tau_{cmg}(t) \in \mathbb{R}^3$ denotes the torque generated via a CMG cluster consisting of four single gimbal CMGs, the term $\dot{J}(t)\omega(t)$ represents the time variation of the satellite inertia matrix due to the motion of the CMGs, and the notation $\zeta^\times \forall \zeta = [\zeta_1, \zeta_2, \zeta_3]^T$ denotes the following skew-symmetric matrix:

$$\zeta^\times = \begin{bmatrix} 0 & -\zeta_3 & \zeta_2 \\ \zeta_3 & 0 & -\zeta_1 \\ -\zeta_2 & \zeta_1 & 0 \end{bmatrix}. \quad (2-2)$$

The satellite inertia matrix in (2-1) can be lower and upper bounded as follows:

$$\frac{1}{2}\lambda_{\min}\{J\}\|\xi\|^2 \leq \xi^T J \xi \leq \frac{1}{2}\lambda_{\max}\{J\}\|\xi\|^2 \quad \forall \xi \in \mathbb{R}^n \quad (2-3)$$

where $\lambda_{\min}\{J\}, \lambda_{\max}\{J\} \in \mathbb{R}$ are the minimum and maximum eigenvalues of $J(\delta)$, respectively. The torque generated from the CMG cluster can be modeled as¹

$$\tau_{cmg} = -\left(\dot{h}_{cmg} + \omega^\times h_{cmg}\right) - AF_d \dot{\delta} - AF_s \text{sgn} \dot{\delta}, \quad (2-4)$$

where $F_d, F_s \in \mathbb{R}^{4 \times 4}$ are diagonal matrices whose elements are the unknown constant dynamic and static friction coefficients, respectively, of the four CMG gimbals, $h_{cmg}(t) \in \mathbb{R}^3$ represents the angular momentum of the CMG cluster, and $\dot{h}_{cmg}(t)$ is modeled as [7]

$$\dot{h}_{cmg} = hA(\delta)\dot{\delta}, \quad (2-5)$$

where $h \in \mathbb{R}$ represents the constant angular momentum of each CMG expressed in the gimbal-fixed frame (i.e., h is the same for all four CMGs). In (2-4) and (2-5), $\dot{\delta}(t) \in \mathbb{R}^4$

¹ The CMG torque expression does not explicitly include gimbal acceleration terms, but these effects are assumed to be included with the other bounded uncertainties, which contribute to the ultimate bound on the tracking error.

denotes the CMG gimbal angular velocity control input, which is defined as

$$\dot{\delta} \triangleq \begin{bmatrix} \dot{\delta}_1 & \dot{\delta}_2 & \dot{\delta}_3 & \dot{\delta}_4 \end{bmatrix}^T, \quad (2-6)$$

where $\dot{\delta}_i(t) \in \mathbb{R}$ denotes the angular velocity of the individual CMG gimbals $\forall i = 1, 2, 3, 4$, $\text{sgn}(\dot{\delta}(t)) \in \mathbb{R}^4$ denotes a vector form of the standard $\text{sgn}(\cdot)$ function where the $\text{sgn}(\cdot)$ is applied to each element of $\dot{\delta}(t)$, and $A(\delta) \in \mathbb{R}^{3 \times 4}$ denotes a measurable Jacobian matrix defined as

$$A = \begin{bmatrix} -\cos \gamma \cos \delta_1 & \sin \delta_1 & \sin \gamma \cos \delta_1 \\ \sin \delta_2 & -\cos \gamma \cos \delta_2 & \sin \gamma \cos \delta_2 \\ \cos \gamma \cos \delta_3 & \sin \delta_3 & \sin \gamma \cos \delta_3 \\ -\sin \delta_4 & \cos \gamma \cos \delta_4 & \sin \gamma \cos \delta_4 \end{bmatrix}^T, \quad (2-7)$$

where $\gamma \in \mathbb{R}$ is the constant angle (54.74 deg) of each wall of the pyramid-shaped CMG cluster as depicted in Figure 2.2. Since the elements of $A(\delta)$ in (2-7) are combinations of

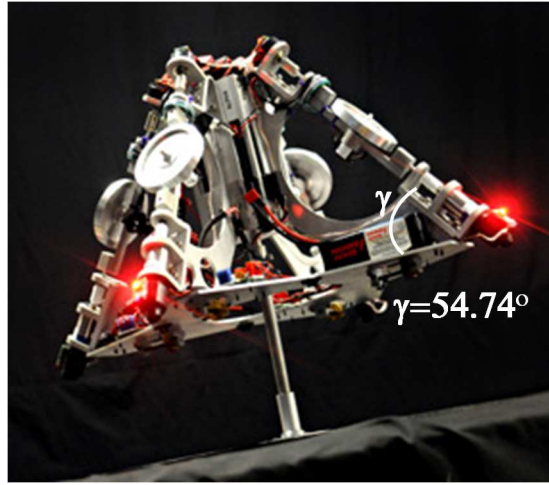


Figure 2-1. The University of Florida control moment gyroscope experimental test bed.

bounded trigonometric terms, the following inequality can be developed:

$$\|A(\delta)\|_{i\infty} \leq \zeta_0, \quad (2-8)$$

where $\zeta_0 \in \mathbb{R}$ is a positive bounding constant, and $\|\cdot\|_{i\infty}$ denotes the induced infinity norm of a matrix.

2.3 Kinematic Model

The rotational kinematics of the rigid-body satellite can be determined as [2]

$$\dot{q}_v = \frac{1}{2} (q_v^\times \omega + q_0 \omega) \quad (2-9)$$

$$\dot{q}_0 = -\frac{1}{2} q_v^T \omega. \quad (2-10)$$

In (2-9) and (2-10), $q(t) \triangleq \{q_0(t), q_v(t)\} \in \mathbb{R} \times \mathbb{R}^3$ represents the unit quaternion [62] describing the orientation of the body-fixed frame \mathcal{F} with respect to \mathcal{I} , subject to the constraint

$$q_v^T q_v + q_0^2 = 1. \quad (2-11)$$

Rotation matrices that bring \mathcal{I} onto \mathcal{F} and \mathcal{I} onto \mathcal{F}_d (desired body-fixed orientation), denoted by $R(q_v, q_0) \in SO(3)$ and $R_d(q_{vd}, q_{0d}) \in SO(3)$, respectively, can be defined as

$$R \triangleq (q_0^2 - q_v^T q_v) I_3 + 2q_v q_v^T - 2q_0 q_v^\times \quad (2-12)$$

$$R_d \triangleq (q_{0d}^2 - q_{vd}^T q_{vd}) I_3 + 2q_{vd} q_{vd}^T - 2q_{0d} q_{vd}^\times, \quad (2-13)$$

where I_3 denotes the 3×3 identity matrix, and $q_d(t) \triangleq \{q_{0d}(t), q_{vd}(t)\} \in \mathbb{R} \times \mathbb{R}^3$ represents the desired unit quaternion that describes the orientation of the body-fixed frame \mathcal{F}_d with respect to \mathcal{I} . Using (2-9) and (2-10), $\omega(t)$ can be expressed in terms of the quaternion as

$$\omega = 2(q_0 \dot{q}_v - q_v \dot{q}_0) - 2q_v^\times \dot{q}_v. \quad (2-14)$$

The desired angular velocity body-fixed frame \mathcal{F}_d with respect to \mathcal{I} expressed in \mathcal{F}_d can also be determined as

$$\omega_d = 2(q_{0d} \dot{q}_{vd} - q_{vd} \dot{q}_{0d}) - 2q_{vd}^\times \dot{q}_{vd}. \quad (2-15)$$

The subsequent analysis is based on the assumption that $q_{0d}(t)$, $q_{vd}(t)$, and their first three time derivatives are bounded for all time. This assumption ensures that $\omega_d(t)$ of (2-15) and its first two time derivatives are bounded for all time.

2.4 Control Objective

The objective in this chapter is to develop a gimbal velocity controller to enable the attitude of \mathcal{F} to track the attitude of \mathcal{F}_d . To quantify the objective, an attitude tracking error denoted by $\tilde{R}(e_v, e_0) \in \mathbb{R}^{3 \times 3}$ is defined that brings \mathcal{F}_d onto \mathcal{F} as

$$\tilde{R} \triangleq RR_d^T = (e_0^2 - e_v^T e_v) I_3 + 2e_v e_v^T - 2e_0 e_v^\times, \quad (2-16)$$

where $R(q_v, q_0)$ and $R_d(q_{vd}, q_{0d})$ were defined in (2-12) and (2-13), respectively, and the quaternion tracking error $e(t) \triangleq \{e_0(t), e_v(t)\} \in \mathbb{R} \times \mathbb{R}^3$ is defined as

$$e_0 \triangleq q_0 q_{0d} + q_v^T q_{vd} \quad (2-17)$$

$$e_v \triangleq q_{0d} q_v - q_0 q_{vd} + q_v^\times q_{vd}. \quad (2-18)$$

Based on (2-16), the attitude control objective can be stated as

$$\tilde{R}(e_v(t), e_0(t)) \rightarrow I_3 \quad \text{as} \quad t \rightarrow \infty. \quad (2-19)$$

Based on the tracking error formulation, the angular velocity of \mathcal{F} with respect to \mathcal{F}_d expressed in \mathcal{F} , denoted by $\tilde{\omega}(t) \in \mathbb{R}^3$, is defined as

$$\tilde{\omega} \triangleq \omega - \tilde{R}\omega_d. \quad (2-20)$$

From the definitions of the quaternion tracking error variables, the following constraint can be developed [2]:

$$e_v^T e_v + e_0^2 = 1, \quad (2-21)$$

where

$$0 \leq \|e_v(t)\| \leq 1 \quad 0 \leq |e_0(t)| \leq 1, \quad (2-22)$$

where $\|\cdot\|$ represents the standard Euclidean norm. From (2-21),

$$\|e_v(t)\| \rightarrow 0 \Rightarrow |e_0(t)| \rightarrow 1, \quad (2-23)$$

and hence, (2-16) can be used to conclude that if (2-23) is satisfied, then the control objective in (2-19) will be achieved.

2.5 Adaptive Control Development

To facilitate the controller design, an auxiliary signal, denoted by $r(t) \in \mathbb{R}^3$, is defined as

$$r \triangleq \omega - \tilde{R}\omega_d + \alpha e_v \quad (2-24)$$

where $\alpha \in \mathbb{R}^{3 \times 3}$ is a constant, positive definite, diagonal control gain matrix. After substituting (2-24) into (2-20), the angular velocity tracking error can be expressed as

$$\tilde{\omega} = r - \alpha e_v. \quad (2-25)$$

Motivation for the design of $r(t)$ is obtained from the subsequent Lyapunov-based stability analysis and the fact that (2-14) - (2-18) can be used to determine the open-loop quaternion tracking error as

$$\dot{e}_v = \frac{1}{2} (e_v^\times + e_0 I) \tilde{\omega} \quad \dot{e}_0 = -\frac{1}{2} e_v^T \tilde{\omega}. \quad (2-26)$$

2.5.1 Tracking Error Dynamics

The open-loop dynamics for $r(t)$ can be determined by taking the time derivative of (2-24) and premultiplying the resulting expression by $J(\delta)$ as

$$J\dot{r} = J\dot{\omega} + J\omega^\times \tilde{R}\omega_d - J\tilde{R}\dot{\omega}_d + J\alpha\dot{e}_v, \quad (2-27)$$

where the fact that

$$\dot{\tilde{R}} = -\omega^\times \tilde{R}$$

was utilized. After using (2-1), (2-4), (2-5), (2-24), and (2-26), the expression in (2-27) can be written as

$$J\dot{r} = -\omega^\times h_{cmg} - \frac{1}{2} \dot{J}r + Y_1 \theta_1 - \Omega_1 \dot{\delta} - hA\dot{\delta} - AF_s \text{sgn} \dot{\delta}. \quad (2-28)$$

In (2–28), $Y_1(e_v, e_0, \omega, \delta, t) \in \mathbb{R}^{3 \times p_1}$ is a known and measurable regression matrix, and $\theta_1 \in \mathbb{R}^{p_1}$ is a vector of p_1 unknown constants (i.e., satellite inertia parameters) where²

$$Y_1 \theta_1 = -\omega^\times J \omega + J \omega^\times \tilde{R} \omega_d - J \tilde{R} \dot{\omega}_d + \frac{1}{2} J \alpha (e_v^\times + e_0 I) \tilde{\omega}. \quad (2-29)$$

Also in (2–28), $\Omega_1(r, e_v, e_0, t) \in \mathbb{R}^{3 \times 4}$ denotes an auxiliary matrix containing parametric uncertainty defined as

$$\Omega_1 \dot{\delta} = \left(\frac{\partial J}{\partial \delta} \dot{\delta} \right) \left(\frac{1}{2} r + \tilde{R} \omega_d + \alpha e_v \right) + A F_d \dot{\delta} \quad (2-30)$$

that can be linearly parameterized in terms of a known regression matrix $Y_2(e_v, e_0, r, \omega, \delta, \dot{\delta}, t) \in \mathbb{R}^{3 \times p_2}$ and a vector of p_2 unknown constants (i.e., inertia parameters and friction coefficients) $\theta_2 \in \mathbb{R}^{p_2}$ as³

$$\Omega_1 \dot{\delta} \triangleq Y_2 \theta_2. \quad (2-31)$$

Some of the control design challenges for the open-loop system in (2–28) are that the control input $\dot{\delta}(t)$ is premultiplied by a nonsquare known time-varying matrix plus a nonsquare unknown time-varying matrix, and $\dot{\delta}(t)$ is embedded inside of a discontinuous nonlinearity (i.e., the *signum* function). To address the fact that $\dot{\delta}(t)$ is premultiplied by a nonsquare unknown time-varying matrix, an estimate of the uncertainty in (2–31), denoted by $\hat{\Omega}_1(r, e_v, e_0, t) \in \mathbb{R}^{3 \times 4}$, is defined as

$$\hat{\Omega}_1 \dot{\delta} \triangleq Y_2 \hat{\theta}_2 \quad (2-32)$$

² The constant p_1 is defined based on the number of uncertain parameters in the parameterization in (2–29). In this case, $p_1 = 6$, corresponding to the 6 uncertain inertia parameters.

³ The constant p_2 is defined based on the number of uncertain elements in (2–30).

where $\hat{\theta}_2(t) \in \mathbb{R}^{p_2}$ is a subsequently designed estimate for the parametric uncertainty in $\Omega_1(r, e_v, e_0, t)$. Based on (2-31) and (2-32), (2-28) can be rewritten as

$$J\dot{r} = -\omega^\times h_{cmg} - \frac{1}{2}\dot{J}r + Y_1\theta_1 - Y_2\tilde{\theta}_2 - B\dot{\delta} - AF_s \text{sgn}\dot{\delta}, \quad (2-33)$$

where $B(r, e_v, e_0, \delta, t) \in \mathbb{R}^{3 \times 4}$ is defined as

$$B = hA + \hat{\Omega}_1 \quad (2-34)$$

and the parameter estimate mismatch $\tilde{\theta}_2(t) \in \mathbb{R}^{p_2}$ is defined as

$$\tilde{\theta}_2 = \theta_2 - \hat{\theta}_2. \quad (2-35)$$

Based on the open-loop dynamics in (2-33) and the subsequent stability analysis, the control input is designed as

$$\dot{\delta} = B^+ \left[Y_1\hat{\theta}_1 - \omega^\times h_{cmg} + kr + k_n r - e_v \right], \quad (2-36)$$

where $k, k_n \in \mathbb{R}$ denote positive control gains, and $B^+(r, e_v, e_0, \delta, t) \in \mathbb{R}^{3 \times 3}$ denotes a pseudoinverse of $B(\delta, e_v, e_0, \hat{\theta}_2, t)$ defined as [20-22]

$$B^+ = B^T (BB^T + \epsilon I_{3 \times 3})^{-1}. \quad (2-37)$$

In (2-37), $\epsilon(t) \in \mathbb{R}$ denotes a singularity avoidance parameter. For example, Nakamura et al. [21] designed $\epsilon(t)$ as

$$\epsilon \triangleq \epsilon_0 \exp [-\det (BB^T)], \quad (2-38)$$

so that $\epsilon(t)$ is negligible when $B(r, e_v, e_0, \delta, t)B^T(r, e_v, e_0, \delta, t)$ is nonsingular but increases to the constant parameter $\epsilon_0 \in \mathbb{R}$ as the singularity is approached. After substituting (2-36) into (2-33), the closed-loop error system for $r(t)$ can be obtained as

$$J\dot{r} = -\frac{1}{2}\dot{J}r + Y_1\tilde{\theta}_1 - Y_2\tilde{\theta}_2 - kr - k_n r + e_v - AF_s \text{sgn}\dot{\delta}, \quad (2-39)$$

where the parameter estimate mismatch $\tilde{\theta}_1(t) \in \mathbb{R}^{p_1}$ is defined as

$$\tilde{\theta}_1 = \theta_1 - \hat{\theta}_1. \quad (2-40)$$

Based on (2-39) and the subsequent stability analysis, the parameter estimates $\hat{\theta}_1(t)$ and $\hat{\theta}_2(t)$ are designed as⁴

$$\dot{\hat{\theta}}_1 = \text{proj}(\Gamma_1 Y_1^T r) \quad \dot{\hat{\theta}}_2 = \text{proj}(-\Gamma_2 Y_2^T r), \quad (2-41)$$

where $\Gamma_1 \in \mathbb{R}^{p_1 \times p_1}$ and $\Gamma_2 \in \mathbb{R}^{p_2 \times p_2}$ denote constant, positive-definite, diagonal adaptation gain matrices, and $\text{proj}(\cdot)$ denotes a projection algorithm utilized to guarantee that the i -th element of $\hat{\theta}_1(t)$ and $\hat{\theta}_2(t)$ can be bounded as

$$\underline{\theta}_{1i} \leq \hat{\theta}_{1i} \leq \bar{\theta}_{1i} \quad \underline{\theta}_{2i} \leq \hat{\theta}_{2i} \leq \bar{\theta}_{2i}, \quad (2-42)$$

where $\underline{\theta}_{1i}, \bar{\theta}_{1i} \in \mathbb{R}$ and $\underline{\theta}_{2i}, \bar{\theta}_{2i} \in \mathbb{R}$ denote known, constant lower and upper bounds for each element of $\hat{\theta}_1(t)$ and $\hat{\theta}_2(t)$, respectively.⁵

While robust or linear control methods (i.e., LQR, H_∞ , LQG) can be applied to linearized versions of satellite systems, such controllers are designed based on worst-case scenarios for the uncertainty in the system. Although high gain and/or high frequency feedback are often needed to compensate for such worst-case scenarios, adaptive control has advantages over linear or robust control approaches in that high gain and/or high frequency feedback is not necessary.

⁴ The adaptive laws given here are designed based on the subsequent Lyapunov-based stability analysis, not to identify the actual values of the uncertain parameters.

⁵ The adaptive control law given in (2-36) and (2-41) requires measurements of angular position and velocity, not acceleration.

2.5.2 Stability Analysis

Theorem 2-1: *Given the closed-loop dynamics given in (2-24) and (2-33), the adaptive controller of (2-36) and (2-41) ensures global uniformly ultimately bounded (GUUB) attitude tracking in the sense that*

$$\|e_v(t)\| \rightarrow \varepsilon_0 \exp(-\varepsilon_1 t) + \varepsilon_2, \quad (2-43)$$

where $\varepsilon_0, \varepsilon_1, \varepsilon_2 \in \mathbb{R}$ denote positive bounding constants.

Proof: Let $V(e_0, e_v, r, t) \in \mathbb{R}$ be defined as the nonnegative function

$$V \triangleq e_v^T e_v + (1 - e_0)^2 + \frac{1}{2} r^T J r + \frac{1}{2} \tilde{\theta}_1^T \Gamma_1^{-1} \tilde{\theta}_1 + \frac{1}{2} \tilde{\theta}_2^T \Gamma_2^{-1} \tilde{\theta}_2. \quad (2-44)$$

The expression in (2-44) can be rewritten as

$$V \triangleq \frac{1}{2} \begin{bmatrix} e_v^T & r^T \end{bmatrix} \begin{bmatrix} e_v \\ J r \end{bmatrix} + (1 - e_0)^2 + \frac{1}{2} \tilde{\theta}_1^T \Gamma_1^{-1} \tilde{\theta}_1 + \frac{1}{2} \tilde{\theta}_2^T \Gamma_2^{-1} \tilde{\theta}_2, \quad (2-45)$$

and it follows directly from the bounds given in (2-3), (2-22), and (2-42) that $V(e_0, e_v, r, t)$ can be upper and lower bound as follows:

$$\lambda_1 \|z\|^2 + c_1 \leq V(t) \leq \lambda_2 \|z\|^2 + c_2, \quad (2-46)$$

where $\lambda_1, \lambda_2, c_1, c_2 \in \mathbb{R}$ are known positive bounding constants, and $z(t) \in \mathbb{R}^6$ is defined as

$$z \triangleq \begin{bmatrix} e_v^T & r^T \end{bmatrix}^T. \quad (2-47)$$

After using (2-26), (2-35), (2-39), and (2-40), the time derivative of $V(e_0, e_v, r, t)$ can be expressed as

$$\begin{aligned} \dot{V} = & e_v^T (e_v^\times + e_0 I) \tilde{\omega} + (1 - e_0) e_v^T \tilde{\omega} + r^T \left(Y_1 \tilde{\theta}_1 - Y_2 \tilde{\theta}_2 - k r - k_n r + e_v - A F_s \operatorname{sgn} \dot{\delta} \right) \\ & - \tilde{\theta}_1^T \Gamma_1^{-1} \dot{\tilde{\theta}}_1 - \tilde{\theta}_2^T \Gamma_2^{-1} \dot{\tilde{\theta}}_2. \end{aligned} \quad (2-48)$$

By using (2-8), (2-25), (2-41), and exploiting the fact that

$$e_v^T e_v^\times \tilde{\omega} = 0,$$

the expression in (2-48) can be written as

$$\dot{V} \leq -\lambda_3 \|z\|^2 - k_n \|r\|^2 + \|r\| \zeta_0 \|F_s\|_{i_\infty}, \quad (2-49)$$

where $\lambda_3 = \lambda_{\min} \{\alpha, k\} \in \mathbb{R}$. After completing the squares, (2-49) can be written as

$$\dot{V}(t) \leq -\lambda_3 \|z\|^2 + \frac{(\zeta_0 \|F_s\|_{i_\infty})^2}{4k_n}. \quad (2-50)$$

Since the inequality in (2-46) can be utilized to lower bound $\|z\|^2$ as

$$\|z\|^2 \geq \frac{1}{\lambda_2} V(t) - \frac{c_2}{\lambda_2}, \quad (2-51)$$

the inequality in (2-50) can be expressed as

$$\dot{V}(t) \leq -\frac{\lambda_3}{\lambda_2} V(t) + \varepsilon, \quad (2-52)$$

where $\varepsilon \in \mathbb{R}$ is a positive constant that is defined as

$$\varepsilon = \frac{(\zeta_0 \|F_s\|_{i_\infty})^2}{4k_n} + \frac{\lambda_3 c_2}{\lambda_2}. \quad (2-53)$$

The linear differential inequality in (2-52) can be solved as

$$V(t) \leq V(0) \exp\left(-\frac{\lambda_3}{\lambda_2} t\right) + \varepsilon \frac{\lambda_2}{\lambda_3} \left[1 - \exp\left(-\frac{\lambda_3}{\lambda_2} t\right)\right]. \quad (2-54)$$

The expressions in (2-44) and (2-54) can be used to conclude that $r(t) \in \mathcal{L}_\infty$. Thus, from (2-22), (2-25), and (2-47), $\tilde{\omega}(t), z(t) \in \mathcal{L}_\infty$, and (2-24) can be used to conclude that $\omega(t) \in \mathcal{L}_\infty$. Equation (2-26) then shows that $\dot{e}_v(t), \dot{e}_0(t) \in \mathcal{L}_\infty$. Hence, (2-29), (2-32), (2-34), and (2-42) can be used to prove that the control input $\delta(t) \in \mathcal{L}_\infty$. Standard signal chasing arguments can then be utilized to prove that all remaining signals remain bounded during closed-loop operation. The inequalities in (2-46) can now be used along

with (2-53) and (2-54) to conclude that

$$\|z\|^2 \leq \left(\frac{\lambda_2 \|z(0)\|^2 + c_2}{\lambda_1} \right) \exp \left\{ -\frac{\lambda_3}{\lambda_2} t \right\} + \left(\frac{\lambda_2 (\zeta_0 \|F_s\|_{i\infty})^2}{4k_n \lambda_3 \lambda_1} + \frac{c_2 - c_1}{\lambda_1} \right). \quad (2-55)$$

The result in (2-43) can now be directly obtained from (2-55).

2.6 Asymptotic Tracking Extension

In this section, a control design is developed for the case when static friction F_s is ignored. The following analysis illustrates that the controller developed in the previous section can be used to achieve asymptotic attitude tracking for this case.

2.6.1 Closed-Loop Error System

In the absence of static friction, letting $k_n = 0$ in (2-36) results in the following expression for the closed-loop tracking error system:

$$J\dot{r} = -\frac{1}{2}\dot{J}r + Y_1\tilde{\theta}_1 - Y_2\tilde{\theta}_2 - kr + e_v. \quad (2-56)$$

2.6.2 Stability Analysis Ignoring Static Friction

Theorem 2-2: *Given the closed-loop dynamics given in (2-56), the adaptive controller of (2-36) and (2-41) ensures asymptotic attitude tracking in the sense that*

$$\|e_v(t)\| \rightarrow 0 \quad \text{and} \quad \|\tilde{\omega}(t)\| \rightarrow 0 \quad (2-57)$$

provided the initial conditions are selected such that

$$\|e_0(0)\| \neq 0, \quad (2-58)$$

and the inertia matrix J satisfies the sufficient condition defined in (2-3).

Proof: To prove Theorem 2-2, the same procedure as in the previous section can be used to calculate the time derivative of the function $V(t)$ defined in (2-44) as

$$\dot{V}(t) \leq -\lambda_3 \|z\|^2, \quad (2-59)$$

where z was defined in (2-47), and λ_3 was defined in (2-49). From (2-59), $\dot{V}(t)$ is negative semi-definite, and $V(t)$ is bounded as shown in (2-46). Furthermore, (2-22), (2-24), (2-41), (2-42), and (2-56) can be used to conclude that $e(t), \dot{e}(t), \dot{r}(t) \in \mathcal{L}_\infty$. Thus, $\dot{z}(t) \in \mathcal{L}_\infty$, and $z(t) \in \mathcal{L}_2 \cap \mathcal{L}_\infty$. Barbalat's Lemma can now be used to conclude that

$$\|z(t)\| \rightarrow 0 \quad \text{as } t \rightarrow \infty.$$

Hence, the adaptive control law given by (2-36) and (2-41) achieves the asymptotic tracking claim given in (2-57) for the case in which static friction is ignored in the dynamics. Verification of the boundedness of the remaining signals during closed-loop operation is similar to that in the previous section.

2.7 Simulation Results

The attitude controller developed in this chapter was simulated based on the University of Florida control moment gyroscope (CMG) test bed (see 2.2). Using (2-1), the dynamic equation of motion in terms of the CMG test bed can be expressed as

$$J_{cmg}\dot{\omega} = -\omega^\times J_{cmg}\omega - \dot{J}_{cmg}\omega - \left(\dot{h}_{cmg} + \omega^\times h_{cmg}\right) - AF_d\dot{\delta} - AF_s \text{sgn}\dot{\delta}, \quad (2-60)$$

where the CMG test bed inertia matrix $J_{cmg}(\delta) \in \mathbb{R}^{3 \times 3}$ is defined using the parallel axis theorem as

$$J_{cmg} \triangleq J_0 + \sum_{i=1}^4 [{}^B J_{gi} + m_{cmg} (r_i^T r_i I_3 - r_i r_i^T)]. \quad (2-61)$$

In (2-61), $J_0 \in \mathbb{R}^{3 \times 3}$ is defined as

$$J_0 \triangleq J_{cmg}(0) = \text{diag} \left\{ 0.0610 \quad 0.0610 \quad 0.0764 \right\} \text{kg} \cdot \text{m}^2, \quad (2-62)$$

$m_{cmg} = 0.1565 \text{ kg}$, and $r_i \in \mathbb{R}^3 \forall i = 1, 2, 3, 4$ are defined as

$$r_1 \triangleq \begin{bmatrix} 0.1591 & 0 & 0.1000 \end{bmatrix}^T m \quad r_2 \triangleq \begin{bmatrix} -0.1591 & 0 & 0.1000 \end{bmatrix}^T m \quad (2-63)$$

$$r_3 \triangleq \begin{bmatrix} 0 & 0.1591 & 0.1000 \end{bmatrix}^T m \quad r_4 \triangleq \begin{bmatrix} 0 & -0.1591 & 0.1000 \end{bmatrix}^T m. \quad (2-64)$$

Also in (2-61), ${}^B J_{gi}(\delta) \in \mathbb{R}^{3 \times 3} \forall i = 1, 2, 3, 4$ denotes the inertia matrix of the i^{th} gimbal as expressed in the CMG test bed body-fixed frame, and is defined as

$${}^B J_{gi} \triangleq [C_{Bgi}] [{}^{gi} J_{gi}] [C_{Bgi}]^T, \quad (2-65)$$

where the coordinate transformation matrix $C_{Bgi} \in SO(3) \forall i = 1, 2, 3, 4$ relates the i^{th} gimbal-fixed frame to the CMG cluster body-fixed frame, and ${}^{gi} J_{gi} = \text{diag} \left\{ 4.89 \times 10^{-5} \quad 2.49 \times 10^{-4} \quad 2.79 \times 10^{-4} \right\} \text{ kg} \cdot \text{m}^2 \forall i = 1, 2, 3, 4$ represents the inertia matrix of the i^{th} gimbal as expressed in the i^{th} gimbal-fixed frame. Also in (2-60), $\dot{h}_{cmg} \in \mathbb{R}^3$ is defined using (2-5), where $h = 0.078$.

The objective is to regulate a satellite's attitude to the desired quaternion defined by

$$q_d = \begin{bmatrix} 0.920 & -0.002 & 0.271 & 0.284 \end{bmatrix}^T, \quad (2-66)$$

with the initial quaternion orientation of the satellite given by

$$q(0) = \begin{bmatrix} 1 & 0 & 0 & 0 \end{bmatrix}^T,$$

and the adaptive estimates initialized as⁶

$$\begin{aligned} \hat{\theta}_1(0) &= \begin{bmatrix} 0 & 0 & 0 & 0 & 0 & 0 \end{bmatrix}^T \\ \hat{\theta}_2(0) &= \begin{bmatrix} 0 & 0 & 0 & 0 & 0 & 0 \end{bmatrix}^T. \end{aligned}$$

The friction matrices F_d and F_s for the simulated CMG test bed are (e.g., see [64])

$$F_d = 0.2I_4 \quad F_s = 0.4I_4, \quad (2-67)$$

⁶ In a realistic scenario, the initial conditions of the adaptive estimates would be initialized to the best guess of the parameter value. The estimates were initialized to a vector of zeros in the simulation for the case when no knowledge is available. This shows that the adaptive control law presented here will work even in a worst-case scenario, when no information of the system parameters is known.

where I_n denotes the $n \times n$ identity matrix. To test the scenario when a sudden increase in the friction occurs, an instantaneous jump (i.e., step function) of 0.3 in the F_d and F_s parameters is programmed to occur 4 seconds into the simulation⁷. Figures 2-2 and 2-3 show the simulation results of the closed-loop system for this case with control gains selected as (e.g., see (2-36), (2-37), (2-38), and (2-41)):

$$k = 0.3 \quad k_n = 0.85 \quad \epsilon_0 = 0.2 \quad \alpha = 2 \quad \Gamma_1 = 0.2I_6 \quad \Gamma_2 = 2I_4.$$

Figure 2-4 illustrates the variation in the inertia parameters during closed loop operation. This effect is only significant for a brief transient period before the adaptation law for $\hat{\theta}_2$ in (2-41) compensates for the disturbance.

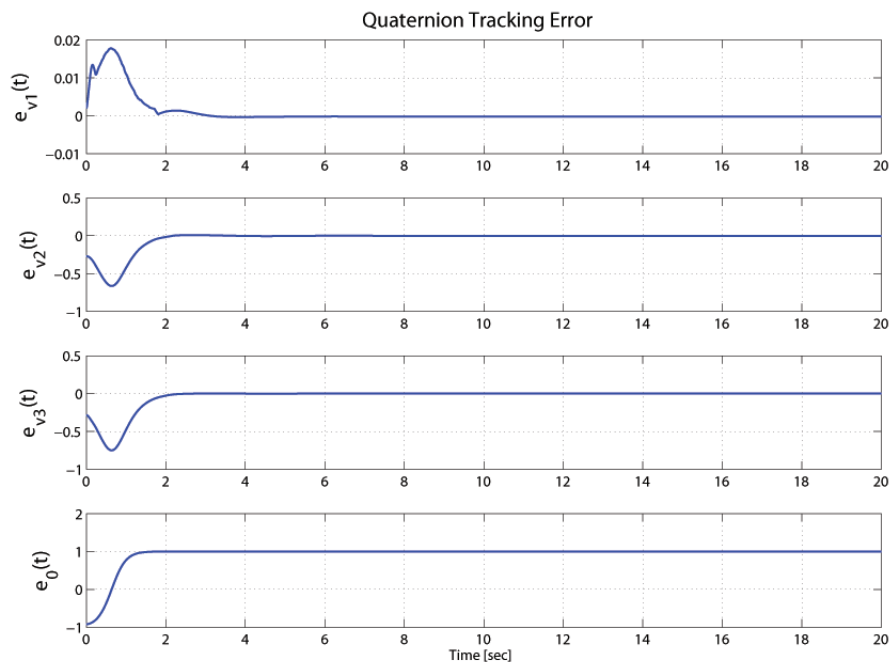


Figure 2-2. Quaternion tracking error.

⁷ In a realistic situation, the gimbal friction would most likely increase gradually over time (e.g., due to bearing degradation, corrosion, etc.), so the sudden spike of friction tested in the simulation tests a worst case scenario.

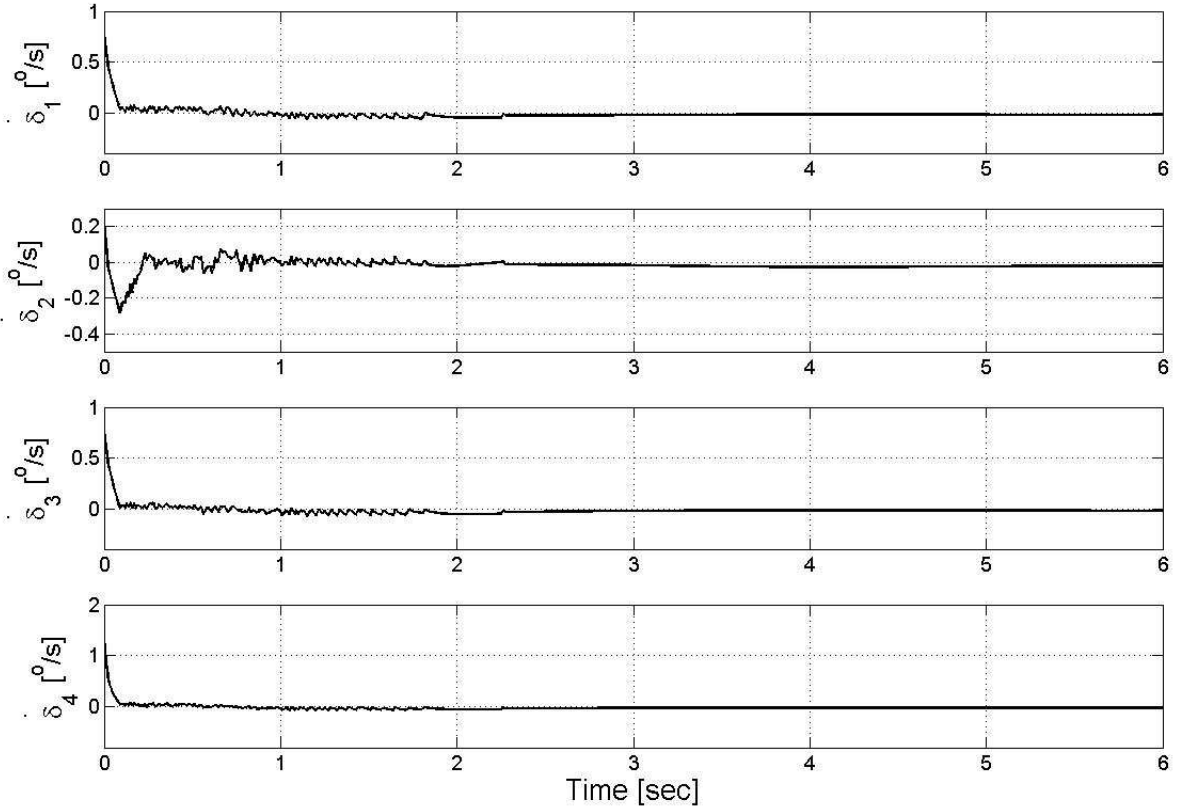


Figure 2-3. Control input gimbal angular rate response.

2.8 Conclusions and Future Work

In this chapter, a uniformly ultimately bounded attitude tracking controller for a rigid body satellite is presented. The controller adapts for parametric uncertainty in the satellite inertia matrix in addition to the uncertainties in the input torque caused by unknown CMG gimbal friction. The gimbal rate input controller achieves uniformly ultimately bounded attitude tracking in the presence of static and dynamic CMG gimbal friction. In the presence of static friction, the control design is complicated due to the control input being embedded in a hard nonlinearity. This difficulty is overcome with the use of a robust tracking control law. In addition, since a singularity robust steering law is incorporated in the control design, the proposed approach avoids singular torque directions inherent to the dynamics of the four single gimbal CMG cluster. Numerical simulation

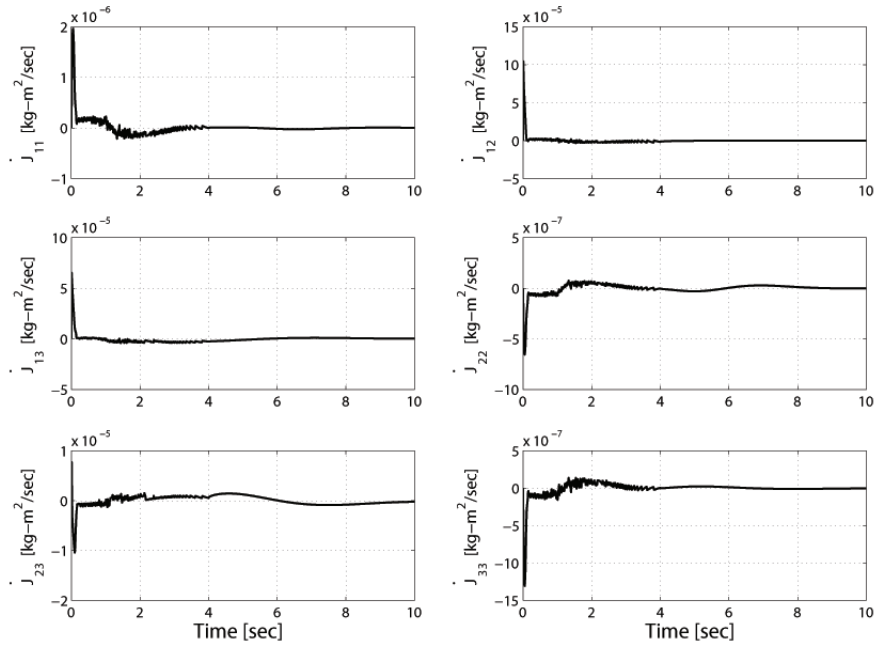


Figure 2-4. $\dot{J}(\delta)$ vs. time.

results are provided to show the efficacy of the proposed controller. An asymptotic tracking extension is also presented in the absence of static friction in the dynamic model. Future work will address the issues of explicit gimbal acceleration dependence in the CMG torque model, variations in CMG wheel speed, and hard stops in the CMG gimbals.

CHAPTER 3
ADAPTIVE NEURAL NETWORK SATELLITE ATTITUDE CONTROL IN THE
PRESENCE OF INERTIA AND CMG ACTUATOR UNCERTAINTIES

3.1 Introduction

An adaptive NN attitude tracking controller is developed in this chapter for CMG-actuated small-sats, which compensates for uncertain satellite inertia, nonlinear disturbance torques, uncertain CMG gimbal friction, and CMG actuator disturbances. The NN weights and thresholds are adjusted on-line, with no off-line learning phase required. In addition to the unknown CMG gimbal friction assumed present in the CMG torque model (e.g., see [23]), unknown electromechanical disturbances are assumed to be present in the CMG actuators. Some of the challenges encountered in the control design are that the control input (i.e., CMG gimbal angular rate) is: premultiplied by a non-square, time-varying, nonlinear uncertain matrix due to dynamic gimbal friction and electromechanical disturbances; and is embedded in a hard nonlinearity due to static gimbal friction. Furthermore, due to the small size of the satellite considered in this development, the motion of the CMGs causes significant time-variation in the satellite inertia characteristics. The time-variation of the satellite inertia manifests itself as a nonlinear disturbance torque in the satellite dynamic model, which is handled via online NN approximation. Simulation results are provided to illustrate the efficacy of the proposed control design.

3.2 Dynamic Model and Properties

The dynamic model for a rigid body CMG-actuated satellite can be expressed as [62, 63]

$$J\dot{\omega} = -\omega^\times J\omega + \tau_{cmg} - \dot{J}\omega + \tau_d. \quad (3-1)$$

In (3-1), $J(\delta) \in \mathbb{R}^{3 \times 3}$ represents the positive definite, symmetric satellite inertia matrix that is a function of the CMG gimbal angular position vector $\delta(t) \in \mathbb{R}^4$, $\omega(t) \in \mathbb{R}^3$ denotes the angular velocity of the satellite body-fixed frame \mathcal{F} with respect to \mathcal{I} expressed in \mathcal{F} , $\tau_{cmg}(t) \in \mathbb{R}^3$ denotes the torque generated via a CMG cluster consisting of four single

gimbal CMGs, the term $\dot{J}(t)\omega(t)$ represents the torque produced by the time variation of the satellite inertia matrix due to the motion of the CMGs, $\tau_d(t) \in \mathbb{R}^3$ denotes a general nonlinear disturbance (e.g., unmodeled effects), and the notation $\zeta^\times \forall \zeta = [\zeta_1, \zeta_2, \zeta_3]^T$ denotes the following skew-symmetric matrix:

$$\zeta^\times = \begin{bmatrix} 0 & -\zeta_3 & \zeta_2 \\ \zeta_3 & 0 & -\zeta_1 \\ -\zeta_2 & \zeta_1 & 0 \end{bmatrix}. \quad (3-2)$$

The torque generated from the CMG cluster can be modeled as

$$\tau_{cmg} = -\left(\dot{h}_{cmg} + \omega^\times h_{cmg}\right) - AF_d \dot{\delta} - AF_s \text{sgn} \dot{\delta} + AT_d, \quad (3-3)$$

where $F_d, F_s \in \mathbb{R}^{4 \times 4}$ are diagonal matrices whose elements are the unknown constant dynamic and static friction coefficients, respectively, of the four CMG gimbals, $h_{cmg}(t) \in \mathbb{R}^3$ represents the angular momentum of the CMG cluster, and $\dot{h}_{cmg}(t)$ is modeled as [7]

$$\dot{h}_{cmg} = hA(\delta) \dot{\delta}, \quad (3-4)$$

where $h \in \mathbb{R}$ represents the constant angular momentum of each CMG expressed in the gimbal-fixed frame (i.e., h is the same for all four CMGs). In (3-3) and (3-4), $\dot{\delta}(t) \in \mathbb{R}^4$ denotes the CMG gimbal angular velocity control input, which is defined as

$$\dot{\delta} \triangleq \begin{bmatrix} \dot{\delta}_1 & \dot{\delta}_2 & \dot{\delta}_3 & \dot{\delta}_4 \end{bmatrix}^T, \quad (3-5)$$

where $\dot{\delta}_i(t) \in \mathbb{R} \forall i = 1, 2, 3, 4$ denotes the angular velocity of the i^{th} CMG gimbal, $\text{sgn}(\dot{\delta}(t)) \in \mathbb{R}^4$ denotes a vector form of the standard $\text{sgn}(\cdot)$ function where the $\text{sgn}(\cdot)$ is applied to each element of $\dot{\delta}(t)$, and $A(\delta) \in \mathbb{R}^{3 \times 4}$ denotes a measurable Jacobian matrix

defined as

$$A = \begin{bmatrix} -\cos \gamma \cos \delta_1 & -\sin \delta_1 & \sin \gamma \cos \delta_1 \\ \sin \delta_2 & -\cos \gamma \cos \delta_2 & \sin \gamma \cos \delta_2 \\ \cos \gamma \cos \delta_3 & \sin \delta_3 & \sin \gamma \cos \delta_3 \\ -\sin \delta_4 & \cos \gamma \cos \delta_4 & \sin \gamma \cos \delta_4 \end{bmatrix}^T, \quad (3-6)$$

where $\gamma \in \mathbb{R}$ is the constant angle (54.74 deg) of each wall of the pyramid-shaped CMG cluster as depicted in Figure 2-1. Also in (3-3), $T_d(\delta, \dot{\delta}) \in \mathbb{R}^4$ represents torques in the gimbal axes due to tachometer disturbances, defined explicitly as [65]

$$T_d \triangleq K_G E_d \dot{\delta}, \quad (3-7)$$

where $K_G \in \mathbb{R}^{4 \times 4}$ denotes a diagonal matrix of uncertain, constant forward loop gains for the four CMG gimbal loops, and $E_d(\delta) \in \mathbb{R}^{4 \times 4}$ is defined as

$$E_d(\delta) \triangleq \text{diag} \left\{ E_{d1}(\delta_1) \quad E_{d2}(\delta_2) \quad E_{d3}(\delta_3) \quad E_{d4}(\delta_4) \right\}, \quad (3-8)$$

where the disturbance voltages $E_{di}(\delta_i) \forall i = 1, 2, 3, 4$ are functions of the i^{th} gimbal angle defined as

$$E_{di} \triangleq \sum_{n=1}^{10} \left\{ \frac{1}{n} \sin(n\delta_i) + \frac{1}{n+1} \cos(n\delta_i) \right\}. \quad (3-9)$$

Property 3-1: The satellite inertia matrix in (3-1) can be lower and upper bounded as

$$\frac{1}{2} \lambda_{\min} \{J\} \|\xi\|^2 \leq \xi^T J \xi \leq \frac{1}{2} \lambda_{\max} \{J\} \|\xi\|^2 \quad \forall \xi \in \mathbb{R}^n, \quad (3-10)$$

where $\lambda_{\min} \{J\}$, $\lambda_{\max} \{J\} \in \mathbb{R}$ are the minimum and maximum eigenvalues of $J(\delta)$, respectively.

Property 3-2: Since the elements of $A(\delta)$ in (3-6) are combinations of bounded trigonometric terms, the following inequality can be developed:

$$\|A(\delta)\|_{i\infty} \leq \zeta_0, \quad (3-11)$$

where $\zeta_0 \in \mathbb{R}$ is a positive bounding constant, and $\|\cdot\|_{i\infty}$ denotes the induced infinity norm of a matrix.

Property 3-3: The static friction matrix F_s can be bounded as $\|F_s\|_{i\infty} < F_M$, where F_M is a known constant.

Property 3-4: The term $\tau_d(t) \in \mathbb{R}^3$ is a disturbance acting on the system due to the gravity-gradient. Similar to [66], $\tau_d(t)$ is assumed to be of the form

$$\tau_d = \frac{p(q)}{R_0^3}, \quad (3-12)$$

where $p(q) \in \mathbb{R}^3$ is an unknown nonlinear function of the quaternion $q(t) \triangleq \{q_0(t), q_v(t)\} \in \mathbb{R} \times \mathbb{R}^3$, and $R_0 \in \mathbb{R}$ is the distance from the center of mass of the aircraft to the center of the Earth.

3.3 Kinematic Model

The rotational kinematics of the rigid-body satellite can be determined as [2]

$$\dot{q}_v = \frac{1}{2} (q_v^\times \omega + q_0 \omega) \quad (3-13)$$

$$\dot{q}_0 = -\frac{1}{2} q_v^T \omega. \quad (3-14)$$

In (3-13) and (3-14), $q(t)$ represents the unit quaternion [62] describing the orientation of the body-fixed frame \mathcal{F} with respect to \mathcal{I} , subject to the constraint

$$q_v^T q_v + q_0^2 = 1, \quad (3-15)$$

and $q_d(t) \triangleq \{q_{0d}(t), q_{vd}(t)\} \in \mathbb{R} \times \mathbb{R}^3$ represents the desired unit quaternion that describes the orientation of the body-fixed frame \mathcal{F}_d with respect to \mathcal{I} . Rotation matrices that bring \mathcal{I} onto \mathcal{F} and \mathcal{I} onto \mathcal{F}_d , denoted by $R(q_v, q_0) \in SO(3)$ and $R_d(q_{vd}, q_{0d}) \in SO(3)$, respectively, can be defined as

$$R \triangleq (q_0^2 - q_v^T q_v) I_3 + 2q_v q_v^T - 2q_0 q_v^\times \quad (3-16)$$

$$R_d \triangleq (q_{0d}^2 - q_{vd}^T q_{vd}) I_3 + 2q_{vd} q_{vd}^T - 2q_{0d} q_{vd}^\times, \quad (3-17)$$

where I_3 denotes the 3×3 identity matrix. Based on (3-13) and (3-14), $\omega(t)$ can be expressed in terms of the quaternion as

$$\omega = 2(q_0\dot{q}_v - q_v\dot{q}_0) - 2q_v^\times\dot{q}_v. \quad (3-18)$$

The desired angular velocity body-fixed frame \mathcal{F}_d with respect to \mathcal{I} expressed in \mathcal{F}_d can also be determined as

$$\omega_d = 2(q_{0d}\dot{q}_{vd} - q_{vd}\dot{q}_{0d}) - 2q_{vd}^\times\dot{q}_{vd}. \quad (3-19)$$

The subsequent analysis is based on the assumption that $q_{0d}(t)$, $q_{vd}(t)$, and their first three time derivatives are bounded for all time. This assumption ensures that $\omega_d(t)$ of (3-19) and its first two time derivatives are bounded for all time.

3.4 Control Objective

The objective in this chapter is to develop a gimbal velocity controller to enable the attitude of \mathcal{F} to track the attitude of \mathcal{F}_d . To quantify the objective, an attitude tracking error denoted by $\tilde{R}(e_v, e_0) \in \mathbb{R}^{3 \times 3}$ is defined that brings \mathcal{F}_d onto \mathcal{F} as

$$\tilde{R} \triangleq RR_d^T = (e_0^2 - e_v^T e_v) I_3 + 2e_v e_v^T - 2e_0 e_v^\times, \quad (3-20)$$

where $R(q_v, q_0)$ and $R_d(q_{vd}, q_{0d})$ were defined in (3-16) and (3-17), respectively, and the quaternion tracking error $e(t) \triangleq \{e_0(t), e_v(t)\} \in \mathbb{R} \times \mathbb{R}^3$ is defined as

$$e_0 \triangleq q_0 q_{0d} + q_v^T q_{vd} \quad (3-21)$$

$$e_v \triangleq q_{0d} q_v - q_0 q_{vd} + q_v^\times q_{vd}. \quad (3-22)$$

Based on (3-20), the attitude control objective can be stated as

$$\tilde{R}(e_v(t), e_0(t)) \rightarrow I_3 \quad \text{as} \quad t \rightarrow \infty. \quad (3-23)$$

Based on the tracking error formulation, the angular velocity of \mathcal{F} with respect to \mathcal{F}_d expressed in \mathcal{F} , denoted by $\tilde{\omega}(t) \in \mathbb{R}^3$, is defined as

$$\tilde{\omega} \triangleq \omega - \tilde{R}\omega_d. \quad (3-24)$$

To facilitate the subsequent controller design, an auxiliary control signal, denoted by $r(t) \in \mathbb{R}^3$, is defined as [67]

$$r \triangleq \omega - \tilde{R}\omega_d + \alpha e_v, \quad (3-25)$$

where $\alpha \in \mathbb{R}^{3 \times 3}$ is a constant, positive definite, diagonal control gain matrix. After substituting (3-25) into (3-24), the angular velocity tracking error can be expressed as

$$\tilde{\omega} = r - \alpha e_v. \quad (3-26)$$

Motivation for the design of $r(t)$ is obtained from the subsequent Lyapunov-based stability analysis and that fact that (3-18)-(3-22) can be used to determine the open-loop quaternion tracking error as

$$\dot{e}_v = \frac{1}{2} (e_v^\times + e_0 I) \tilde{\omega} \quad \dot{e}_0 = -\frac{1}{2} e_v^T \tilde{\omega}. \quad (3-27)$$

From the definitions of the quaternion tracking error variables, the following constraint can be developed [2]:

$$e_v^T e_v + e_0^2 = 1, \quad (3-28)$$

where

$$0 \leq \|e_v(t)\| \leq 1 \quad 0 \leq |e_0(t)| \leq 1, \quad (3-29)$$

where $\|\cdot\|$ represents the standard Euclidean norm. From (3-28),

$$\|e_v(t)\| \rightarrow 0 \Rightarrow |e_0(t)| \rightarrow 1, \quad (3-30)$$

and hence, (3-20) can be used to conclude that if (3-30) is satisfied, then the control objective in (3-23) will be achieved.

3.5 Feedforward NN Estimation

NN-based estimation methods are well suited for dynamic models containing unstructured uncertainties and disturbances as in (3-1). The main feature that empowers NN-based controllers is the universal approximation property. Let \mathbb{S} be a compact simply connected set of \mathbb{R}^{N_1+1} . Let $\mathbb{C}^n(\mathbb{S})$ be defined as the space where $f : \mathbb{S} \rightarrow \mathbb{R}^n$ is continuous. The universal approximation property states that there exist weights and thresholds such that some function $f(x) \in \mathbb{C}^n(\mathbb{S})$ can be represented by a three-layer NN as [68, 69]

$$f(x) = W^T \sigma(V^T x) + \varepsilon(x) \quad (3-31)$$

for some given input $x(t) \in \mathbb{R}^{N_1+1}$. In (3-31), $V \in \mathbb{R}^{(N_1+1) \times N_2}$ and $W \in \mathbb{R}^{(N_2+1) \times n}$ are bounded constant ideal weight matrices for the first-to-second and second-to-third layers, respectively, where N_1 is the number of neurons in the input layer, N_2 is the number of neurons in the hidden layer, and n is the number of neurons in the third layer. The activation function in (3-31) is denoted by $\sigma(\cdot) : \mathbb{R}^{N_2+1} \rightarrow \mathbb{R}^{N_2+1}$, and $\varepsilon(x) : \mathbb{R}^{N_1+1} \rightarrow \mathbb{R}^n$ is the functional reconstruction error. Based on (3-31), the typical three-layer NN approximation for $f(x)$ is given as [68, 69]

$$\hat{f}(x) = \hat{W}^T \sigma(\hat{V}^T x), \quad (3-32)$$

where $\hat{V}(t) \in \mathbb{R}^{(N_1+1) \times N_2}$ and $\hat{W}(t) \in \mathbb{R}^{(N_2+1) \times n}$ are subsequently designed estimates of the ideal weight matrices. The estimate mismatch for the ideal weight matrices, denoted by $\tilde{V}(t) \in \mathbb{R}^{(N_1+1) \times N_2}$ and $\tilde{W}(t) \in \mathbb{R}^{(N_2+1) \times n}$, are defined as

$$\tilde{V} \triangleq V - \hat{V} \quad \tilde{W} \triangleq W - \hat{W}, \quad (3-33)$$

and the mismatch for the hidden layer output error for a given $x(t)$, denoted by $\tilde{\sigma}(x) \in \mathbb{R}^{N_2+1}$, is defined as

$$\tilde{\sigma} \triangleq \sigma - \hat{\sigma} = \sigma(V^T x) - \sigma(\hat{V}^T x). \quad (3-34)$$

The neural network estimate has several properties that facilitate the subsequent development. These properties are described as follows.

Property 3-5: (*Taylor Series Approximation*) The Taylor series expansion for $\sigma(V^T x)$ for a given x may be written as [68, 69]

$$\sigma(V^T x) = \sigma(\hat{V}^T x) + \sigma'(\hat{V}^T x) \tilde{V}^T x + O(\tilde{V}^T x)^2, \quad (3-35)$$

where $\sigma'(\hat{V}^T x) \equiv d\sigma(V^T x)/d(V^T x)|_{V^T x = \hat{V}^T x}$, and $O(\tilde{V}^T x)^2$ denotes the higher order terms. After substituting (3-35) into (3-34), the following expression can be obtained:

$$\tilde{\sigma} = \hat{\sigma}' \tilde{V}^T x + O(\tilde{V}^T x)^2, \quad (3-36)$$

where $\hat{\sigma}' \triangleq \sigma'(\hat{V}^T x)$.

Property 3-6: (*Boundedness of the Ideal Weights*) The ideal weights are assumed to exist and be bounded by known positive values so that

$$\|V\|_F^2 = \text{tr}(V^T V) \leq \bar{V}_B \quad (3-37)$$

$$\|W\|_F^2 = \text{tr}(W^T W) \leq \bar{W}_B, \quad (3-38)$$

where $\|\cdot\|_F$ is the Frobenius norm of a matrix, and $\text{tr}(\cdot)$ is the trace of a matrix.

For notational convenience, let the matrix containing all NN weights be defined as follows:

$$Z \triangleq \begin{bmatrix} W & 0 \\ 0 & V \end{bmatrix}. \quad (3-39)$$

3.6 Control Development

The contribution of this chapter is control development that shows how the aforementioned standard NN feedforward estimation strategy can be combined with robust control methods as a means to achieve tracking control for satellite systems described by (3-1) and (3-3), which contain nonlinear disturbances and parametric uncertainty in addition to uncertainty caused by actuator dynamics.

3.6.1 Open-Loop Error System

The open-loop dynamics for $r(t)$ can be determined by taking the time derivative of (3-25) and premultiplying the resulting expression by $J(\delta)$ as

$$J\dot{r} = J\dot{\omega} + J\omega^\times \tilde{R}\omega_d - J\tilde{R}\dot{\omega}_d + J\alpha\dot{e}_v, \quad (3-40)$$

where the fact that

$$\dot{\tilde{R}} = -\omega^\times \tilde{R}$$

was utilized. After using (3-1), (3-3), (3-4), (3-7), (3-25), and (3-27), the expression in (3-40) can be expressed as

$$J\dot{r} = f - \Omega_1\dot{\delta} - hA\dot{\delta} - \omega^\times h_{cmg} - AF_s \text{sgn}\dot{\delta} - \frac{1}{2}\dot{J}r. \quad (3-41)$$

In (3-41), the uncertain function $f(r, q_v, q_0, e_v, e_0, \omega, \omega_d, \dot{\omega}_d, \delta, t) \in \mathbb{R}^3$ is defined as

$$f \triangleq -\omega^\times J\omega + J\omega^\times \tilde{R}\omega_d - J\tilde{R}\dot{\omega}_d + \frac{1}{2}J\alpha(e_v^\times + e_0I)\tilde{\omega} + \tau_d, \quad (3-42)$$

where $\Omega_1(r, q_v, q_0, e_v, e_0, \omega_d, \dot{\omega}_d, \delta, t) \in \mathbb{R}^{3 \times 4}$ denotes an uncertain auxiliary matrix, which is defined via the parameterization

$$\Omega_1\dot{\delta} = \left[\frac{\partial J}{\partial \delta} \dot{\delta} \right] \left(\frac{1}{2}r + \tilde{R}\omega_d - \alpha e_v \right) + AF_d\dot{\delta} + AK_G E_d\dot{\delta}. \quad (3-43)$$

The expression in (3-43) can be linearly parameterized in terms of a known regression matrix $Y_1(r, q_v, q_0, e_v, e_0, \omega, \omega_d, \dot{\omega}_d, \delta, \dot{\delta}, t) \in \mathbb{R}^{3 \times p_1}$ and a vector of p_1 unknown constants $\theta_1 \in \mathbb{R}^{p_1}$ as

$$\Omega_1\dot{\delta} \triangleq Y_1\theta_1. \quad (3-44)$$

Some of the control design challenges for the open-loop system in (3-41) are that the control input $\dot{\delta}(t)$ is premultiplied by a nonsquare, uncertain time-varying matrix, and is embedded inside of a discontinuous nonlinearity (i.e., the *signum* function). To address the fact that $\dot{\delta}(t)$ is premultiplied by a nonsquare unknown time-varying matrix, an estimate of the uncertainty in (3-44), denoted by $\hat{\Omega}_1(r, q_v, q_0, e_v, e_0, \omega_d, \dot{\omega}_d, \delta, t) \in \mathbb{R}^{3 \times 4}$, is

defined as

$$\hat{\Omega}_1 \dot{\delta} \triangleq Y_1 \hat{\theta}_1, \quad (3-45)$$

where $\hat{\theta}_1(t) \in \mathbb{R}^{p_1}$ is a subsequently designed estimate for the parametric uncertainty in $\Omega_1(r, q_v, q_0, e_v, e_0, \omega_d, \dot{\omega}_d, \delta, t)$. Based on (3-44) and (3-45), (3-41) can be rewritten as

$$J\dot{r} = f - B\dot{\delta} - \omega^\times h_{cmg} - \frac{1}{2}Jr - Y_1 \tilde{\theta}_1 - AF_s \text{sgn}\dot{\delta}, \quad (3-46)$$

where $B(r, q_v, q_0, e_v, e_0, \omega_d, \dot{\omega}_d, \delta, t) \in \mathbb{R}^{3 \times 4}$ is defined as

$$B = hA + \hat{\Omega}_1, \quad (3-47)$$

and the parameter estimate mismatch $\tilde{\theta}_1(t) \in \mathbb{R}^{p_1}$ is defined as

$$\tilde{\theta}_1 \triangleq \theta_1 - \hat{\theta}_1. \quad (3-48)$$

The auxiliary function in (3-42) can be represented by a three-layer NN as

$$f = W^T \sigma(V^T x) + \varepsilon(x). \quad (3-49)$$

In (3-49), the input $x(t) \in \mathbb{R}^{25}$ is defined as

$$x(t) \triangleq \left[1 \quad r(t) \quad q_v(t) \quad q_0(t) \quad e_v(t) \quad e_0(t) \quad \omega(t) \quad \omega_d(t) \quad \dot{\omega}_d(t) \quad \delta(t) \right]^T, \quad (3-50)$$

so that $N_1 = 24$, where N_1 was introduced in (3-31). Based on the assumption that the actual and desired trajectories are bounded, the following inequality holds:

$$\|\varepsilon(x)\| \leq \varepsilon_{b1}, \quad (3-51)$$

where $\varepsilon_{b1} \in \mathbb{R}$ is a known positive constant.

3.6.2 Closed-Loop Error System

Based on the open-loop dynamics in (3-46) and the subsequent stability analysis, the control input is designed as

$$\dot{\delta} = B^+ \left[\hat{f} - \omega^\times h_{cmg} + K_v r - v + e_v \right], \quad (3-52)$$

where $K_v \in \mathbb{R}$ denotes a positive control gain, and $v(t) \in \mathbb{R}^3$ denotes a robustifying term, defined as [70]

$$v \triangleq -K_Z \left(\left\| \hat{Z} \right\|_F + Z_M \right) r - k_n r, \quad (3-53)$$

where $k_n \in \mathbb{R}$ denotes a positive control gain (i.e., nonlinear damping term), $\hat{Z} \in \mathbb{R}^{(N_1+N_2+2) \times (N_2+n)}$ is a subsequently designed estimate of Z , $Z_M \in \mathbb{R}$ satisfies the inequality

$$\|Z\|_F \leq Z_M, \quad (3-54)$$

and $K_Z \in \mathbb{R}$ is a control gain designed to satisfy the inequality

$$K_Z > c_2, \quad (3-55)$$

where c_2 is defined in (3-69). Also in (3-52), $B^+(r, q_v, q_0, e_v, e_0, \omega_d, \dot{\omega}_d, \delta, t) \in \mathbb{R}^{4 \times 3}$ denotes the generalized inverse of $B(r, q_v, q_0, e_v, e_0, \omega_d, \dot{\omega}_d, \delta, t)$, which could be defined using the Moore-Penrose definition or the singularity robust pseudoinverse definition coined by Nakamura et al. as (e.g., see [20-22])

$$B^+ = B^T (BB^T + \epsilon I_{3 \times 3})^{-1}. \quad (3-56)$$

In (3-56), $\epsilon(t) \in \mathbb{R}$ denotes a singularity avoidance parameter. For example, in [21] Nakamura et al. designed $\epsilon(t)$ as

$$\epsilon \triangleq \epsilon_0 \exp \left\{ -\det (BB^T) \right\}, \quad (3-57)$$

so that $\epsilon(t)$ is negligible when BB^T is nonsingular but increases to the constant parameter $\epsilon_0 \in \mathbb{R}$ as the singularity is approached. Also in (3-52), the feedforward NN component,

denoted as $\hat{f}(t) \in \mathbb{R}^3$, is given by

$$\hat{f} \triangleq \hat{W}^T \sigma(\hat{V}^T x), \quad (3-58)$$

where the state vector $x(t) \in \mathbb{R}^{25}$ was defined in (3-49). The estimates of the NN weights in (3-58) are generated on-line (there is no off-line learning phase) as [70]

$$\dot{\hat{W}} \triangleq \Gamma_1(\hat{\sigma}r^T - \hat{\sigma}'\hat{V}^T x r^T - \kappa \|r\| \hat{W}) \quad (3-59)$$

$$\dot{\hat{V}} \triangleq \Gamma_2 x r^T (\hat{\sigma}'^T \hat{W})^T - \kappa \Gamma_2 \|r\| \hat{V}, \quad (3-60)$$

where $\Gamma_1 \in \mathbb{R}^{(N_1+1) \times (N_1+1)}$, $\Gamma_2 \in \mathbb{R}^{(N_2+1) \times (N_2+1)}$ are constant, positive definite, symmetric control gain matrices, and $\kappa \in \mathbb{R}^+$ is a constant control gain.

Remark 3-1: *The adaptive update laws given in (3-59) and (3-60) ensure that $\hat{W}(t)$ and $\hat{V}(t)$ remain bounded provided $x(t)$ remains bounded. This fact will be exploited in the subsequent stability analysis.*

The closed-loop tracking error system can be developed by substituting (3-52) into (3-46) as

$$J\dot{r} = -\frac{1}{2}Jr + \tilde{f} - Y_1\tilde{\theta}_1 - K_v r + v - e_v - AF_s \text{sgn}\dot{\delta}, \quad (3-61)$$

where $\tilde{f}(x) \in \mathbb{R}^3$ represents a function estimation error vector defined as

$$\tilde{f} \triangleq f - \hat{f}. \quad (3-62)$$

Based on (3-61) and the subsequent stability analysis, the parameter estimate $\hat{\theta}_1(t)$ is designed as

$$\dot{\hat{\theta}}_1 = \text{proj}(-\Gamma_3 Y_1^T r), \quad (3-63)$$

where $\Gamma_3 \in \mathbb{R}^{p_1 \times p_1}$ denotes a constant, positive-definite, diagonal adaptation gain matrix, and $\text{proj}(\cdot)$ denotes a projection algorithm utilized to guarantee that the i^{th} element of $\hat{\theta}_1(t)$ can be bounded as

$$\underline{\theta}_{1i} \leq \hat{\theta}_{1i} \leq \bar{\theta}_{1i}, \quad (3-64)$$

where $\underline{\theta}_{1i}, \bar{\theta}_{1i} \in \mathbb{R}$ denote known, constant lower and upper bounds for each element of $\hat{\theta}_1(t)$.

Remark 3-2: To determine $\hat{\theta}_1$, the adaptation law in (3-63) assumes the availability of angular position and velocity measurements only.

Using (3-49), (3-58) and (3-62), the closed-loop error system in (3-61) can be expressed as

$$J\dot{r} = -\frac{1}{2}\dot{J}r + W^T\sigma(V^Tx) - \hat{W}^T\sigma(\hat{V}^Tx) + v - Y_1\tilde{\theta}_1 - K_v r + \varepsilon(x) - e_v - AF_s \text{sgn}\dot{\delta}. \quad (3-65)$$

After adding and subtracting the terms $W^T\hat{\sigma}$ and $\hat{W}^T\tilde{\sigma}$ to (3-65), the following expression is obtained:

$$J\dot{r} = -\frac{1}{2}\dot{J}r + \tilde{W}^T\hat{\sigma} + \hat{W}^T\tilde{\sigma} + \tilde{W}^T\tilde{\sigma} + \varepsilon(x) - Y_1\tilde{\theta}_1 - K_v r + v - e_v - AF_s \text{sgn}\dot{\delta} \quad (3-66)$$

where the notations $\hat{\sigma}$ and $\tilde{\sigma}$ were introduced in (3-34). The Taylor series approximation described in (3-35) and (3-36) can now be used to rewrite (3-66) as

$$J\dot{r} = -\frac{1}{2}\dot{J}r + w - K_v r + v - e_v - Y_1\tilde{\theta}_1 + \tilde{W}^T(\hat{\sigma} - \hat{\sigma}'\hat{V}^Tx) + \hat{W}^T\hat{\sigma}'\tilde{V}^Tx, \quad (3-67)$$

where $w(t) \in R^3$ is defined as

$$w = \tilde{W}^T\hat{\sigma}'V^Tx + W^TO(\tilde{V}^Tx)^2 - AF_s \text{sgn}\dot{\delta} + \varepsilon(x). \quad (3-68)$$

The NN reconstruction error $\varepsilon(x)$, the higher order terms in the Taylor series expansion of $f(x)$, and the static friction term $AF_s \text{sgn}\dot{\delta}(t)$ can be treated as disturbances in the error system. Moreover, these disturbances can be upper bounded as [70]

$$\|w(t)\| \leq c_0 + c_1 \left\| \tilde{Z} \right\|_F + c_2 \left\| \tilde{Z} \right\|_F \|r\|, \quad (3-69)$$

where $c_i \in R \forall i = 0, 1, 2$ are known positive constants, and c_0 is explicitly defined as

$$c_0 \triangleq \|A\|_{i\infty} F_M + \varepsilon_{b1} + c_3 Z_M, \quad (3-70)$$

and $c_3 \in \mathbb{R}$ is a known positive constant.

3.6.3 Stability Analysis

Theorem 3-1: *Given the closed-loop dynamics in (3-67), the adaptive controller of (3-52), (3-59), (3-60), and (3-63) ensures global uniformly ultimately bounded (GUUB) attitude tracking in the sense that*

$$\|e_v(t)\| \rightarrow \varepsilon_0 \exp\{-\varepsilon_1 t\} + \varepsilon_2, \quad (3-71)$$

where $\varepsilon_0, \varepsilon_1, \varepsilon_2 \in \mathbb{R}$ denote positive bounding constants.

Proof: Let $V(e_0, e_v, r, t) \in \mathbb{R}$ be defined as the nonnegative function

$$V(t) \triangleq e_v^T e_v + (1 - e_0)^2 + \frac{1}{2} r^T J r + \frac{1}{2} \text{tr} \left(\tilde{W}^T \Gamma_1^{-1} \tilde{W} \right) + \frac{1}{2} \text{tr} \left(\tilde{V}^T \Gamma_2^{-1} \tilde{V} \right) + \frac{1}{2} \tilde{\theta}_1^T \Gamma_3^{-1} \tilde{\theta}_1. \quad (3-72)$$

Based on (3-10), (3-29), (3-48), (3-59), (3-60), and (3-64), (3-72) can be upper and lower bounded as

$$\lambda_1 \|y\|^2 + c_4 \leq V(t) \leq \lambda_2 \|y\|^2 + c_5, \quad (3-73)$$

where $\lambda_1, \lambda_2, c_4, c_5 \in \mathbb{R}$ are known positive bounding constants, and $y(t) \in \mathbb{R}^6$ is defined as

$$y \triangleq \begin{bmatrix} e_v^T & r^T \end{bmatrix}^T. \quad (3-74)$$

After using (3-26), (3-27), (3-67), and exploiting the fact that

$$e_v^T e_v^\times \tilde{\omega} = 0,$$

the time derivative of $V(t)$ can be expressed as

$$\begin{aligned} \dot{V}(t) = & -\alpha e_v^T e_v + r^T \left(w - K_v r + v - Y_1 \tilde{\theta}_1 \right) - \text{tr} \tilde{W}^T \left(\Gamma_1^{-1} \dot{\tilde{W}}_1 - \hat{\sigma} r^T + \hat{\sigma}' \hat{V}^T x r^T \right) \\ & - \text{tr} \tilde{V}^T \left(\Gamma_2^{-1} \dot{\tilde{V}}_1 - x r^T \hat{W}^T \hat{\sigma}' \right) - \tilde{\theta}_1^T \Gamma_3^{-1} \dot{\tilde{\theta}}_1. \end{aligned} \quad (3-75)$$

After substituting for the tuning rules given in (3-59), (3-60), and (3-63), (3-75) can be expressed as

$$\dot{V} = -\alpha e_v^T e_v + r^T (w - K_v r + v) + \kappa \|r\| \text{tr} \tilde{Z}^T (Z - \tilde{Z}). \quad (3-76)$$

After substituting (3-53) and using the fact that $\text{tr} \tilde{Z}^T (Z - \tilde{Z}) = \langle \tilde{Z}, Z \rangle_F - \|\tilde{Z}\|_F^2 \leq \|\tilde{Z}\|_F \|Z\|_F - \|\tilde{Z}\|_F^2$, (3-76) can be upper bounded as follows [70]:

$$\begin{aligned} \dot{V}(t) &\leq -\alpha \|e_v\|^2 - K_{v \min} \|r\|^2 - k_n \|r\|^2 + \|r\| \|w\| - K_Z \left(\|\hat{Z}\|_F + Z_M \right) \|r\|^2 \\ &\quad + \kappa \|r\| \left(\|\tilde{Z}\|_F \left(Z_M - \|\tilde{Z}\|_F \right) \right). \end{aligned} \quad (3-77)$$

After substituting the upper bound for $\|w\|$ given in (3-69) and utilizing inequality (3-55), $\dot{V}(t)$ can be bounded as

$$\dot{V}(t) \leq -\lambda_3 \|y\|^2 - k_n \|r\|^2 + \gamma \|r\|, \quad (3-78)$$

where $\lambda_3 \triangleq \min \{ \alpha, K_{v \min} \}$, and $\gamma \triangleq c_0 + c_1 \|\tilde{Z}\|_F + \kappa \|\tilde{Z}\|_F \left(Z_M - \|\tilde{Z}\|_F \right)$. Completing the squares in (3-78) yields

$$\dot{V}(t) \leq -\lambda_3 \|y\|^2 + \frac{\gamma^2}{4k_n}. \quad (3-79)$$

Based on (3-73), (3-79) can be expressed as

$$\dot{V}(t) \leq -\frac{\lambda_3}{\lambda_2} V(t) + \varepsilon, \quad (3-80)$$

where $\varepsilon \in \mathbb{R}$ is a positive constant that is defined as

$$\varepsilon = \frac{\gamma^2}{4k_n} + \frac{\lambda_3 c_5}{\lambda_2}. \quad (3-81)$$

The linear differential inequality in (3-80) can be solved as

$$V(t) \leq \exp \left\{ -\frac{\lambda_3}{\lambda_2} t \right\} V(0) + \varepsilon \frac{\lambda_2}{\lambda_3} \left(1 - \exp \left\{ -\frac{\lambda_3}{\lambda_2} t \right\} \right). \quad (3-82)$$

The expressions in (3-72), (3-73), and (3-82) can be used to conclude that $r(t) \in \mathcal{L}_\infty$.

Thus, from (3-26), (3-29), and (3-74), $\tilde{\omega}(t), y(t) \in \mathcal{L}_\infty$, and (3-25) can be used to

conclude that $\omega(t) \in \mathcal{L}_\infty$. Equation (3-27) then shows that $\dot{e}_v(t), \dot{e}_0(t) \in \mathcal{L}_\infty$. Hence, (3-47), (3-52), (3-53), and (3-58)-(3-60) can be used to prove that the control input $\dot{\delta}(t) \in \mathcal{L}_\infty$. Standard signal chasing arguments can then be utilized to prove that all remaining signals remain bounded during closed-loop operation. The inequalities in (3-73) can now be used along with (3-81) and (3-82) to conclude that

$$\|y\|^2 \leq \left(\frac{\lambda_2 \|y(0)\|^2 + c_5}{\lambda_1} \right) \exp \left\{ -\frac{\lambda_3}{\lambda_2} t \right\} + \left(\frac{\lambda_2 \gamma^2}{4k_n \lambda_3 \lambda_1} + \frac{c_5 - c_4}{\lambda_1} \right). \quad (3-83)$$

The result in (3-71) can now be directly obtained from (3-83).

3.7 Simulation Results

The NN attitude controller developed in this chapter was simulated based on the University of Florida control moment gyroscope (CMG) testbed (see 2.2). Using (3-1), the dynamic equation of motion in terms of the CMG testbed can be expressed as

$$J_{cmg} \dot{\omega} = -\omega^\times J_{cmg} \omega - \dot{J}_{cmg} \omega - \left(\dot{h}_{cmg} + \omega^\times h_{cmg} \right) - AF_d \dot{\delta} - AF_s \text{sgn} \dot{\delta} + \tau_d + AT_d, \quad (3-84)$$

where $\dot{h}_{cmg} \in \mathbb{R}^3$ is defined using (3-4), where $h = 0.078 \text{ kg} \cdot \text{m}^2/\text{s}$, and $h_{cmg} \in \mathbb{R}^3$ was defined in (3-3), and the CMG testbed inertia matrix $J_{cmg}(\delta) \in \mathbb{R}^{3 \times 3}$ is defined using the parallel axis theorem as

$$J_{cmg} \triangleq J_0 + \sum_{i=1}^4 \left[{}^B J_{gi} + m_{cmg} (r_i^T r_i I_3 - r_i r_i^T) \right]. \quad (3-85)$$

In (3-85), J_0 is defined as

$$J_0 \triangleq J_{cmg}(0) = \text{diag} \left\{ 0.0610 \quad 0.0610 \quad 0.0764 \right\} \text{ kg} \cdot \text{m}^2, \quad (3-86)$$

$m_{cmg} = 0.1565 \text{ kg}$, and $r_i \in \mathbb{R}^3 \forall i = 1, 2, 3, 4$ are defined as

$$r_1 \triangleq \begin{bmatrix} 0.1591 & 0 & 0.1000 \end{bmatrix}^T m \quad r_2 \triangleq \begin{bmatrix} -0.1591 & 0 & 0.1000 \end{bmatrix}^T m \quad (3-87)$$

$$r_3 \triangleq \begin{bmatrix} 0 & 0.1591 & 0.1000 \end{bmatrix}^T m \quad r_4 \triangleq \begin{bmatrix} 0 & -0.1591 & 0.1000 \end{bmatrix}^T m. \quad (3-88)$$

Also in (3–85), ${}^B J_{gi}(\delta) \in \mathbb{R}^{3 \times 3} \forall i = 1, 2, 3, 4$ denotes the inertia matrix of the i^{th} gimbal expressed in the CMG testbed body-fixed frame, defined as

$${}^B J_{gi} \triangleq [C_{Bgi}] [{}^{gi} J_{gi}] [C_{Bgi}]^T. \quad (3-89)$$

In (3–89), the coordinate transformation matrix $C_{Bgi} \in SO(3) \forall i = 1, 2, 3, 4$

relates the i^{th} gimbal-fixed frame to the CMG cluster body-fixed frame, and

${}^{gi} J_{gi} = \text{diag} \left\{ 4.89 \times 10^{-5} \quad 2.49 \times 10^{-4} \quad 2.79 \times 10^{-4} \right\} \text{ kg} \cdot \text{m}^2 \forall i = 1, 2, 3, 4$ represents the inertia matrix of the i^{th} gimbal expressed in the i^{th} gimbal-fixed frame. In (3–84), the friction matrices $F_d \in \mathbb{R}^{4 \times 4}$ and $F_s \in \mathbb{R}^{4 \times 4}$ for the simulated CMG testbed are (e.g., see [64])

$$F_d = 0.2I_4 \quad F_s = 0.3I_4, \quad (3-90)$$

where I_n denotes the $n \times n$ identity matrix, and the Jacobian matrix $A(\delta) \in \mathbb{R}^{3 \times 4}$

was defined in (3–6). The nonlinear disturbance terms $\tau_d(t)$ and $T_d(\delta, \dot{\delta}) \triangleq$

$\left[T_{d1} \quad T_{d2} \quad T_{d3} \quad T_{d4} \right]^T$ are given by

$$\tau_d = 0.1 \begin{bmatrix} \sin 10t + \cos 20t \\ \sin 20t + \cos 30t \\ \sin 40t + \cos 50t \end{bmatrix} \quad (3-91)$$

$$T_{di} = K_{Gi} \sum_{n=1}^{10} \left\{ \frac{1}{n} \sin(n\delta_i) + \frac{1}{n+1} \cos(n\delta_i) \right\} \dot{\delta}_i, \quad (3-92)$$

where the CMG torquer control loop gain for the the i^{th} gimbal $K_{Gi} = 1.6 \forall i = 1, 2, 3, 4$.

The objective is to regulate a satellite's attitude to the desired quaternion defined by

$$q_d = \begin{bmatrix} 0.292 & 0.577 & 0.303 & -0.700 \end{bmatrix}^T, \quad (3-93)$$

with the initial quaternion orientation of the satellite given by

$$q(0) = \begin{bmatrix} 1 & 0 & 0 & 0 \end{bmatrix}^T,$$

and the NN weight estimates initialized as⁸

$$\hat{W}(0) = 0_{21 \times 3} \quad \hat{V}(0) = 0_{25 \times 20}, \quad (3-94)$$

where the notation $0_{m \times n}$ denotes an $m \times n$ matrix of zeros.

To test the scenario when a sudden increase in the friction occurs, instantaneous jumps (i.e., step functions) of 0.6 and 0.3 in the F_d and F_s parameters, respectively, are programmed to occur 4 seconds into the simulation⁹. Figures 3-1 and 3-2 show the simulation results of the closed-loop system with control gains selected as follows (e.g., see (3-52), (3-53), (3-56), (3-57), (3-59), (3-60), and (3-63)):

$$\begin{aligned} K_v = 0.2 \quad k_n = 0.7 \quad K_Z = 0.05 \quad \kappa = 2.5 \quad \alpha = 2 \quad \epsilon_0 = 0.2 \\ \Gamma_1 = 10.2I_{21} \quad \Gamma_2 = 5I_{21} \quad \Gamma_3 = 0.1I_6 \end{aligned}$$

Figure 3-3 illustrates the variation in the inertia parameters during closed loop operation.

Remark 3-3: *The gimbal rate control inputs remained bounded during closed-loop operation for the case when saturation limiting was not included in the simulation. However, the above simulation results were achieved using a gimbal rate saturation limit of 7.5 °/sec to test the tracking capability of the controller in the presence of actuator limitations (see [6] for a more detailed discussion of CMG gimbal rate ranges). The largest angular excursion (i.e., δ_{\max}) during the simulation interval is approximately 1.6°.*

⁸ In practice the initial conditions of the NN weight estimates would be initialized to the best guess of the ideal values. The estimates were initialized to matrices of zeros in the simulation for the case when no knowledge is available.

⁹ In a realistic situation, the gimbal friction would most likely increase gradually over time (e.g., due to bearing degradation, corrosion, etc.), so the sudden spike of friction tested in the simulation tests a worst case scenario.

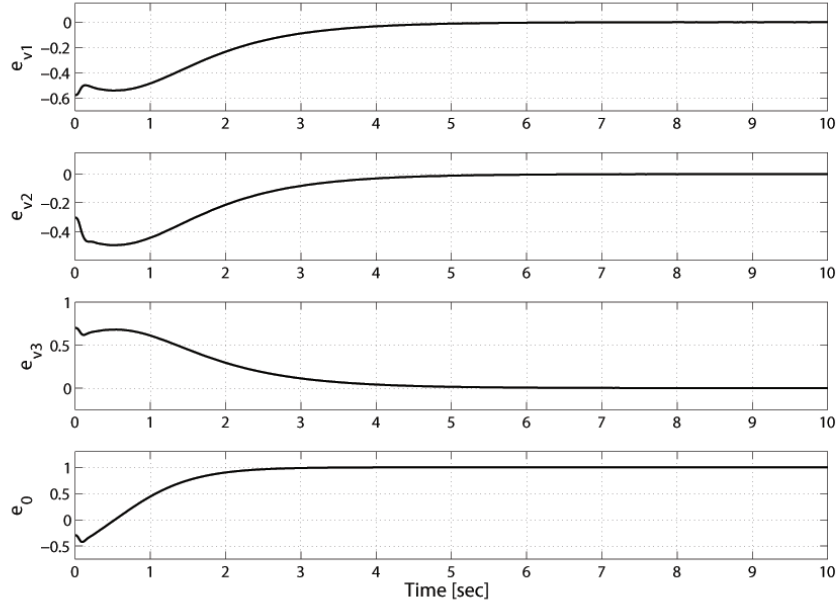


Figure 3-1. Quaternion tracking error of closed-loop system.

3.8 Conclusion

In this chapter, a uniformly ultimately bounded NN attitude tracking controller for a rigid body satellite is presented. The controller adapts for parametric uncertainty in the satellite inertia matrix and time varying satellite inertia parameters. In addition, the NN controller compensates for uncertainties in the input torque caused by unknown CMG gimbal friction and electromechanical disturbances in the gimbal loops. The gimbal rate input controller achieves uniformly ultimately bounded attitude tracking in the presence of static and dynamic CMG gimbal friction. In the presence of static friction, the control design is complicated due to the control input being embedded in a hard nonlinearity. This difficulty is overcome with the use of a robust tracking control law. In addition, since a singularity robust steering law is incorporated in the control design, the proposed approach avoids singular torque directions inherent to the dynamics of the four single gimbal CMG cluster. Numerical simulation results are provided to show the efficacy of the proposed NN controller.

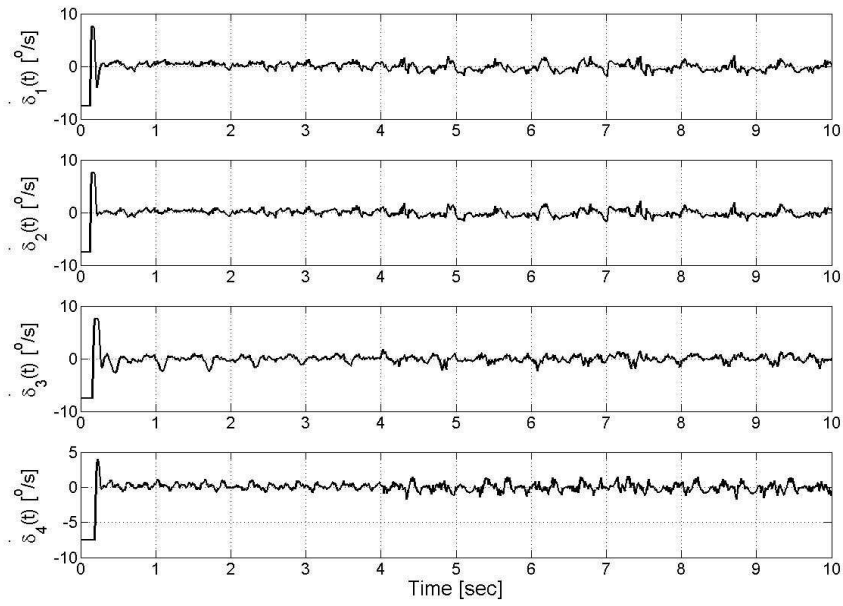


Figure 3-2. Control input gimbal angular rates.

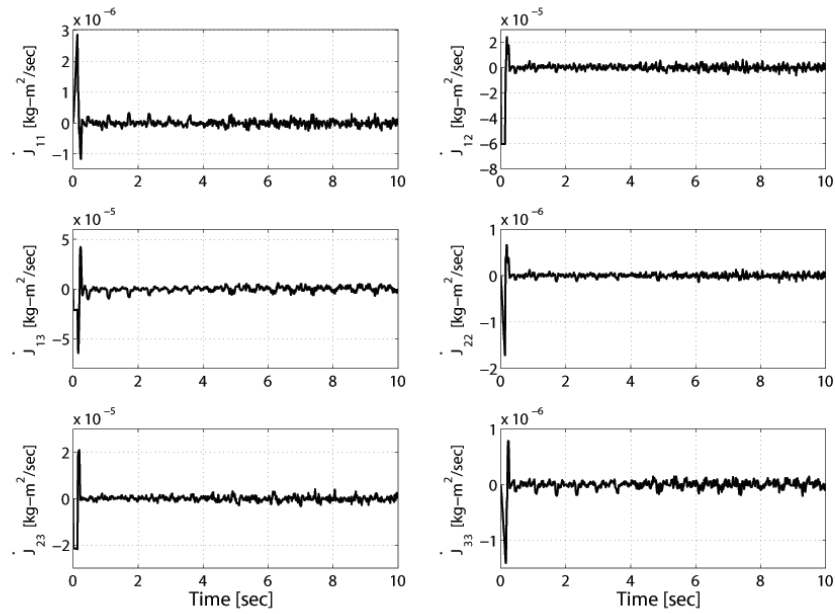


Figure 3-3. Time variation of the inertia matrix (i.e., $\dot{J}(\delta)$) during closed-loop operation.

CHAPTER 4
ASYMPTOTIC TRACKING FOR AIRCRAFT VIA AN UNCERTAIN DYNAMIC
INVERSION METHOD

4.1 Introduction

The contribution in this chapter is the use of a robust control approach (coined RISE control in [53]) to achieve asymptotic tracking control of a model reference system, where the plant dynamics contain a bounded additive disturbance (e.g., potential disturbances include: gravity, inertial coupling, nonlinear gust modeling, etc.). The RISE-based control structure has been used for a variety of fully actuated systems in [52–60]. The result in this chapter represents the first ever application of the RISE method where the controller is multiplied by a non-square matrix containing parametric uncertainty. To achieve the result, the typical RISE control structure is modified by adding a robust control term, which is designed to compensate for the uncertainty in the input matrix. The result is proven via Lyapunov-based stability analysis and demonstrated through numerical simulation.

4.2 Aircraft Model and Properties

The aircraft system under consideration in this chapter can be modeled via the following state space representation [25, 29, 34, 71, 72]:

$$\dot{x} = Ax + Bu + f(x) \tag{4-1}$$

$$y = Cx, \tag{4-2}$$

where $A \in \mathbb{R}^{n \times n}$ denotes the state matrix, $B \in \mathbb{R}^{n \times m}$ for $m < n$ represents the input matrix, $C \in \mathbb{R}^{m \times n}$ is the known output matrix, $u \in \mathbb{R}^m$ is a vector of control inputs, and $f(x) \in \mathbb{R}^n$ represents an unknown, nonlinear disturbance.

Assumption 4-1: *The A and B matrices given in (4-1) contain parametric uncertainty.*

Property 4-1: The nonlinear disturbance term $f(x)$ and its time derivative can be expressed as:

$$f(x) = f_1(t) + f_2(x) \quad (4-3)$$

$$\dot{f}(x, \dot{x}) = \dot{f}_1(t) + \dot{f}_2(x, \dot{x}), \quad (4-4)$$

where the auxiliary functions $f_1(t), \dot{f}_1(t) \in \mathbb{R}^n$ and the second derivative $\ddot{f}_1(t) \in \mathbb{R}^n$ can be upper bounded as

$$\|f_1(t)\| \leq \zeta_1 \quad \|\dot{f}_1(t)\| \leq \zeta_2 \quad (4-5)$$

$$\|\ddot{f}_1(t)\| \leq \zeta_3, \quad (4-6)$$

where $\zeta_i \forall i = 1, 2, 3$ are known positive bounding constants, $f_2(x) \in \mathbb{R}^n$ is an unknown second-order differentiable function, and $\|\cdot\|$ denotes the standard Euclidean norm.

In this research, the equations of motion given in 4-1 will be utilized, where the state and input matrices are based on the dynamic parameters of the Osprey fixed wing aerial vehicle (see Figure 4-1). The Osprey is a commercially available, low-cost experimental flight testbed for investigating novel control approaches. Based on the



Figure 4-1. Photograph of the Osprey aircraft testbed.

standard assumption that the longitudinal and lateral modes of the aircraft are decoupled, the state space model for the Osprey aircraft testbed can be represented using (4-1) and

(4-2), where the state matrix $A \in \mathbb{R}^{8 \times 8}$ and input matrix $B \in \mathbb{R}^{8 \times 4}$ are given as

$$A = \begin{bmatrix} A_{lon} & 0_{4 \times 4} \\ 0_{4 \times 4} & A_{lat} \end{bmatrix} \quad B = \begin{bmatrix} B_{lon} & 0_{4 \times 2} \\ 0_{4 \times 2} & B_{lat} \end{bmatrix}, \quad (4-7)$$

and the output matrix $C \in \mathbb{R}^{4 \times 8}$ is designed as

$$C = \begin{bmatrix} C_{lon} & 0_{2 \times 4} \\ 0_{2 \times 4} & C_{lat} \end{bmatrix}, \quad (4-8)$$

where $A_{lon}, A_{lat} \in \mathbb{R}^{4 \times 4}$, $B_{lon}, B_{lat} \in \mathbb{R}^{4 \times 2}$, and $C_{lon}, C_{lat} \in \mathbb{R}^{2 \times 4}$ denote the state matrices, input matrices, and output matrices, respectively, for the longitudinal and lateral subsystems, and the notation $0_{i \times j}$ denotes an $i \times j$ matrix of zeros. The state vector $x(t) \in \mathbb{R}^8$ is given as

$$x = \begin{bmatrix} x_{lon}^T & x_{lat}^T \end{bmatrix}^T, \quad (4-9)$$

where $x_{lon}(t), x_{lat}(t) \in \mathbb{R}^4$ denote the longitudinal and lateral state vectors defined as

$$x_{lon} \triangleq \begin{bmatrix} V & \alpha & q & \theta \end{bmatrix}^T \quad (4-10)$$

$$x_{lat} \triangleq \begin{bmatrix} \beta & p & r & \phi \end{bmatrix}^T, \quad (4-11)$$

where the state variables are defined as

$V = velocity$ $\alpha = angle\ of\ attack$

$q = pitch\ rate$ $\theta = pitch\ angle$

$\beta = sideslip\ angle$ $p = roll\ rate$

$r = yaw\ rate$ $\phi = bank\ angle$

and the control input vector is defined as

$$u \triangleq \begin{bmatrix} u_{lon}^T & u_{lat}^T \end{bmatrix}^T = \begin{bmatrix} \delta_{elev} & \delta_{thrust} & \delta_{ail} & \delta_{rud} \end{bmatrix}^T. \quad (4-12)$$

In (4-12), $\delta_{elev} \in \mathbb{R}$ denotes the elevator deflection angle, $\delta_{thrust} \in \mathbb{R}$ is the control thrust, $\delta_{ail} \in \mathbb{R}$ is the aileron deflection angle, and $\delta_{rud} \in \mathbb{R}$ is the rudder deflection angle.

The disturbance $f(x)$ introduced in (4-1) can represent several bounded nonlinearities. The more promising example of disturbances that can be represented by $f(x)$ is the nonlinear form of a selectively extracted portion of the state space matrix $A_{lon} \in \mathbb{R}^{4 \times 4}$ that would normally be linearized. This nonlinearity would then be added to the new state space plant by superposition, resulting in the following quasi-linear plant model:

$$\dot{x}_{lon} = A'_{lon}x_{lon} + B_{lon}u_{lon} + f(x_{lon}), \quad (4-13)$$

where $A'_{lon} \in \mathbb{R}^{4 \times 4}$ is the state space matrix A_{lon} with the linearized portion removed, and $f(x_{lon}) \in \mathbb{R}^4$ denotes the nonlinear disturbances present in the longitudinal dynamics. Some physical examples of this would be the selective nonlinearities that cannot be ignored, such as when dealing with supermaneuvering vehicles, where post-stall angles of attack and inertia coupling, for example, are encountered. Given that the Osprey is essentially a very benign maneuvering vehicle, $f(x)$ in this dissertation will represent less rigorous nonlinearities for illustrative purposes. A similar technique can be followed with the lateral direction state space representation, where the nonlinear part of A_{lat} is extracted, and a new quasi-linear model for the lateral dynamics is developed as

$$\dot{x}_{lat} = A'_{lat}x_{lat} + B_{lat}u_{lat} + f(x_{lat}), \quad (4-14)$$

where $A'_{lat} \in \mathbb{R}^{4 \times 4}$ is the new lateral state matrix with the linearized components removed, and $f(x_{lat}) \in \mathbb{R}^4$ denotes the nonlinear disturbances present in the lateral dynamics. Another example of bounded nonlinear disturbances, which can be represented by $f(x)$ in (4-1), is a discrete vertical gust. The formula given in [73], for example, defines such a

bounded nonlinearity in the longitudinal axis as

$$f(x_{lon}) = \begin{bmatrix} -11.1 \\ 7.2 \\ 37.4 \\ 0 \end{bmatrix} \frac{1}{V_0} \left\{ \frac{U_{ds}}{2} \left[1 - \cos\left(\frac{\pi s}{H}\right) \right] \right\}, \quad (4-15)$$

where H denotes the distance (between 35 feet and 350 feet) along the airplane's flight path for the gust to reach its peak velocity, V_0 is the forward velocity of the aircraft when it enters the gust, $s \in [0, 2H]$ represents the distance penetrated into the gust (e.g., $s = \int_{t_1}^{t_2} V(t) dt$), and U_{ds} is the design gust velocity as specified in [73]. This regulation is intended to be used to evaluate both vertical and lateral gust loads, so a similar representation can be developed for the lateral dynamics. Another source of bounded nonlinear disturbances that could be represented by $f(x)$ is transport delay from communication with a ground station.

4.3 Control Development

To facilitate the subsequent control design, a reference model can be developed as:

$$\dot{x}_m = A_m x_m + B_m \delta \quad (4-16)$$

$$y_m = C x_m, \quad (4-17)$$

with $A_m \in \mathbb{R}^{n \times n}$ and $B_m \in \mathbb{R}^{n \times m}$ designed as

$$A_m = \begin{bmatrix} A_{lonm} & 0_{4 \times 4} \\ 0_{4 \times 4} & A_{latm} \end{bmatrix} \quad B_m = \begin{bmatrix} B_{lonm} & 0_{4 \times 2} \\ 0_{4 \times 2} & B_{latm} \end{bmatrix}, \quad (4-18)$$

where A_m is Hurwitz, $\delta(t) \in \mathbb{R}^m$ is the reference input, $x_m \triangleq \begin{bmatrix} x_{lonm}^T & x_{latm}^T \end{bmatrix}^T \in \mathbb{R}^n$ represents the reference states, $y_m \in \mathbb{R}^m$ are the reference outputs, and C was defined in (4-2). The lateral and longitudinal reference models were chosen with the specific purpose of decoupling the longitudinal mode velocity and pitch rate as well as decoupling the

lateral mode roll rate and yaw rate. In addition to this criterion, the design is intended to exhibit favorable transient response characteristics and to achieve zero steady-state error. Simultaneous and uncorrelated commands are input into each of the longitudinal and lateral model simulations to illustrate that each model indeed behaves as two completely decoupled second order systems.

The control objective is to ensure that the system tracks a desired reference trajectory despite unknown, nonlinear, non-LP disturbances in the dynamic model. To quantify this objective, a tracking error, denoted by $e(t) \in \mathbb{R}^m$, is defined as

$$e = y - y_m = C(x - x_m). \quad (4-19)$$

To facilitate the subsequent analysis, a filtered tracking error [74], denoted by $r(t) \in \mathbb{R}^m$, is defined as:

$$r \triangleq \dot{e} + \alpha e, \quad (4-20)$$

where $\alpha \in \mathbb{R}^{m \times m}$ denotes a matrix of positive, constant control gains.

4.3.1 Open-loop Error System

The open-loop tracking error dynamics can be developed by taking the time derivative of (4-20) and utilizing the expressions in (4-1), (4-2), (4-16), and (4-17) to obtain the following expression:

$$\dot{r} = \tilde{N} + N_d + C\tilde{A}(\dot{e} + \alpha e) + C\tilde{B}(\dot{u} + \alpha u) + C\hat{B}(\dot{u} + \alpha u) - e, \quad (4-21)$$

where the auxiliary function $\tilde{N}(x, \dot{x}, e, \dot{e}) \in \mathbb{R}^m$ is defined as

$$\tilde{N} \triangleq C\hat{A}\dot{e} + C\left(\dot{f}_2(x) - \dot{f}_2(x_m)\right) + \alpha CAe + \alpha C(f_2(x) - f_2(x_m)) + e, \quad (4-22)$$

the auxiliary function $N_d(x_m, \dot{x}_m, \delta, \dot{\delta})$ is defined as

$$\begin{aligned} N_d = & -CA_m\dot{x}_m - CB_m\dot{\delta} + C\hat{A}\dot{x}_m - \alpha CA_mx_m - \alpha CB_m\delta + \alpha C\hat{A}x_m \\ & + Cf_1 + \alpha Cf_1 + Cf_2(x_m) + \alpha Cf_2(x_m), \end{aligned} \quad (4-23)$$

$\hat{A} \in \mathbb{R}^{n \times n}$ and $\hat{B} \in \mathbb{R}^{n \times m}$ are subsequently designed adaptive estimates for the matrices A and B , and the estimate mismatch terms, denoted by $\tilde{A} \in \mathbb{R}^{n \times n}$ and $\tilde{B} \in \mathbb{R}^{n \times m}$, are defined as

$$\tilde{A} \triangleq A - \hat{A} \quad \tilde{B} \triangleq B - \hat{B}. \quad (4-24)$$

To simplify the notation in the subsequent development, the constant, unknown matrix $\Omega \in \mathbb{R}^{m \times m}$ is defined as

$$\Omega \triangleq CB, \quad (4-25)$$

and the estimate and estimate mismatch for Ω are defined as

$$\hat{\Omega} \triangleq C\hat{B} \quad \tilde{\Omega} \triangleq C\tilde{B}, \quad (4-26)$$

respectively. The quantities $\tilde{N}(x, \dot{x}, e, \dot{e})$ and $N_d(x_m, \dot{x}_m, \delta, \dot{\delta})$ and the derivative $\dot{N}_d(x_m, \dot{x}_m, \ddot{x}_m, \delta, \dot{\delta}, \ddot{\delta})$ can be upper bounded as follows:

$$\|\tilde{N}\| \leq \rho(\|z\|) \|z\| \quad (4-27)$$

$$\|N_d\| \leq \zeta_{N_d} \quad \|\dot{N}_d\| \leq \zeta_{\dot{N}_d}, \quad (4-28)$$

where $z \in \mathbb{R}^{2m}$ is defined as

$$z \triangleq \begin{bmatrix} e^T & r^T \end{bmatrix}^T, \quad (4-29)$$

$\zeta_{N_d}, \zeta_{\dot{N}_d} \in \mathbb{R}$ are known positive bounding constants, and the function $\rho(\|z\|)$ is a positive, globally invertible, nondecreasing function. Based on the expression in (4-21) and the subsequent stability analysis, the control input is designed as

$$\begin{aligned} u = & -\alpha \int_0^t u(\tau) d\tau - (k_s + 1) \hat{\Omega}^{-1} e(t) + (k_s + 1) \hat{\Omega}^{-1} e(0) - \int_0^t k_\gamma \hat{\Omega}^{-1} \text{sgn}(r(\tau)) d\tau \\ & - \hat{\Omega}^{-1} \int_0^t [(k_s + 1) \alpha e(\tau) + \beta \text{sgn}(e(\tau))] d\tau, \end{aligned} \quad (4-30)$$

where $\beta, k_s, k_\gamma \in \mathbb{R}^{m \times m}$ are diagonal matrices of positive, constant control gains, α was defined in (4-20), and the constant feedforward estimate $\hat{\Omega} \in \mathbb{R}^{m \times m}$ is defined as

$$\hat{\Omega} \triangleq C\hat{B}. \quad (4-31)$$

To simplify the notation in the subsequent stability analysis, the constant auxiliary matrix $\tilde{\Omega} \in \mathbb{R}^{m \times m}$ is defined as

$$\tilde{\Omega} \triangleq \Omega\hat{\Omega}^{-1}, \quad (4-32)$$

where $\tilde{\Omega}$ can be separated into diagonal and off-diagonal components as

$$\tilde{\Omega} = \Lambda + \Delta, \quad (4-33)$$

where $\Lambda \in \mathbb{R}^{m \times m}$ contains only the diagonal elements of $\tilde{\Omega}$, and $\Delta \in \mathbb{R}^{m \times m}$ contains the off-diagonal elements.

4.3.2 Closed-loop Error System

After substituting the time derivative of (4-30) into (4-21), the following closed-loop error system is obtained:

$$\dot{r} = \tilde{N} + N_d - (k_s + 1)\tilde{\Omega}r - k_\gamma\tilde{\Omega}sgn(r) - \tilde{\Omega}\beta sgn(e(t)) - e. \quad (4-34)$$

Assumption 4-2: *The constant estimate $\hat{\Omega}$ given in (4-31) is selected such that the following condition is satisfied:*

$$\lambda_{\min}(\Lambda) - \sqrt{m}\|\Delta\| > \varepsilon, \quad (4-35)$$

where $\varepsilon \in R$ is a known positive constant, and $\lambda_{\min}(\cdot)$ denotes the minimum eigenvalue of the argument.

Remark 4-1: *Preliminary testing results show that Assumption 2 is mild in the sense that (4-35) is satisfied for a wide range of $\hat{\Omega} \neq \Omega$.*

Remark 4-2: *A possible deficit of this control design is that the acceleration-dependent term r appears in the control input given in (4-30). This is undesirable*

from a controls standpoint; however many aircraft controllers are designed based on the assumption that acceleration measurements are available [75–79]. Further, from (4-30), the sign of the acceleration is all that is required for measurement in this control design.

4.4 Stability Analysis

Theorem 4-1: *The controller given in (4-30) ensures that all system signals are bounded during closed-loop operation and that the position tracking error is regulated in the sense that*

$$\|e(t)\| \rightarrow 0 \quad \text{as } t \rightarrow \infty, \quad (4-36)$$

provided the control gain k_s introduced in (4-30) is selected sufficiently large (see the subsequent stability proof), and β and k_γ are selected according to the following sufficient conditions:

$$\beta > \frac{(\zeta_{N_d} + \frac{1}{\alpha}\zeta_{\dot{N}_d})}{\lambda_{\min}(\Lambda)} \quad (4-37)$$

$$k_\gamma > \frac{\sqrt{m}\beta \|\Delta\|}{\varepsilon}, \quad (4-38)$$

where ζ_{N_d} and $\zeta_{\dot{N}_d}$ were introduced in (4-28), ε was defined in (4-35), and Λ and Δ were introduced in (4-33).

Before proving Theorem 4-1, the following lemma will be set forth.

Lemma 4-1: *To facilitate the subsequent stability analysis, the auxiliary function $P(t) \in R$ is defined as*

$$P(t) \triangleq \beta \|e(0)\| \|\Lambda\| - e(0)^T N_d(0) + \sqrt{m} \int_0^t \beta \|\Delta\| \|r(\tau)\| d\tau - \int_0^t L(\tau) d\tau, \quad (4-39)$$

where the auxiliary function $L(t) \in R$ is defined as

$$L(t) \triangleq r^T \left(N_d(t) - \beta \tilde{\Omega} \text{sgn}(e) \right). \quad (4-40)$$

Provided the sufficient condition in (4-37) is satisfied, the following inequality can be obtained¹⁰ :

$$\int_0^t L(\tau) d\tau \leq \beta \|e(0)\| \|\Lambda\| - e(0)^T N_d(0) + \sqrt{m} \int_0^t \beta \|\Delta\| \|r(\tau)\| d\tau. \quad (4-41)$$

Hence, (4-41) can be used to conclude that $P(t) \geq 0$.

Proof: (See Theorem 4-1) Let $\mathcal{D} \subset \mathbb{R}^{2m+1}$ be a domain containing $y(t) = 0$, where $y(t) \in \mathbb{R}^{2m+1}$ is defined as

$$y(t) \triangleq \begin{bmatrix} z^T & \sqrt{P(t)} \end{bmatrix}^T. \quad (4-42)$$

Let $V(y, t) : \mathcal{D} \times [0, \infty) \rightarrow \mathbb{R}$ be a continuously differentiable, positive definite function defined as

$$V \triangleq \frac{1}{2} e^T e + \frac{1}{2} r^T r + P, \quad (4-43)$$

where $V(y, t)$ satisfies the inequality

$$U_1(y) \leq V(y, t) \leq U_2(y), \quad (4-44)$$

provided the sufficient condition introduced in (4-37) is satisfied. In (4-44), the continuous, positive definite functions $U_1(y), U_2(y) \in \mathbb{R}$ are defined as

$$U_1 \triangleq \frac{1}{2} \|y\|^2 \quad U_2 \triangleq \|y\|^2. \quad (4-45)$$

After taking the derivative of (4-43) and utilizing (4-20), (4-33), (4-34), (4-39), and (4-40), $\dot{V}(y, t)$ can be expressed as

$$\begin{aligned} \dot{V}(y, t) = & -\alpha e^T e + r^T \tilde{N} - (k_s + 1) r^T \Lambda r - (k_s + 1) r^T \Delta r + \sqrt{m} \beta \|r\| \|\Delta\| \\ & - k_\gamma r^T \Delta \text{sgn}(r) - k_\gamma r^T \Lambda \text{sgn}(r). \end{aligned} \quad (4-46)$$

¹⁰ See Appendix for the details on the bound of $\int_0^t L(\tau) d\tau$.

By utilizing (4-27), $\dot{V}(y, t)$ can be upper bounded as

$$\dot{V}(y, t) \leq -\alpha e^T e - \varepsilon \|r\|^2 - k_s \varepsilon \|r\|^2 + \rho(\|z\|) \|r\| \|z\| + [-k_\gamma \varepsilon + \sqrt{m} \beta \|\Delta\|] \|r\|, \quad (4-47)$$

Clearly, if (4-38) is satisfied, the bracketed term in (4-47) is negative, and $\dot{V}(y, t)$ can be upper bounded using the squares of the components of $z(t)$ as follows:

$$\dot{V}(y, t) \leq -\alpha \|e\|^2 - \varepsilon \|r\|^2 + [\rho(\|z\|) \|r\| \|z\| - k_s \varepsilon \|r\|^2], \quad (4-48)$$

Completing the squares for the bracketed terms in (4-48) yields

$$\dot{V}(y, t) \leq -\eta_3 \|z\|^2 + \frac{\rho^2(\|z\|) \|z\|^2}{4k_s \varepsilon}, \quad (4-49)$$

where $\eta_3 \triangleq \min\{\alpha, \varepsilon\}$, and $\rho(\|z\|)$ is introduced in (4-27). The following expression can be obtained from (4-49):

$$\dot{V}(y, t) \leq -U(y), \quad (4-50)$$

where $U(y) = c \|z\|^2$, for some positive constant $c \in \mathbb{R}$, is a continuous, positive semi-definite function that is defined on the following domain:

$$\mathcal{D} \triangleq \left\{ y \in \mathbb{R}^{2m+1} \mid \|y\| < \rho^{-1} \left(2\sqrt{\varepsilon \eta_3 k_s} \right) \right\}. \quad (4-51)$$

The inequalities in (4-44) and (4-50) can be used to show that $V(t) \in \mathcal{L}_\infty$ in \mathcal{D} ; hence $e(t), r(t) \in \mathcal{L}_\infty$ in \mathcal{D} . Given that $e(t), r(t) \in \mathcal{L}_\infty$ in \mathcal{D} , standard linear analysis methods can be used to prove that $\dot{e}(t) \in \mathcal{L}_\infty$ in \mathcal{D} from (4-20). Since $e(t), \dot{e}(t) \in \mathcal{L}_\infty$ in \mathcal{D} , (4-19) can be used along with the assumption that $y_m, \dot{y}_m \in \mathcal{L}_\infty$ in \mathcal{D} to prove that $y(t), \dot{y}(t) \in \mathcal{L}_\infty$. Given that $r(t) \in \mathcal{L}_\infty$ in \mathcal{D} , the assumption that $\hat{\Omega}^{-1} \in \mathcal{L}_\infty$ in \mathcal{D} can be used along with time derivative of (4-30) to show that $\dot{u}(t) \in \mathcal{L}_\infty$ in \mathcal{D} . Further, Equation 2.78 of [80] can be used to show that $\dot{u}(t)$ can be upper bounded as $\dot{u}(t) \leq -\alpha u(\tau) + M$, $\forall t \geq 0$, where $M \in \mathbb{R}^+$ is a bounding constant. Theorem 1.1 of [81] can then be utilized to prove that $u(t) \in \mathcal{L}_\infty$ in \mathcal{D} . Hence, (4-34) can be used to show that $\dot{r}(t) \in \mathcal{L}_\infty$ in \mathcal{D} . Since $\dot{e}(t), \dot{r}(t) \in \mathcal{L}_\infty$ in \mathcal{D} , the definitions for $U(y)$ and $z(t)$ can be used to prove that

$U(y)$ is uniformly continuous in \mathcal{D} . Let $S \subset \mathcal{D}$ denote a set defined as follows:

$$S \triangleq \left\{ y(t) \in \mathcal{D} \mid U_2(y(t)) < \frac{1}{2} \left(\rho^{-1} \left(2\sqrt{\varepsilon\eta_3 k_s} \right) \right)^2 \right\}. \quad (4-52)$$

Theorem 8.4 of [82] can now be invoked to state that

$$c \|z\|^2 \rightarrow 0 \quad \text{as} \quad t \rightarrow \infty \quad \forall y(0) \in S. \quad (4-53)$$

Based on the definition of z , (4-53) can be used to show that

$$\|e(t)\| \rightarrow 0 \quad \text{as} \quad t \rightarrow \infty \quad \forall y(0) \in S. \quad (4-54)$$

4.5 Simulation Results

A numerical simulation was created to test the efficacy of the proposed controller.

The simulation is based on the aircraft state space system given in (4-1) and (4-2), where the state matrix A , input authority matrix B , and nonlinear disturbance function $f(x)$ are given by the state space model for the Osprey aircraft given in (4-7)-(4-12). The reference model for the simulation is represented by the state space system given in (4-16)-(4-18), with state matrices A_{lonm} and A_{latm} , input matrices B_{lonm} and B_{latm} , and output matrices C_{lon} and C_{lat} selected as

$$A_{lonm} = \begin{bmatrix} 0.6 & -1.1 & 0 & 0 \\ 2.0 & -2.2 & 0 & 0 \\ 0 & 0 & -4.0 & -600.0 \\ 0 & 0 & 0.1 & -10 \end{bmatrix} \quad (4-55)$$

$$A_{latm} = \begin{bmatrix} -4.0 & -600.0 & 0 & 0 \\ 0.1 & -10.00 & 0 & 0 \\ 0 & 0 & 0.6 & -1.1 \\ 0 & 0 & 2.0 & -2.2 \end{bmatrix} \quad (4-56)$$

$$B_{lonm} = \begin{bmatrix} 0 & 0.5 \\ 0 & 0 \\ 10 & 0 \\ 0 & 0 \end{bmatrix} \quad B_{latm} = \begin{bmatrix} 10 & 0 \\ 0 & 0 \\ 0 & 0.5 \\ 0 & 0 \end{bmatrix}, \quad (4-57)$$

and

$$C_{lon} = \begin{bmatrix} 0 & 0 & 1 & 0 \\ 1 & 0 & 0 & 0 \end{bmatrix} \quad C_{lat} = \begin{bmatrix} 0 & 1 & 0 & 0 \\ 0 & 0 & 1 & 0 \end{bmatrix}. \quad (4-58)$$

The longitudinal and lateral dynamic models for the Osprey aircraft flying at 25 m/s at an altitude of 60 meters are represented using (4-13) and (4-14), where A'_{lon} , A'_{lat} , B_{lon} , and B_{lat} are given as

$$A'_{lon} = \begin{bmatrix} -0.15 & 11.08 & 0.08 & 0 \\ -0.03 & -7.17 & 0.83 & 0 \\ 0 & -37.35 & -9.96 & 0 \\ 0 & 0 & 1.00 & 0 \end{bmatrix} \quad (4-59)$$

$$A'_{lat} = \begin{bmatrix} -0.69 & -0.03 & -0.99 & 0 \\ -3.13 & -12.92 & 1.10 & 0 \\ 17.03 & -0.10 & -0.97 & 0 \\ 0 & 1.00 & -0.03 & 0 \end{bmatrix} \quad (4-60)$$

$$B_{lon} = \begin{bmatrix} 3E^{-3} & 0.06 \\ 1E^{-5} & 1E^{-4} \\ 0.98 & 0 \\ 0 & 0 \end{bmatrix} \quad B_{lat} = \begin{bmatrix} 0 & 0 \\ 1.50 & -0.02 \\ -0.09 & 0.17 \\ 0 & 0 \end{bmatrix}, \quad (4-61)$$

respectively. The nonlinear disturbance terms $f(x_{lon})$ and $f(x_{lat})$ introduced in (4-13) and (4-14), respectively, are defined as

$$f(x_{lon}) = \begin{bmatrix} -9.81 \sin \theta + g(x) & 0 & 0 & 0 \end{bmatrix}^T \quad (4-62)$$

$$f(x_{lat}) = \begin{bmatrix} 0.39 \sin \phi & 0 & 0 & 0 \end{bmatrix}^T, \quad (4-63)$$

where $g(x)$ represents a disturbance due to a discrete vertical wind gust as defined in (4-15), where $U_{ds} = 10.12 \text{ m/s}$, $H = 15.24 \text{ m}$, and $V_0 = 25 \text{ m/s}$ (cruise velocity). Figure 4-2 shows a plot of the wind gust used in the simulation. The remainder of the additive

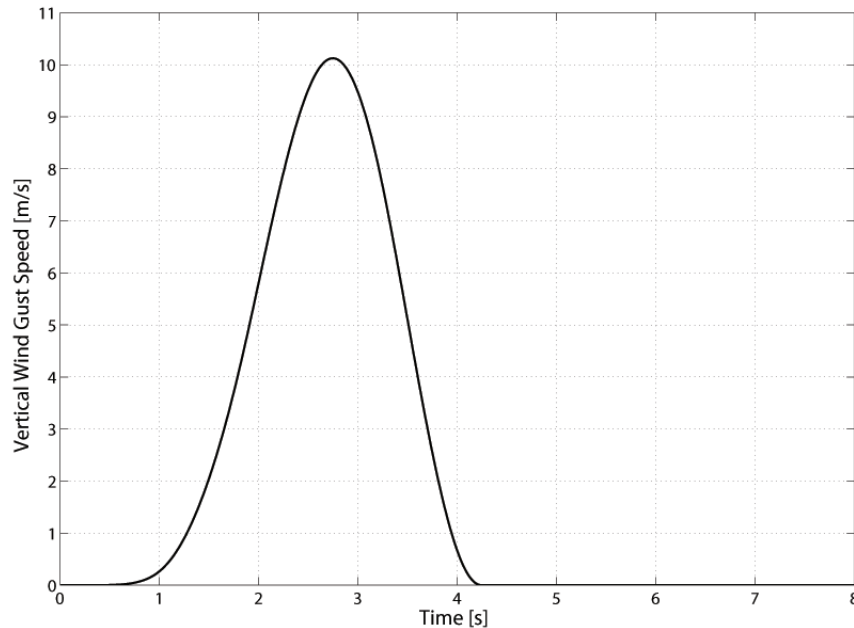


Figure 4-2. Plot of the discrete vertical (upward) wind gust used in the controller simulation.

disturbances in (4-62) and (4-63) represent nonlinearities not captured in the linearized state space model (e.g., due to small angle assumptions). All states and control inputs were initialized to zero for the simulation.

The feedforward estimates \hat{B}_{lon} and \hat{B}_{lat} were selected as

$$\hat{B}_{lon} = \begin{bmatrix} 0.01 & 0.1 \\ 0 & 0 \\ 1.4 & 0 \\ 0 & 0 \end{bmatrix} \quad \hat{B}_{lat} = \begin{bmatrix} 0 & 0 \\ 1.7 & -0.05 \\ -0.1 & 0.25 \\ 0 & 0 \end{bmatrix}. \quad (4-64)$$

Remark 4-3: For the choices for \hat{B}_{lon} and \hat{B}_{lat} given in (4-64), the inequality in (4-35) is satisfied. Specifically, the choice for \hat{B}_{lon} yields

$$\lambda_{\min}(\Lambda) = 0.6450 > 0.0046 = \|\Delta\|, \quad (4-65)$$

and the choice for \hat{B}_{lat} yields

$$\lambda_{\min}(\Lambda) = 0.6828 > 0.0842 = \|\Delta\|. \quad (4-66)$$

In order to develop a realistic stepping stone to an actual experimental demonstration of the proposed aircraft controller, the simulation parameters were selected based on detailed data analyses and specifications. The sensor noise values are based upon Cloud Cap Technology's Piccolo Autopilot and analysis of data logged during straight and level flight. These values are also corroborated with the specifications given for Cloud Cap Technology's Crista Inertial Measurement Unit (IMU). The thrust limit and estimated rate limit was measured via a static test using a fish scale. The control surface rate and position limits were determined via the geometry of the control surface linkages in conjunction with the detailed specifications sheet given with the Futaba S3010 standard ball bearing servo. The simulation parameters are summarized in the following table:

The objectives for the longitudinal controller simulation are to track pitch rate and forward velocity commands. Figures 4-3 and 4-4 show the simulation results of the closed-loop longitudinal system with control gains selected as follows (e.g., see (4-30) and

Table 4-1. Parameters used in the DI controller simulation.

Sampling Time	0.01 sec
Pitch Rate Sensor Noise	$\pm 1.7^\circ/\text{sec}$
Velocity Sensor Noise	$\pm 0.4 \frac{m}{\text{sec}}$
Roll Rate Sensor Noise	$\pm 1.7^\circ/\text{sec}$
Yaw Rate Sensor Noise	$\pm 1.7^\circ/\text{sec}$
Control Thrust Saturation Limit	$\pm 200 N$
Control Thrust Rate Limit	$\pm 200 \frac{N}{\text{sec}}$
Elevator Saturation Limit	$\pm 30^\circ$
Elevator Rate Limit	$\pm 300^\circ/\text{sec}$
Aileron Saturation Limit	$\pm 30^\circ$
Aileron Rate Limit	$\pm 300^\circ/\text{sec}$
Rudder Saturation Limit	$\pm 30^\circ$
Rudder Rate Limit	$\pm 300^\circ/\text{sec}$

(4-25))¹¹ :

$$\beta = \text{diag} \left\{ \begin{array}{cc} 0.1 & 130 \end{array} \right\} \quad k_s = \text{diag} \left\{ \begin{array}{cc} 0.2 & 160 \end{array} \right\}$$

$$\alpha = \text{diag} \left\{ \begin{array}{cc} 0.7 & 0.1 \end{array} \right\} \quad k_\gamma = 0.1 I_{2 \times 2},$$

where the notation $I_{j \times j}$ denotes the $j \times j$ identity matrix. Figure 4-3 shows the reference and actual pitch rates during closed-loop operation, and Figure 4-4 shows the reference and actual forward velocity responses.

For the lateral controller simulation, the objectives are to track roll rate and yaw rate commands. Figures 4-5 and 4-6 show the simulation results of the closed-loop lateral

¹¹ The k_γ used in the longitudinal controller simulation does not satisfy the sufficient condition given in (4-38); however, this condition is not necessary for stability, it is sufficient for the Lyapunov stability proof.

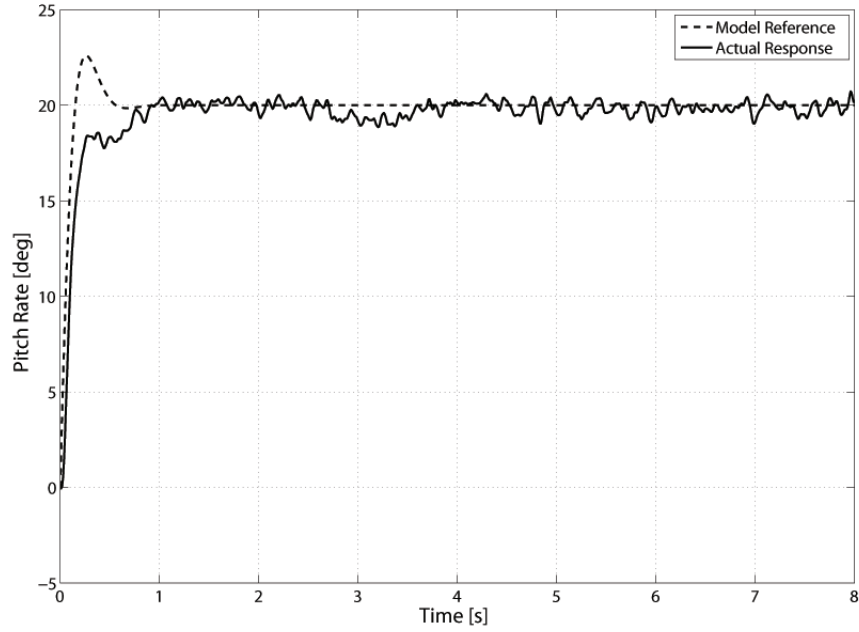


Figure 4-3. Pitch rate response achieved during closed-loop longitudinal controller operation.

system with control gains selected as follows:

$$\beta = \text{diag} \left\{ \begin{array}{cc} 0.2 & 0.6 \end{array} \right\} \quad k_s = \text{diag} \left\{ \begin{array}{cc} 0.2 & 3 \end{array} \right\}$$

$$\alpha = \text{diag} \left\{ \begin{array}{cc} 1.0 & 0.2 \end{array} \right\} \quad k_\gamma = I_{2 \times 2}.$$

Figure 4-5 shows the reference and actual roll rates during closed-loop operation, and Figure 4-6 shows the reference and actual yaw rates. The control actuation (relative to trim conditions) used during closed-loop operation for the robust controller is shown in Figure 4-7.

4.6 Conclusion

An aircraft controller is presented, which achieves asymptotic tracking control of a model reference system where the plant dynamics contain input uncertainty and a bounded non-LP disturbance. This result represents the first ever application of a continuous control strategy in a DI and MRAC framework to a nonlinear system with

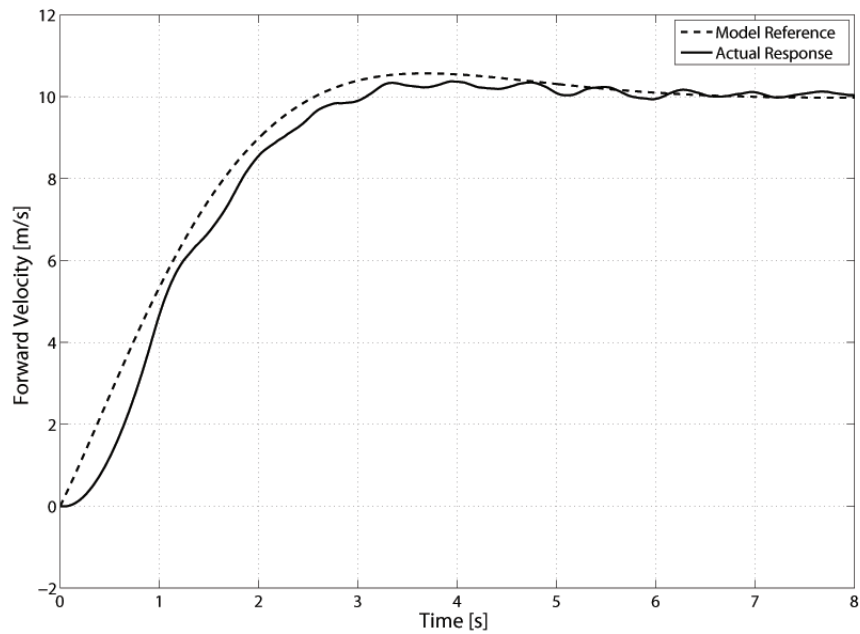


Figure 4-4. Forward velocity response achieved during closed-loop longitudinal controller operation.

additive, non-LP disturbances, where the control input is multiplied by a non-square matrix containing parametric uncertainty. To achieve the result, a novel robust control technique is combined with a RISE control structure. A Lyapunov-based stability analysis is provided to verify the theoretical result, and numerical simulation results are provided to demonstrate the efficacy of the proposed controller.

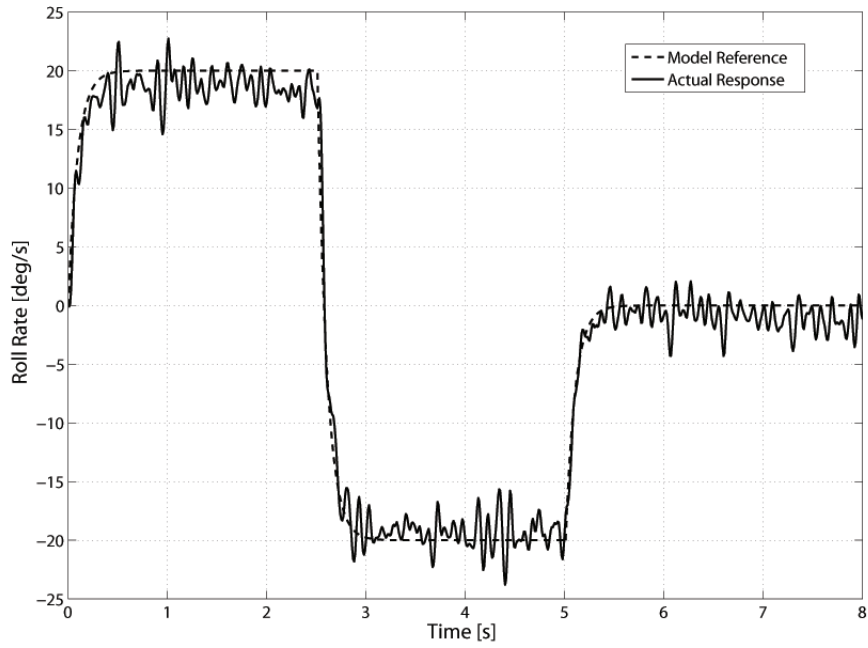


Figure 4-5. Roll rate response achieved during closed-loop lateral controller operation.

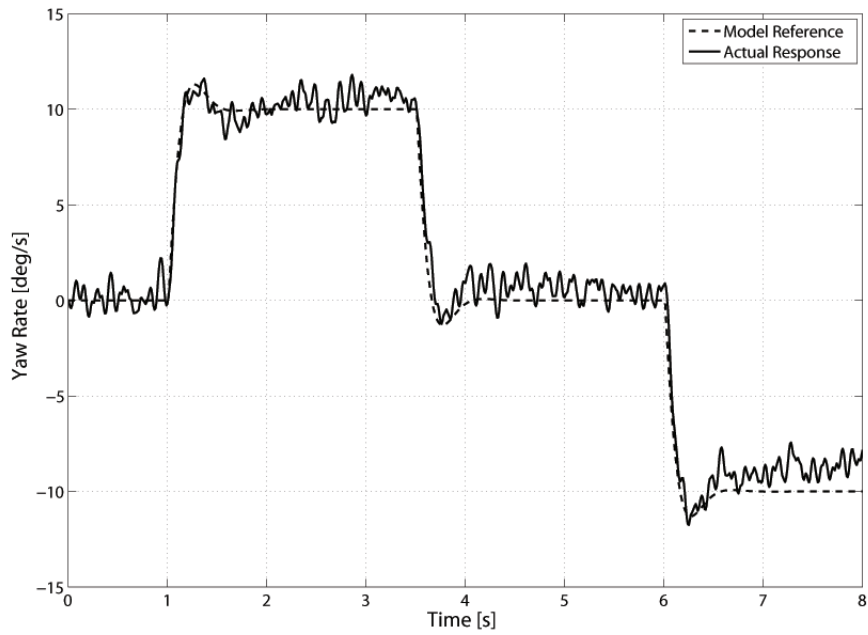


Figure 4-6. Yaw rate response achieved during closed-loop lateral controller operation.

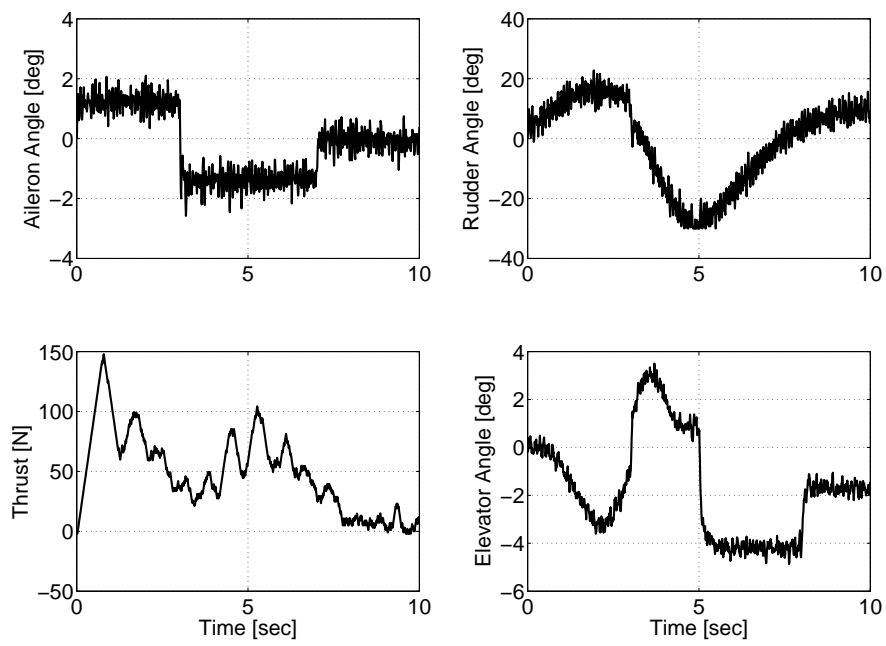


Figure 4-7. Control actuation away from trim used during closed-loop robust dynamic inversion controller operation for the lateral subsystem (top) and the longitudinal subsystem (bottom)

CHAPTER 5
ADAPTIVE DYNAMIC INVERSION FOR ASYMPTOTIC TRACKING OF AN
AIRCRAFT REFERENCE MODEL

5.1 Introduction

Adaptive dynamic inversion (ADI) is a promising area of controls research (e.g., see [27, 29, 30, 33]). Specific difficulties exist, however, in designing ADI controllers for systems containing uncertainty in the input matrix. While robust control methods are often utilized to compensate for the inversion error in such cases [35–38], the required control effort can be large due to the high gain or high frequency feedback typically required in the robust control design. Motivated by the desire to develop an adaptive method as opposed to robust, neural network (NN)-based controllers have been typically used to compensate for unstructured uncertainty (e.g., see [61]). One drawback of NN-based control is that asymptotic stability is difficult to prove due to the inherent functional reconstruction error. A contribution in this chapter is the use of a new robust control technique in conjunction with an adaptive control law to achieve an asymptotic tracking result in the presence of parametric uncertainty in the input and state matrices and an additive, nonvanishing nonlinear disturbance. An asymptotic tracking result is proven via a Lyapunov stability analysis, and a high fidelity numerical simulation is provided to show the performance of the proposed control design.

5.2 Aircraft Model

The development in this chapter is based on the following state-space representation of an aircraft [25, 29, 34, 71, 72]:

$$\dot{x} = Ax + Bu + f(x, t) \tag{5-1}$$

$$y = Cx. \tag{5-2}$$

In (5-1) and (5-2), $A \in \mathbb{R}^{n \times n}$ denotes a state matrix composed of unknown constant elements, $B \in \mathbb{R}^{n \times m}$ denotes an input matrix composed of uncertain constant elements with $m < n$, $C \in \mathbb{R}^{m \times n}$ denotes a known output matrix, $x(t) \in \mathbb{R}^n$ denotes the state

vector, $u(t) \in \mathbb{R}^m$ denotes a vector of control inputs, and $f(x, t) \in \mathbb{R}^n$ represents a state- and time-dependent unknown, nonlinear disturbance.

Assumption 5-1: *The nonlinear disturbance $f(x, t)$ and its first two time derivatives are assumed to exist and be bounded. The disturbance $f(x, t)$ introduced in (5-1) can represent several bounded nonlinearities (e.g., errors due to linearization, inertial coupling, discrete vertical gusts, etc.). For a detailed discussion of nonlinearities that can be represented by $f(x, t)$ see [35].*

Assumption 5-2: *For some given output matrix, the matrix product CB is invertible for all elements of B contained within some bounded region.*

While the model in (5-1) and (5-2) is generic to a broad class of aircraft, this section describes how a specific aircraft can be related to (5-1). Based on the standard assumption that the longitudinal and lateral modes of the aircraft are decoupled, the state-space model for the commercially available Osprey fixed wing aerial vehicle (see Figure 4-1) can be represented using (5-1) and (5-2), where the state matrix $A \in \mathbb{R}^{8 \times 8}$ and input matrix $B \in \mathbb{R}^{8 \times 4}$ are given as

$$A = \begin{bmatrix} A_{lon} & 0_{4 \times 4} \\ 0_{4 \times 4} & A_{lat} \end{bmatrix} \quad B = \begin{bmatrix} B_{lon} & 0_{4 \times 2} \\ 0_{4 \times 2} & B_{lat} \end{bmatrix}, \quad (5-3)$$

and the output matrix $C \in \mathbb{R}^{4 \times 8}$ is designed as

$$C = \begin{bmatrix} C_{lon} & 0_{2 \times 4} \\ 0_{2 \times 4} & C_{lat} \end{bmatrix}. \quad (5-4)$$

In (5-3) and (5-4), $A_{lon}, A_{lat} \in \mathbb{R}^{4 \times 4}$, $B_{lon}, B_{lat} \in \mathbb{R}^{4 \times 2}$, and $C_{lon}, C_{lat} \in \mathbb{R}^{2 \times 4}$ denote the state matrices, input matrices, and output matrices, respectively, for the longitudinal and lateral subsystems, and the notation $0_{i \times j}$ denotes an $i \times j$ matrix of zeros. The Osprey state-vector $x(t) \in \mathbb{R}^8$ is given as

$$x = \begin{bmatrix} x_{lon}^T & x_{lat}^T \end{bmatrix}^T, \quad (5-5)$$

where $x_{lon}(t), x_{lat}(t) \in \mathbb{R}^4$ denote the longitudinal and lateral state vectors defined as

$$x_{lon} \triangleq \begin{bmatrix} V & \alpha & q & \theta \end{bmatrix}^T \quad (5-6)$$

$$x_{lat} \triangleq \begin{bmatrix} \beta & p & r & \phi \end{bmatrix}^T, \quad (5-7)$$

where the components of the state are defined as

$$V = \text{velocity} \quad \alpha = \text{angle of attack}$$

$$q = \text{pitch rate} \quad \theta = \text{pitch angle}$$

$$\beta = \text{sideslip angle} \quad p = \text{roll rate}$$

$$r = \text{yaw rate} \quad \phi = \text{bank angle}$$

and the control input vector is defined as

$$u \triangleq \begin{bmatrix} u_{lon}^T & u_{lat}^T \end{bmatrix}^T = \begin{bmatrix} \delta_{elev} & \delta_{thrust} & \delta_{ail} & \delta_{rud} \end{bmatrix}^T. \quad (5-8)$$

In (5-8), $\delta_{elev}(t) \in \mathbb{R}$ denotes the elevator deflection angle, $\delta_{thrust}(t) \in \mathbb{R}$ is the control thrust, $\delta_{ail}(t) \in \mathbb{R}$ is the aileron deflection angle, and $\delta_{rud}(t) \in \mathbb{R}$ is the rudder deflection angle.

5.3 Control Development

To facilitate the subsequent control design, a reference model is developed as

$$\dot{x}_m = A_m x_m + B_m \delta \quad (5-9)$$

$$y_m = C x_m, \quad (5-10)$$

with $A_m \in \mathbb{R}^{n \times n}$ and $B_m \in \mathbb{R}^{n \times m}$ designed as

$$A_m = \begin{bmatrix} A_{lonm} & 0_{q \times q} \\ 0_{q \times q} & A_{latm} \end{bmatrix} \quad B_m = \begin{bmatrix} B_{lonm} & 0_{q \times p} \\ 0_{q \times p} & B_{latm} \end{bmatrix}, \quad (5-11)$$

where A_m is Hurwitz, $\delta(t) \in \mathbb{R}^m$ is the reference input, $x_m(t) \in \mathbb{R}^n$ is the reference state, defined as

$$x_m(t) \triangleq \begin{bmatrix} x_{lonm}^T(t) & x_{latm}^T(t) \end{bmatrix}^T, \quad (5-12)$$

$y_m \in \mathbb{R}^m$ are the reference outputs, and C was defined in (5-2). Also in (5-11), $A_{lonm}, A_{latm} \in \mathbb{R}^{q \times q}$, $B_{lonm}, B_{latm} \in \mathbb{R}^{q \times p}$ denote the state matrices and input matrices, respectively, for the longitudinal and lateral subsystems¹². The lateral and longitudinal reference models were chosen with the specific purpose of decoupling the longitudinal velocity and pitch rate as well as decoupling the lateral roll rate and yaw rate. In addition to this criterion, the design is intended to exhibit favorable transient response characteristics and to achieve zero steady-state error. Simultaneous and uncorrelated commands are input into each of the longitudinal and lateral model simulations to illustrate that each model indeed behaves as two completely decoupled second order systems.

The control objective is to ensure that the aircraft output states track a desired time-varying reference trajectory despite parametric uncertainty and unknown, nonlinear, non-LP disturbances in the dynamic model. To quantify this objective, a tracking error, denoted by $e(t) \in \mathbb{R}^m$, is defined as

$$e \triangleq y - y_m = C(x - x_m). \quad (5-13)$$

To facilitate the subsequent analysis, a filtered tracking error [74], denoted by $r(t) \in \mathbb{R}^m$, is defined as

$$r \triangleq \dot{e} + \alpha e, \quad (5-14)$$

¹² The dimensions of reference model subsystem matrices A_{lonm} , A_{latm} , B_{lonm} , and B_{latm} will match those of the plant model. Thus, if the Osprey model is used as the plant, $q = 4$, and $p = 2$ (see (5-3) and (5-4)).

where $\alpha \in \mathbb{R}$ is a positive, constant control gain. The subsequent development is based on the assumption that $y(t)$ and $\dot{y}(t)$ are measurable, and hence, $e(t)$, $\dot{e}(t)$, and $r(t)$ are measurable [75–79].

The open-loop tracking error dynamics can be developed by taking the time derivative of (5–14) and utilizing the expressions in (5–1), (5–2), (5–9), and (5–10) to obtain

$$\dot{r} = \tilde{N} + N_d + Y_B \tilde{\theta}_B + C \hat{B} (\dot{u} + \alpha u) - e. \quad (5-15)$$

In (5–15), the auxiliary functions $\tilde{N}(x, \dot{x}, e, x_m, \dot{x}_m, t) \in \mathbb{R}^m$ and $N_d(x_m, \dot{x}_m, \delta, \dot{\delta}, t) \in \mathbb{R}^m$ are defined as

$$\begin{aligned} \tilde{N} \triangleq & C \left(\dot{f}(x, \dot{x}, t) - \dot{f}(x_m, \dot{x}_m, t) \right) + \alpha C (f(x, t) - f(x_m, t)) + e \\ & + CA((\dot{x} + \alpha x) - (\dot{x}_m + \alpha x_m)), \end{aligned} \quad (5-16)$$

and

$$N_d \triangleq -C(A_m - A)(\dot{x}_m + \alpha x_m) - CB_m(\dot{\delta} + \alpha \delta) + C(\dot{f}(x_m, \dot{x}_m, t) + \alpha f(x_m, t)). \quad (5-17)$$

Motivation for the selective grouping of the terms in (5–16) and (5–17) is derived from the fact that the following inequalities can be developed [52, 53]:

$$\|\tilde{N}\| \leq \rho(\|z\|) \|z\| \quad (5-18)$$

$$\|N_d\| \leq \zeta_{N_d} \quad \|\dot{N}_d\| \leq \zeta_{\dot{N}_d}, \quad (5-19)$$

where $z(t) \in \mathbb{R}^{2m}$ is defined as

$$z \triangleq \begin{bmatrix} e^T & r^T \end{bmatrix}^T, \quad (5-20)$$

$\zeta_{N_d}, \zeta_{\dot{N}_d} \in \mathbb{R}$ are known positive bounding constants, and $\rho(\cdot) \in \mathbb{R}$ is a positive, globally invertible, nondecreasing function. Also in (5–15), $Y_B(u, \dot{u}) \in \mathbb{R}^{m \times p_1}$ denotes a measurable regression matrix, and $\theta_B \in \mathbb{R}^{p_1}$ is a vector containing the unknown parameters of the B

matrix, defined as

$$Y_B \theta_B \triangleq CB(\dot{u} + \alpha u). \quad (5-21)$$

In (5-15) and the subsequent stability analysis, $\tilde{\theta}_B(t) \in \mathbb{R}^{p_1}$ denotes the parameter estimation error defined as

$$\tilde{\theta}_B \triangleq \theta_B - \hat{\theta}_B, \quad (5-22)$$

where $\hat{\theta}_B(t) \in \mathbb{R}^{p_1}$ denotes a subsequently designed parameter estimate vector. The estimate matrix $\hat{B}(t) \in \mathbb{R}^{n \times m}$ is introduced in (5-15) to facilitate the control development, where the elements of the matrix are composed of the elements of $\hat{\theta}_B(t)$.

Based on the expression in (5-15) and the subsequent stability analysis, the control input is designed as

$$u = - \int_0^t [\alpha u(\tau) + \Omega(\tau)] d\tau, \quad (5-23)$$

where the auxiliary function $\Omega(t) \in \mathbb{R}^m$ is defined as

$$\Omega \triangleq (C\hat{B})^{-1} [(k_s + 1)r + \beta \text{sgn}(e)], \quad (5-24)$$

where $\beta, k_s \in \mathbb{R}^{m \times m}$ are constant, positive definite, diagonal control gain matrices, and α is defined in (5-14). The adaptive estimate $\hat{B}(t)$ (or $\hat{\theta}_B(t)$ in vector form) in (5-24) is generated online according to the adaptive update law

$$\dot{\hat{\theta}}_B = \text{proj} \{ \Gamma_B Y_B^T r \}. \quad (5-25)$$

In (5-25), $\Gamma_B \in \mathbb{R}^{p_1 \times p_1}$ is a constant, positive definite, symmetric adaptation gain matrix, and $\text{proj}(\cdot)$ denotes a projection operator utilized to guarantee that the i^{th} element of $\hat{\theta}_B(t)$ is bounded as

$$\underline{\theta}_{Bi} \leq \hat{\theta}_{Bi} \leq \bar{\theta}_{Bi}, \quad (5-26)$$

where $\bar{\theta}_{Bi}, \underline{\theta}_{Bi} \in \mathbb{R}$ denote known, constant upper and lower bounds, respectively, for each element of $\hat{\theta}_B(t)$. After substituting the time derivative of (5-23) into (5-15), the

closed-loop error system can be determined as

$$\dot{r} = \tilde{N} + N_d + Y_B \tilde{\theta}_B - (k_s + 1)r - \beta \text{sgn}(e) - e. \quad (5-27)$$

Remark 5-1: The projection operator in (5-25) ensures that the matrix estimate $C\hat{B}(t)$ is invertible under the standard assumption that CB is invertible [25, 34, 83] for all elements of B contained within some bounded region (i.e., $\underline{\theta}_{Bi} \leq \theta_{Bi} \leq \bar{\theta}_{Bi}$). For example, the estimate $C\hat{B}(t)$ for the Osprey longitudinal dynamics could be selected as

$$\begin{aligned} (C\hat{B})_{lon} &= \begin{bmatrix} 1 & 0 \\ 0 & 1 \\ 0 & 0 \\ 0 & 0 \end{bmatrix}^T \begin{bmatrix} [\underline{\theta}_{B1}, \bar{\theta}_{B1}] & [\underline{\theta}_{B2}, \bar{\theta}_{B2}] \\ [\underline{\theta}_{B3}, \bar{\theta}_{B3}] & [\underline{\theta}_{B4}, \bar{\theta}_{B4}] \\ [\underline{\theta}_{B5}, \bar{\theta}_{B5}] & [\underline{\theta}_{B6}, \bar{\theta}_{B6}] \\ [\underline{\theta}_{B7}, \bar{\theta}_{B7}] & [\underline{\theta}_{B8}, \bar{\theta}_{B8}] \end{bmatrix} \\ &= \begin{bmatrix} [\underline{\theta}_{B1}, \bar{\theta}_{B1}] & [\underline{\theta}_{B2}, \bar{\theta}_{B2}] \\ [\underline{\theta}_{B3}, \bar{\theta}_{B3}] & [\underline{\theta}_{B4}, \bar{\theta}_{B4}] \end{bmatrix}, \end{aligned} \quad (5-28)$$

where $[\cdot, \cdot]$ denotes an interval between a lower and upper bound. Assumption 2 (and hence, the invertibility of $C\hat{B}(t)$) is valid for this particular example provided

$$[\underline{\theta}_{B1}, \bar{\theta}_{B1}] \cdot [\underline{\theta}_{B4}, \bar{\theta}_{B4}] \neq [\underline{\theta}_{B2}, \bar{\theta}_{B2}] \cdot [\underline{\theta}_{B3}, \bar{\theta}_{B3}]. \quad (5-29)$$

5.4 Stability Analysis

Theorem 5-1: The controller given in (5-23) ensures that all system signals are bounded during closed-loop operation and that the position tracking error is regulated in the sense that

$$\|e(t)\| \rightarrow 0 \quad \text{as } t \rightarrow \infty, \quad (5-30)$$

provided the control gain matrix k_s introduced in (5-23) is selected sufficiently large (see the subsequent stability proof), and the control gain matrix β introduced in (5-24) is

selected such the following sufficient condition is satisfied:

$$\lambda_{\min} \{\beta\} > \zeta_{N_d} + \frac{1}{\alpha} \zeta_{\dot{N}_d}, \quad (5-31)$$

where ζ_{N_d} and $\zeta_{\dot{N}_d}$ were introduced in (5-19).

The following lemma is provided to facilitate the main result in Theorem 5-1.

Lemma 5-1: *To facilitate the subsequent stability analysis, the auxiliary function*

$P(t) \in R$ *is defined as*

$$P(t) \triangleq \|\beta\|_{i_\infty} \|e(0)\| - e(0)^T N_d(0) - \int_0^t L(\tau) d\tau, \quad (5-32)$$

where $\|\cdot\|_{i_\infty}$ denotes the induced infinity norm of a matrix, and the auxiliary function

$L(t) \in R$ *is defined as*

$$L(t) \triangleq r^T (N_d(t) - \beta \operatorname{sgn}(e)). \quad (5-33)$$

Provided β is selected according to the sufficient condition the following inequality can be obtained:

$$\int_0^t L(\tau) d\tau \leq \|\beta\|_{i_\infty} \|e(0)\| - e(0)^T N_d(0). \quad (5-34)$$

Hence, (5-34) can be used to conclude that $P(t) \geq 0$.

Proof: See [52, 53] for proof of Lemma 5-1.

Proof: (See Theorem 5-1) Let $\mathcal{D} \subset \mathbb{R}^{2m+p_1+1}$ be a domain containing $y(t) = 0$, where $y(t) \in \mathbb{R}^{2m+p_1+1}$ is defined as

$$y(t) \triangleq \begin{bmatrix} z^T(t) & \tilde{\theta}_B^T(t) & \sqrt{P(t)} \end{bmatrix}^T. \quad (5-35)$$

Let $V(y, t) : \mathcal{D} \times [0, \infty) \rightarrow \mathbb{R}$ be a continuously differentiable, positive definite function defined as

$$V \triangleq \frac{1}{2} e^T e + \frac{1}{2} r^T r + \frac{1}{2} \tilde{\theta}_B^T \Gamma_B^{-1} \tilde{\theta}_B + P \quad (5-36)$$

that satisfies the following inequalities:

$$\eta_1 \|y\|^2 \leq V(y, t) \leq \eta_2 \|y\|^2 \quad (5-37)$$

provided the sufficient condition introduced in (5-31) is satisfied, where $\eta_1 \triangleq \frac{1}{2} \min \{1, \lambda_{\min} \{\Gamma_B^{-1}\}\}$, and $\eta_2 \triangleq \max \{\frac{1}{2} \lambda_{\max} \{\Gamma_B^{-1}\}, 1\}$. After taking the time derivative of (5-36) and utilizing (5-14), (5-23), (5-27), (5-32), and (5-33), $\dot{V}(y, t)$ can be expressed as

$$\dot{V}(y, t) = -\alpha e^T e + r^T \dot{N} + r^T Y_B \dot{\theta}_B - (k_s + 1) r^T r - \dot{\theta}_B^T \Gamma_B^{-1} \dot{\theta}_B. \quad (5-38)$$

After utilizing (5-18) and (5-25), $\dot{V}(y, t)$ can be upper bounded as

$$\dot{V}(y, t) \leq -\alpha e^T e - \|r\|^2 - [k_s \|r\|^2 - \rho(\|z\|) \|r\| \|z\|]. \quad (5-39)$$

Completing the squares for the bracketed terms in (5-39) yields

$$\dot{V}(y, t) \leq -\eta_3 \|z\|^2 + \frac{\rho^2(\|z\|) \|z\|^2}{4k_s}, \quad (5-40)$$

where $\eta_3 \triangleq \min \{\alpha, 1\}$, and $\rho(\|z\|)$ is introduced in (5-18). The following expression can be obtained from (5-40):

$$\dot{V}(y, t) \leq -U(y), \quad (5-41)$$

where $U(y) = c \|z\|^2$, for some positive constant $c \in \mathbb{R}$, is a continuous, positive semi-definite function that is defined on the following domain:

$$\mathcal{D} \triangleq \left\{ y \in \mathbb{R}^{2m+p_1+1} \mid \|y\| < \rho^{-1} \left(2\sqrt{\eta_3 k_s} \right) \right\}. \quad (5-42)$$

The inequalities in (5-37) and (5-41) can be used to show that $V(t) \in \mathcal{L}_\infty$ in \mathcal{D} ; hence, $e(t), r(t), \tilde{\theta}_B(t), P(t) \in \mathcal{L}_\infty$ in \mathcal{D} . Given that $e(t), r(t) \in \mathcal{L}_\infty$ in \mathcal{D} , standard linear analysis methods can be used to prove that $\dot{e}(t) \in \mathcal{L}_\infty$ in \mathcal{D} from (5-14). Since $e(t), \dot{e}(t) \in \mathcal{L}_\infty$, (5-13) can be used along with the assumption that $y_m, \dot{y}_m \in \mathcal{L}_\infty$ to prove that $y(t), \dot{y}(t) \in \mathcal{L}_\infty$. Given that $r(t), \left(C\hat{B}(t)\right)^{-1} \in \mathcal{L}_\infty$ in \mathcal{D} , (5-24) can be used to show that $\Omega(t) \in \mathcal{L}_\infty$ in \mathcal{D} . Since $\Omega(t) \in \mathcal{L}_\infty$ in \mathcal{D} , Equation 2.78 of [80] can be used to show that $\|\Omega(t)\| \leq M, \forall t \geq 0$, where $M \in \mathbb{R}^+$ is a bounding constant. The time derivative of (5-23) can then be used to prove that $\dot{u}(t) \in \mathcal{L}_\infty$ in \mathcal{D} . Given that $\dot{u}(t) \in \mathcal{L}_\infty$ in \mathcal{D} and $\|\Omega(t)\| \leq M$, the time derivative of (5-23) can be used to upper bound $\dot{u}(t)$ as

$\dot{u}(t) \leq -\alpha u(\tau) + M$. Theorem 1.1 of [81] can then be utilized to prove that $u(t) \in \mathcal{L}_\infty$ in \mathcal{D} . Given that $u(t), \dot{u}(t) \in \mathcal{L}_\infty$ in \mathcal{D} , (5-21) can be used to prove that $Y_B \in \mathcal{L}_\infty$ in \mathcal{D} . Hence, (5-27) can be used to show that $\dot{r}(t) \in \mathcal{L}_\infty$ in \mathcal{D} . Since $\dot{e}(t), \dot{r}(t) \in \mathcal{L}_\infty$ in \mathcal{D} , the definitions for $U(y)$ and $z(t)$ can be used to prove that $U(y)$ is uniformly continuous in \mathcal{D} . Let $S \subset \mathcal{D}$ denote a set defined as

$$S \triangleq \left\{ y(t) \in \mathcal{D} \mid \eta_2 \|y\|^2 < \frac{1}{2} \left(\rho^{-1} \left(2\sqrt{\eta_3 k_s} \right) \right)^2 \right\}. \quad (5-43)$$

Theorem 8.4 of [82] can now be invoked to state that

$$c \|z\|^2 \rightarrow 0 \quad \text{as} \quad t \rightarrow \infty \quad \forall y(0) \in S. \quad (5-44)$$

Based on the definition of $z(t)$, (5-44) can be used to show that

$$\|e(t)\| \rightarrow 0 \quad \text{as} \quad t \rightarrow \infty \quad \forall y(0) \in S. \quad (5-45)$$

5.5 Simulation Results

A numerical simulation was created to test the efficacy of the proposed controller.

The simulation is based on the aircraft state space system given in (5-1) and (5-2), where the state matrix A , input authority matrix B , and nonlinear disturbance function $f(x)$ are given by the state space model for the Osprey aircraft given in (5-3)-(5-8). The reference model for the simulation is represented by the state space system given in (5-9)-(5-11), with state matrices A_{lonm} and A_{latm} , input matrices B_{lonm} and B_{latm} , and output matrices C_{lon} and C_{lat} selected as

$$A_{lonm} = \begin{bmatrix} 0.6 & -1.1 & 0 & 0 \\ 2.0 & -2.2 & 0 & 0 \\ 0 & 0 & -4.0 & -600.0 \\ 0 & 0 & 0.1 & -10 \end{bmatrix} \quad (5-46)$$

$$A_{latm} = \begin{bmatrix} -4.0 & -600.0 & 0 & 0 \\ 0.1 & -10.00 & 0 & 0 \\ 0 & 0 & 0.6 & -1.1 \\ 0 & 0 & 2.0 & -2.2 \end{bmatrix} \quad (5-47)$$

$$B_{lonm} = \begin{bmatrix} 0 & 0.5 \\ 0 & 0 \\ 10 & 0 \\ 0 & 0 \end{bmatrix} \quad B_{latm} = \begin{bmatrix} 10 & 0 \\ 0 & 0 \\ 0 & 0.5 \\ 0 & 0 \end{bmatrix}, \quad (5-48)$$

and

$$C_{lon} = \begin{bmatrix} 0 & 0 & 1 & 0 \\ 1 & 0 & 0 & 0 \end{bmatrix} \quad C_{lat} = \begin{bmatrix} 0 & 1 & 0 & 0 \\ 0 & 0 & 1 & 0 \end{bmatrix}. \quad (5-49)$$

The state and input matrices for the longitudinal and lateral dynamic models of the Osprey aircraft flying at 25 m/s at an altitude of 60 meters are given as

$$A_{lon} = \begin{bmatrix} -0.15 & 11.08 & 0.08 & 0 \\ -0.03 & -7.17 & 0.83 & 0 \\ 0 & -37.35 & -9.96 & 0 \\ 0 & 0 & 1.00 & 0 \end{bmatrix} \quad (5-50)$$

$$A_{lat} = \begin{bmatrix} -0.69 & -0.03 & -0.99 & 0 \\ -3.13 & -12.92 & 1.10 & 0 \\ 17.03 & -0.10 & -0.97 & 0 \\ 0 & 1.00 & -0.03 & 0 \end{bmatrix} \quad (5-51)$$

$$B_{lon} = \begin{bmatrix} 3E^{-3} & 0.06 \\ 1E^{-5} & 1E^{-4} \\ -0.98 & 0 \\ 0 & 0 \end{bmatrix} \quad B_{lat} = \begin{bmatrix} 0 & 0 \\ 1.50 & -0.02 \\ -0.09 & 0.17 \\ 0 & 0 \end{bmatrix}, \quad (5-52)$$

Table 5-1. Parameters used in the ADI controller simulation.

Sampling Time	0.01 sec
Pitch Rate Sensor Noise	$\pm 1.7^\circ/\text{sec}$
Velocity Sensor Noise	$\pm 0.4 \frac{m}{\text{sec}}$
Roll Rate Sensor Noise	$\pm 1.2^\circ/\text{sec}$
Yaw Rate Sensor Noise	$\pm 1.2^\circ/\text{sec}$

respectively. The nonlinear disturbance terms, denoted $f(x_{lon})$ and $f(x_{lat})$, are defined as

$$f(x_{lon}) = \begin{bmatrix} -9.81 \sin \theta + g(x) & 0 & 0 & 0 \end{bmatrix}^T \quad (5-53)$$

$$f(x_{lat}) = \begin{bmatrix} 0.39 \sin \phi & 0 & 0 & 0 \end{bmatrix}^T, \quad (5-54)$$

where $g(x)$ represents a disturbance due to a discrete vertical wind gust as defined in [73], where $U_{ds} = 10.12 \text{ m/s}$, $H = 15.24 \text{ m}$, and $V_0 = 25 \text{ m/s}$ (cruise velocity). Figure 3-2 shows a plot of the wind gust used in the simulation. The remainder of the additive disturbances in (5-53) and (5-54) represent nonlinearities not captured in the linearized state space model (e.g., due to small angle assumptions). All states and control inputs were initialized to zero for the simulation.

In order to develop a realistic stepping stone to an actual experimental demonstration of the proposed aircraft controller, the simulation parameters were selected based on detailed data analyses and specifications. The sensor noise values are based upon Cloud Cap Technology's Piccolo Autopilot and analysis of data logged during straight and level flight. These values are also corroborated with the specifications given for Cloud Cap Technology's Crista Inertial Measurement Unit (IMU). The simulation parameters are summarized in the following table:

The objectives for the longitudinal controller simulation are to track pitch rate and forward velocity commands. Figures 5-1 and 5-2 show the simulation results of the closed-loop longitudinal system with control gains selected as follows (e.g., see

(5-23)-(5-25)):

$$\beta = \text{diag} \left\{ \begin{array}{cc} 20 & 50 \end{array} \right\} \quad k_s = \text{diag} \left\{ \begin{array}{cc} 70 & 60 \end{array} \right\}$$

$$\alpha = 0.02I_{2 \times 2} \quad \Gamma_B = 1E^{-5}I_{4 \times 4}$$

where the notation $I_{j \times j}$ denotes the $j \times j$ identity matrix. Figure 5-1 shows the reference and actual pitch rates during closed-loop operation, and Figure 5-2 shows the reference and actual forward velocity responses. For the lateral controller simulation, the

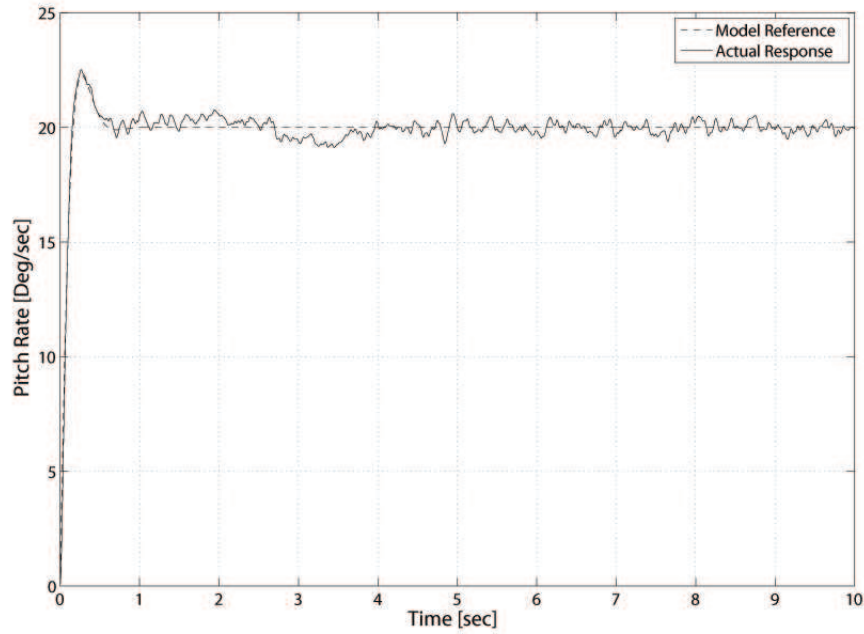


Figure 5-1. Pitch rate response achieved during closed-loop longitudinal controller operation.

objectives are to track roll rate and yaw rate commands. Figures 5-3 and 5-4 show the simulation results of the closed-loop lateral system with control gains selected as follows:

$$\beta = 40I_{2 \times 2} \quad k_s = 60I_{2 \times 2} \quad \alpha = 0.02I_{2 \times 2} \quad \Gamma_B = 0.01I_{4 \times 4}$$

Figure 5-3 shows the reference and actual roll rates during closed-loop operation, and Figure 5-4 shows the reference and actual yaw rates.

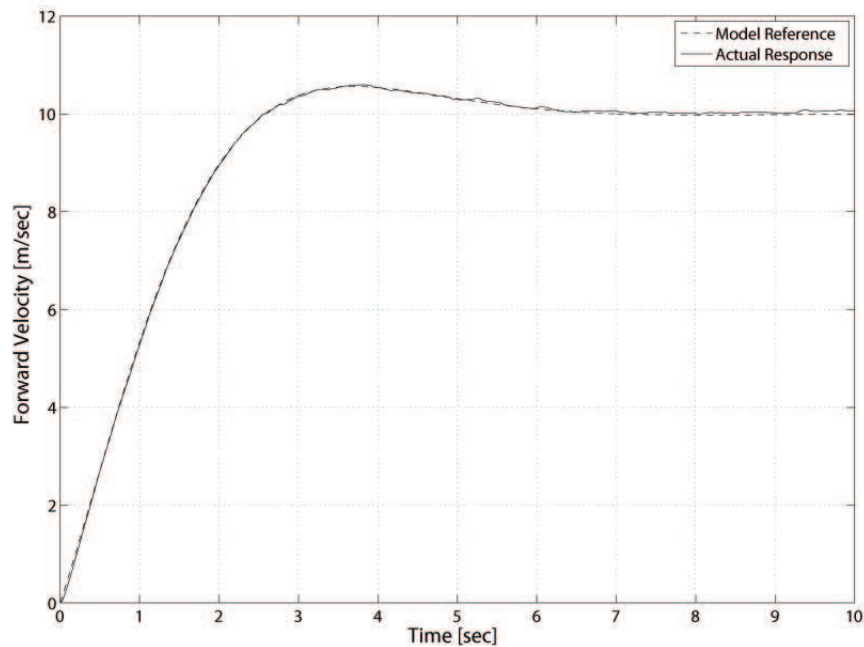


Figure 5-2. Forward velocity response achieved during closed-loop longitudinal controller operation.

The control actuation (relative to trim conditions) used during closed-loop operation for the adaptive controller is shown in Figure 5-5.

To further test the performance of the proposed control design, an additional simulation was created to test the adaptive longitudinal controller's ability to track simultaneous angle of attack (provided an angle of attack sensor is available (e.g., a pitot tube)) and forward velocity commands. The angle of attack and forward velocity responses of the closed-loop adaptive longitudinal system are shown in Figure 5-6, and the control actuation used during closed loop operation is shown in Figure 5-7. The control actuation values shown in Figure 5-7 are measured with respect to trim. The simulation parameters summarized in Table 1 were used for the angle of attack simulation. The motivation for including the angle of attack tracking results in Figure 5-6 is to illustrate that angle of attack control can be achieved using the developed adaptive control design (similar results can also be obtained for the robust controller), so the sudden, individual

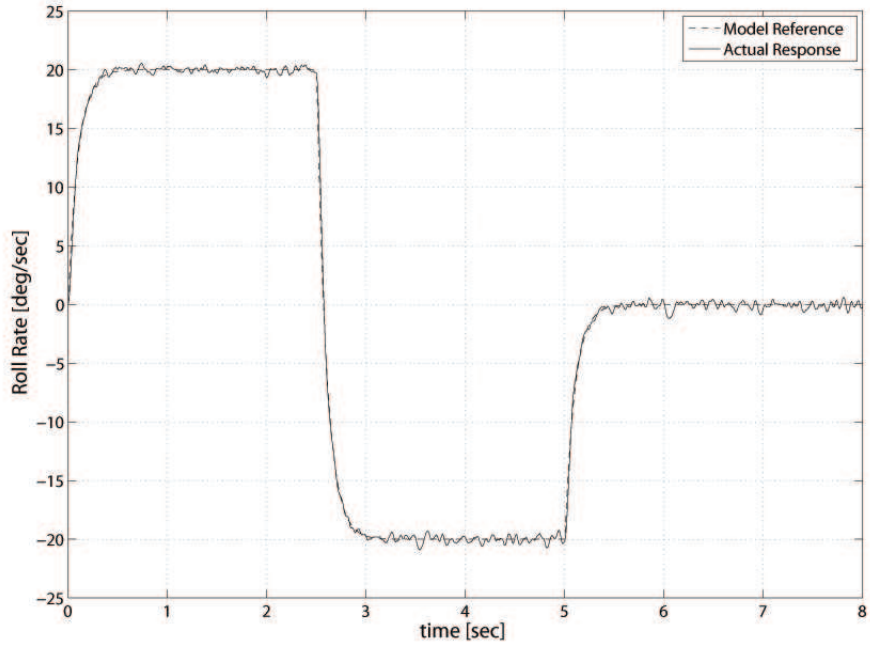


Figure 5-3. Roll rate response achieved during closed-loop lateral controller operation.

gust was not included in the angle of attack simulation. For the angle of attack simulation, the output matrix is

$$C_{lon} = \begin{bmatrix} 0 & 1 & 0 & 0 \\ 1 & 0 & 0 & 0 \end{bmatrix}, \quad (5-55)$$

and the model reference and plant input matrices are

$$B_{lon} = \begin{bmatrix} 0.003 & 0.065 \\ -0.010 & 0.0001 \\ -0.98 & 0 \\ 0 & 0 \end{bmatrix} \quad B_{lonm} = \begin{bmatrix} 0 & 0.5 \\ 0 & 0 \\ 11.5 & 0 \\ 0 & 0 \end{bmatrix}. \quad (5-56)$$

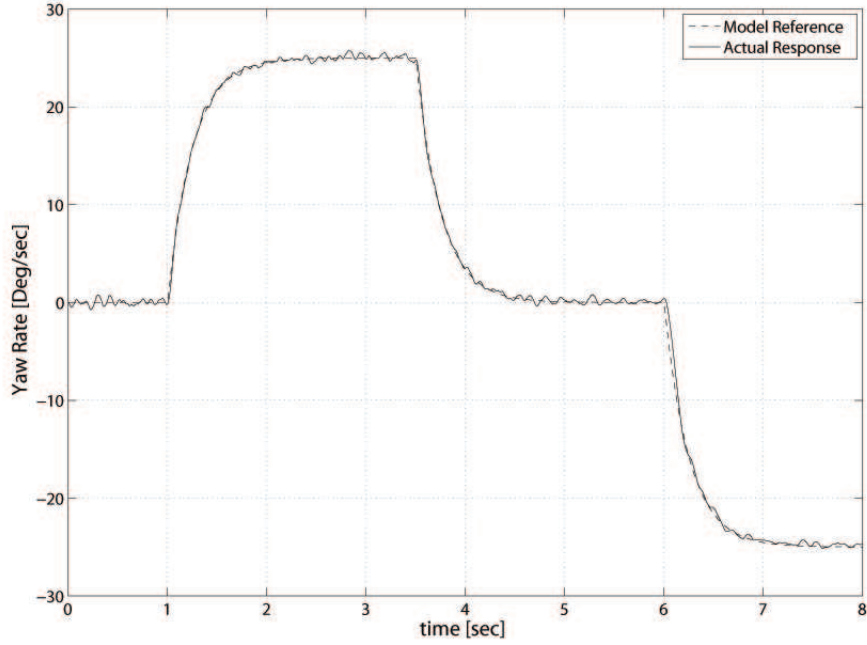


Figure 5-4. Yaw rate response achieved during closed-loop lateral controller operation.

The constant feedforward estimate \hat{B}_{lon} was selected as

$$\hat{B}_{lon} = \begin{bmatrix} 0.001 & 0.05 \\ 0 & 0 \\ -1 & 0 \\ 0 & 0 \end{bmatrix}. \quad (5-57)$$

Note that for the choice of \hat{B}_{lon} given in (5-57), the inequality in (4-35) is satisfied.

Specifically, the choice for \hat{B}_{lon} yields

$$\lambda_{\min}(\Lambda) = 1.2907 > 0.2620 = \|\Delta\|_{i\infty}. \quad (5-58)$$

5.6 Conclusion

An aircraft controller is presented, which achieves asymptotic tracking control of a model reference system where the plant dynamics contain input uncertainty and a bounded non-LP disturbance. This result represents application of a continuous control

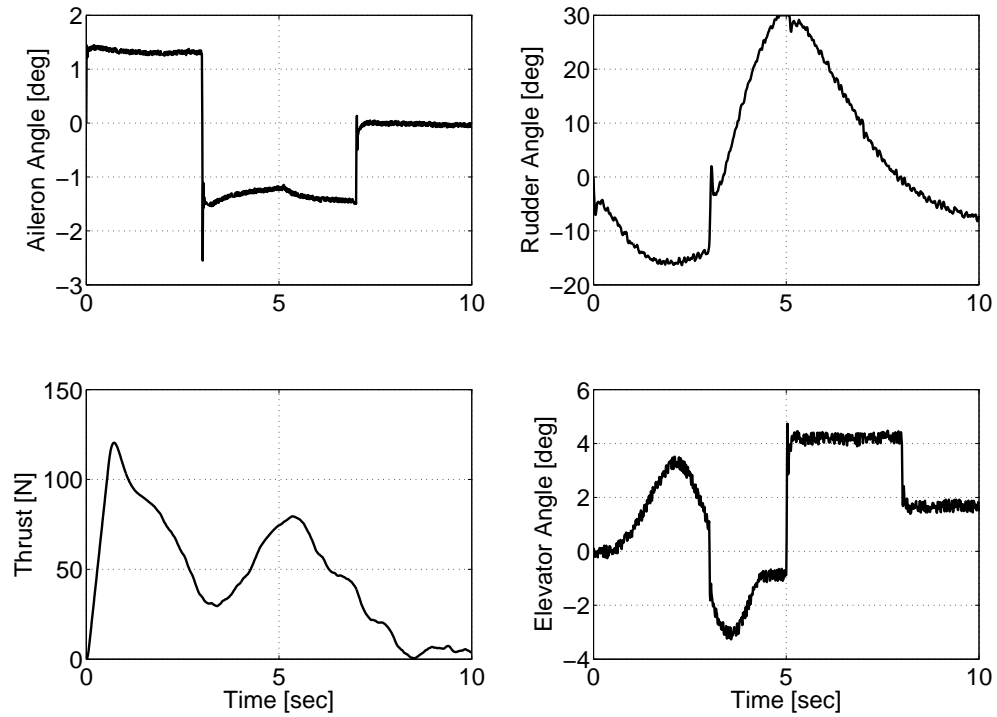


Figure 5-5. Control actuation away from trim used during closed-loop adaptive dynamic inversion controller operation for the lateral subsystem (top) and the longitudinal subsystem (bottom).

strategy in an ADI framework to a nonlinear system with additive, non-LP disturbances, where the control input is multiplied by a non-square matrix containing parametric uncertainty. A Lyapunov-based stability analysis is provided to verify the theoretical result, and numerical simulation results are provided to demonstrate the efficacy of the proposed controller.

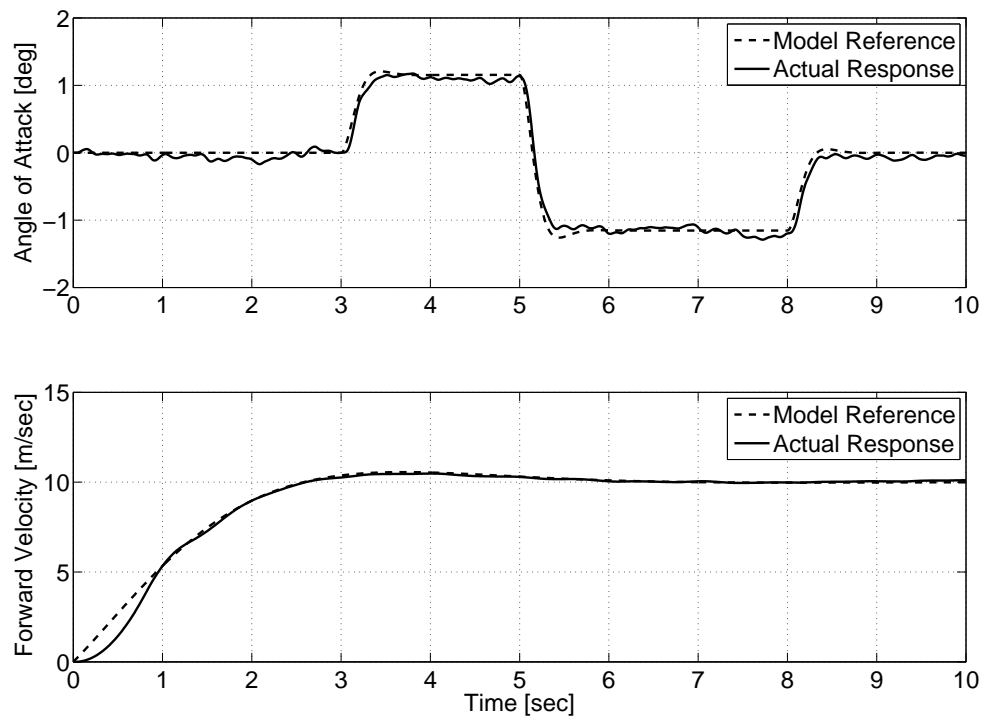


Figure 5-6. Angle of attack (top) and forward velocity away from trim (bottom) responses for the closed-loop adaptive longitudinal system.

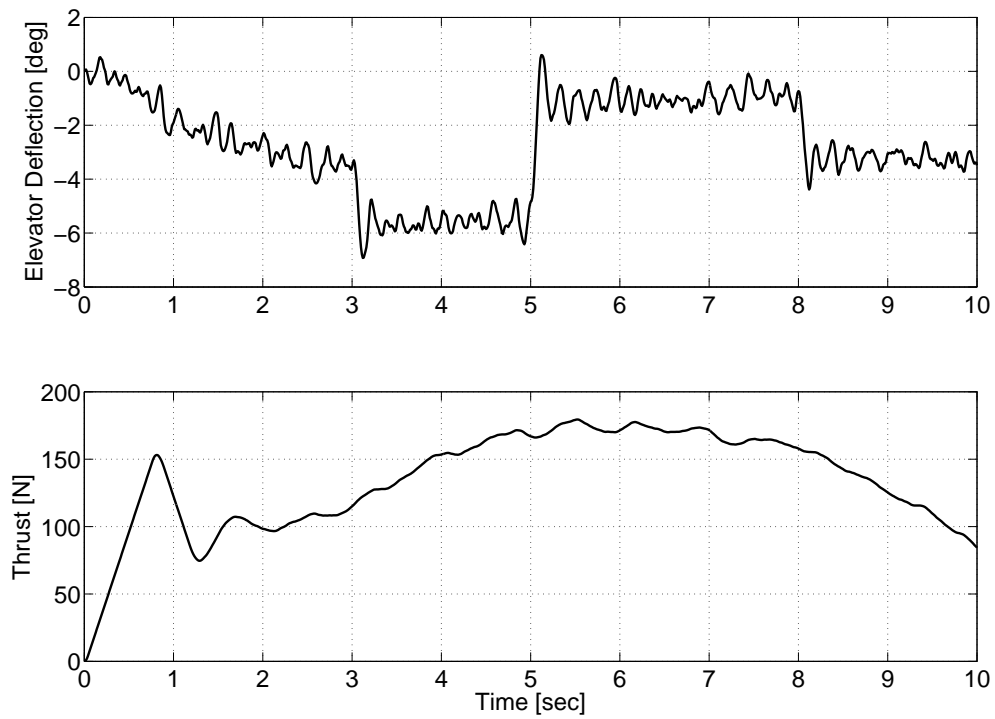


Figure 5-7. Control actuation away from trim used during closed-loop adaptive controller operation for the angle of attack tracking objective. Elevator deflection angle (top) and thrust (bottom).

CHAPTER 6 GLOBAL ADAPTIVE OUTPUT FEEDBACK MRAC

6.1 Introduction

The contribution in this chapter is the development of a continuous output feedback controller that achieves global asymptotic tracking of the outputs of a reference model, where the plant model contains a non-square, column deficient, uncertain input matrix and a non-vanishing disturbance that cannot be linearly parameterized. The developed controller combines a continuous robust feedback structure to compensate for the additive nonlinear disturbance with an adaptive feedforward structure to compensate for uncertainty in the state and input matrices. In comparison with the results in [41], the unknown nonlinearity in the current result does not satisfy the linear-in-the-parameters assumption. In comparison with our previous results in [35, 47], the current development exploits the matrix decomposition technique in [42, 43] so that the controller depends only on the output states, and not the respective time derivatives. Global asymptotic tracking is proven via a Lyapunov stability analysis, and a high fidelity numerical simulation is provided to show the performance of the developed controller.

6.2 System Model

The subsequent development is based on the following state-space system:

$$\dot{x} = Ax + Bu + f(x, t) \tag{6-1}$$

$$y = Cx. \tag{6-2}$$

In (6-1) and (6-2), $A \in \mathbb{R}^{n \times n}$ denotes a state matrix composed of unknown constant elements, $B \in \mathbb{R}^{n \times m}$ denotes a column deficient input matrix composed of uncertain constant elements with $m < n$, $C \in \mathbb{R}^{m \times n}$ denotes a known output matrix, $x(t) \in \mathbb{R}^n$ denotes the state vector, $u(t) \in \mathbb{R}^m$ denotes a vector of control inputs, and $f(x, t) \in \mathbb{R}^n$ represents a state- and time-dependent unknown, nonlinear disturbance. Based on (6-1)

and (6-2), a reference model is defined as

$$\dot{x}_m = A_m x_m + B_m \delta \quad (6-3)$$

$$y_m = C x_m, \quad (6-4)$$

where $A_m \in \mathbb{R}^{n \times n}$ is Hurwitz, $B_m \in \mathbb{R}^{n \times m}$ is the reference input matrix, $\delta(t) \in \mathbb{R}^m$ is the reference input, $x_m(t) \in \mathbb{R}^n$ represents the reference states, $y_m(t) \in \mathbb{R}^m$ are the reference outputs, and C is introduced in (6-2).

Assumption 6-1: The nonlinear disturbance $f(x, t)$ and its first two time derivatives are assumed to exist and be bounded by known constants. A discussion of nonlinearities that can be represented by $f(x, t)$ for an aircraft is provided in [35].

6.3 Control Development

6.3.1 Control Objective

The control objective is to ensure that the outputs $y(t)$ track the time-varying outputs generated from the reference model outputs in (6-4). To quantify the control objective, an output tracking error, denoted by $e(t) = \begin{bmatrix} e_1(t) & e_2(t) & \cdots & e_m(t) \end{bmatrix}^T \in \mathbb{R}^m$, is defined as

$$e \triangleq y - y_m = C(x - x_m). \quad (6-5)$$

To facilitate the subsequent analysis, a filtered tracking error [74], denoted by $r(t) = \begin{bmatrix} r_1(t) & r_2(t) & \cdots & r_m(t) \end{bmatrix}^T \in \mathbb{R}^m$, is defined as

$$r \triangleq \dot{e} + \alpha e, \quad (6-6)$$

where $\alpha \in \mathbb{R}$ is a positive, constant control gain. The subsequent development is based on the assumption that only the output measurements $y(t)$ (and therefore $e(t)$ in (6-5)) are available. Hence, $\dot{e}(t)$ and $r(t)$ are defined to simplify the stability analysis. The unmeasurable signal $r(t)$ is contained inside an integral in the subsequent adaptive update law, but is not required for the control implementation due to integration by parts.

To facilitate the subsequent robust output feedback control development and stability analysis, the state vector $x(t)$ will be segregated in terms of its measurable and unmeasurable components. This step enables the segregation of terms that can be bounded as functions of the error states from those that are bounded by constants. To this end, the state vector $x(t)$ can be expressed as

$$x(t) = \underline{x}(t) + x_u(t), \quad (6-7)$$

where $\underline{x}(t) \in \mathbb{R}^n$ contains the m output states, and $x_u \in \mathbb{R}^n$ contains the $n - m$ remaining states. Likewise, the reference states $x_m(t)$ can also be separated as in (6-7).

Assumption 6-2: The states $x_u(t)$ in (6-7) and the corresponding time derivatives can be further separated as

$$\begin{aligned} x_u(t) &= x_{\rho u}(t) + x_{\zeta u}(t) \\ \dot{x}_u(t) &= \dot{x}_{\rho u}(t) + \dot{x}_{\zeta u}(t), \end{aligned} \quad (6-8)$$

where $x_{\rho u}(t), \dot{x}_{\rho u}(t), x_{\zeta u}(t), \dot{x}_{\zeta u}(t) \in \mathbb{R}^n$ are assumed to be upper bounded as

$$\begin{aligned} \|x_{\rho u}(t)\| &\leq c_1 \|z\| & \|x_{\zeta u}(t)\| &\leq \zeta_{xu} \\ \|\dot{x}_{\rho u}(t)\| &\leq c_2 \|z\| & \|\dot{x}_{\zeta u}(t)\| &\leq \zeta_{\dot{x}u} \end{aligned}$$

where $z(t) \in \mathbb{R}^{2m}$ is defined as

$$z \triangleq \begin{bmatrix} e^T & r^T \end{bmatrix}^T, \quad (6-9)$$

and $c_1, c_2, \zeta_{xu}, \zeta_{\dot{x}u} \in \mathbb{R}$ are known non-negative bounding constants (i.e., the constants could be zero for different classes of systems).

6.3.2 Open-Loop Error System

The open-loop tracking error dynamics can be developed by taking the time derivative of (6-6) and utilizing the expressions in (6-1)-(6-4) to obtain

$$\dot{r} = \tilde{N}_0 + N_{d0} + CA(\dot{\underline{x}}_m + \alpha \underline{x}_m) + CB(\dot{i} + \alpha u), \quad (6-10)$$

where $\underline{x}_m(t) \in \mathbb{R}^n$ contains the reference states that correspond to the output states in $\underline{x}(t)$, and $\dot{\underline{x}}_m(t)$ denotes the respective time derivative. The auxiliary functions $\tilde{N}_0(x, \dot{x}, x_m, \dot{x}_m, t) \in \mathbb{R}^m$ and $N_{d0}(x, x_m, \dot{x}_m, \delta, \dot{\delta}, t) \in \mathbb{R}^m$ in (6–10) are defined as

$$\begin{aligned} \tilde{N}_0 \triangleq & CA(\dot{\underline{x}} - \dot{\underline{x}}_m) + \alpha CA(\underline{x} - \underline{x}_m) \\ & + CA(\dot{x}_{\rho u} + \alpha x_{\rho u}), \end{aligned} \quad (6-11)$$

$$\begin{aligned} N_{d0} \triangleq & C\left(\dot{f}(x, t) + \alpha f(x, t)\right) + CA(\dot{x}_{\zeta u} + \alpha x_{\zeta u}) \\ & - CA_m(\dot{x}_m + \alpha x_m) - CB_m(\dot{\delta} + \alpha \delta). \end{aligned} \quad (6-12)$$

Motivation for the selective grouping of the terms in (6–11) and (6–12) is derived from the fact that the following inequalities can be developed [52, 84]:

$$\left\| \tilde{N}_0 \right\| \leq \rho_0 \|z\| \quad \|N_{d0}\| \leq \zeta_{N_{d0}} \quad \left\| \dot{N}_{d0} \right\| \leq \zeta_{\dot{N}_{d0}}, \quad (6-13)$$

where $\rho_0, \zeta_{N_{d0}}, \zeta_{\dot{N}_{d0}} \in \mathbb{R}$ are known positive bounding constants.

6.3.3 Closed-Loop Error System

Based on the expression in (6–10) and the subsequent stability analysis, the control input is designed as

$$u = - \int_0^t \alpha u(\tau) d\tau + \left(C\hat{B}\right)^{-1} (\mu_0 - \mu_1), \quad (6-14)$$

where $\mu_0(t), \mu_1(t) \in \mathbb{R}^m$ denote subsequently defined feedback control terms, and $\hat{B} \in \mathbb{R}^{n \times m}$ is a constant feedforward estimate of the uncertain matrix B . After substituting the time derivative of (6–14) into (6–10), the error dynamics can be expressed as

$$\dot{r} = \tilde{N}_0 + N_{d0} + CA(\dot{\underline{x}}_m + \alpha \underline{x}_m) + CB \left(C\hat{B}\right)^{-1} (\dot{\mu}_0 - \dot{\mu}_1). \quad (6-15)$$

Assumption 6-3: Upper and lower bounds of the uncertain input matrix B are known such that the constant feedforward estimate \hat{B} can be selected such that

$CB(C\hat{B})^{-1}$ can be decomposed as follows [41–43, 56]:

$$CB(C\hat{B})^{-1} = ST, \quad (6-16)$$

where $S \in \mathbb{R}^{m \times m}$ is symmetric and positive definite, and $T \in \mathbb{R}^{m \times m}$ is a unity upper triangular matrix, which is diagonally dominant in the sense that

$$\varepsilon \leq |T_{ii}| - \sum_{k=i+1}^m |T_{ik}| \leq Q \quad \forall i = 1, \dots, m-1. \quad (6-17)$$

In (6-17), $\varepsilon \in (0, 1)$ and $Q \in \mathbb{R}^+$ are known bounding constants, and $T_{ik} \in \mathbb{R}$ denotes the $(i, k)^{th}$ element of the matrix T . Preliminary results indicate that this assumption is mild in the sense that the decomposition in (6-16) results in a diagonally dominant T for a wide range of $\hat{B} \neq B$.

Based on (6-16), the error dynamics in (6-15) are

$$S^{-1}\dot{r} = \tilde{N}_1 + N_{d1} + S^{-1}CA(\dot{x}_m + \alpha x_m) + T(\dot{\mu}_0 - \dot{\mu}_1) - e, \quad (6-18)$$

where

$$\tilde{N}_1 \triangleq S^{-1}\tilde{N}_0 + e \quad N_{d1} \triangleq S^{-1}N_{d0}.$$

Since S is positive definite, the following inequalities can be developed:

$$\|\tilde{N}_1\| \leq \rho_1 \|z\| \quad \|N_{d1}\| \leq \zeta_{N_{d1}} \quad \|\dot{N}_{d1}\| \leq \zeta_{\dot{N}_{d1}}, \quad (6-19)$$

where $\rho_1, \zeta_{N_{d1}}, \zeta_{\dot{N}_{d1}} \in \mathbb{R}$ are positive bounding constants. The error dynamics in (6-18) can now be rewritten as

$$S^{-1}\dot{r} = \tilde{N}_1 + N_{d1} + Y_A\theta_A + \bar{T}\dot{\mu}_0 + \dot{\mu}_0 - T\dot{\mu}_1 - e, \quad (6-20)$$

where $\bar{T} \triangleq T - I_{m \times m}$ is a strictly upper triangular matrix, $I_{m \times m}$ is an $m \times m$ identity matrix, $Y_A(x_m, \dot{x}_m) \in \mathbb{R}^{m \times p_1}$ denotes a measurable regression matrix, and $\theta_A \in \mathbb{R}^{p_1}$ is a vector containing the unknown elements of the A and S matrices, defined via the

parametrization

$$Y_A \theta_A \triangleq S^{-1} C A (\dot{x}_m + \alpha x_m). \quad (6-21)$$

Based on the open-loop error dynamics in (6-20), the auxiliary control term $\mu_0(t)$ is designed as

$$\begin{aligned} \mu_0 \triangleq & -(k_s + I_{m \times m}) e(t) + (k_s + I_{m \times m}) e(0) \\ & - \int_0^t \left[Y_A \hat{\theta}_A + \alpha (k_s + I_{m \times m}) e(\tau) \right] d\tau, \end{aligned} \quad (6-22)$$

and the auxiliary control term $\mu_1(t)$ is designed as

$$\mu_1 = \int_0^t \beta \operatorname{sgn}(e(\tau)) d\tau, \quad (6-23)$$

where $\beta \in \mathbb{R}$ is a constant, positive control gain, $k_s \in \mathbb{R}^{m \times m}$ is a constant, positive definite, diagonal control gain matrix, and α is introduced in (6-6). The adaptive estimate $\hat{\theta}_A(t) \in \mathbb{R}^{p_1}$ in (6-22) is generated according to the adaptive update law

$$\dot{\hat{\theta}}_{Ai} = \operatorname{proj}(\Xi_i), \quad (6-24)$$

where $\Xi_i(x_m, \dot{x}_m, r)$ denotes the i^{th} component of $\Xi(x_m, \dot{x}_m, r) \forall i = 1, \dots, p_1$, where the auxiliary term $\Xi(x_m, \dot{x}_m, r) \in \mathbb{R}^{p_1}$ is defined as

$$\Xi(x_m, \dot{x}_m, r) \triangleq \Gamma_A Y_A^T(x_m, \dot{x}_m) r. \quad (6-25)$$

For the adaptation law in (6-24) and (6-25), $\Gamma_A \in \mathbb{R}^{p_1 \times p_1}$ is a constant, positive definite, symmetric adaptation gain matrix. Since the measurable regression matrix $Y_A(\cdot)$ contains only the reference trajectories x_m and \dot{x}_m , the expression in (6-24) can be integrated by parts to prove that the adaptive estimate $\hat{\theta}_A(t)$ can be generated using only measurements of $e(t)$ (i.e., no $r(t)$ measurements, and hence, no $\dot{x}(t)$ measurements are required).

Property 6-2: The projection algorithm in (6-24) ensures that the following inequality is satisfied (for further details, see [85, 86]):

$$\underline{\theta}_{Ai} \leq \hat{\theta}_{Ai} \leq \bar{\theta}_{Ai}. \quad (6-26)$$

After substituting the time derivative of (6-22) into (6-20), the closed-loop error system can be determined as

$$\begin{aligned} S^{-1}\dot{r} &= \tilde{N}_1 + \bar{T}\dot{\mu}_0 + N_{d1} - (k_s + I_{m \times m})r \\ &+ Y_A\tilde{\theta}_A - T\dot{\mu}_1 - e, \end{aligned} \quad (6-27)$$

where $\tilde{\theta}_A(t) \in \mathbb{R}^{p_1}$ denotes the parameter estimation error defined as

$$\tilde{\theta}_A \triangleq \theta_A - \hat{\theta}_A. \quad (6-28)$$

Using the time derivative of (6-22), the vector $\bar{T}\dot{\mu}_0$ can be expressed as

$$\bar{T}\dot{\mu}_0 = \begin{bmatrix} \sum_{j=2}^m \bar{T}_{1j}\dot{\mu}_{0j} \\ \sum_{j=3}^m \bar{T}_{2j}\dot{\mu}_{0j} \\ \vdots \\ \bar{T}_{(m-1)m}\dot{\mu}_{0m} \\ 0 \end{bmatrix} = \begin{bmatrix} \Lambda_\rho \\ 0 \end{bmatrix} + \begin{bmatrix} \Lambda_\zeta \\ 0 \end{bmatrix}, \quad (6-29)$$

where the auxiliary signals $\Lambda_\rho \triangleq \begin{bmatrix} \Lambda_{\rho 1} & \Lambda_{\rho 2} & \cdots & \Lambda_{\rho(m-1)} \end{bmatrix}^T \in \mathbb{R}^{m-1}$ and $\Lambda_\zeta \triangleq \begin{bmatrix} \Lambda_{\zeta 1} & \Lambda_{\zeta 2} & \cdots & \Lambda_{\zeta(m-1)} \end{bmatrix}^T \in \mathbb{R}^{m-1}$, and the individual elements are defined as

$$\Lambda_{\rho i} \triangleq - \sum_{j=i+1}^m \bar{T}_{ij} (k_{sj} + 1) r_j \quad (6-30)$$

$$\Lambda_{\zeta i} \triangleq - \sum_{j=i+1}^m \bar{T}_{ij} \Omega_{jk}, \quad (6-31)$$

$\forall i = 1, \dots, m-1$, where the subscript j denotes the j^{th} element of the corresponding vector, and $\Omega_{jk} \in \mathbb{R}^m$ is defined as

$$\Omega_{jk} \triangleq \sum_{k=1}^{p_1} Y_{Ajk} \hat{\theta}_{Ak} \quad \forall j = 1, \dots, m. \quad (6-32)$$

Based on (6-30)-(6-32), the following inequalities can be developed [41, 56]:

$$\|\Lambda_\rho\| \leq \rho_{\Lambda 1} \|z\| \quad \|\Lambda_\zeta\| \leq \zeta_1, \quad (6-33)$$

where $z(t)$ is defined in (6-9), and $\rho_{\Lambda 1}, \zeta_1 \in \mathbb{R}$ are known positive bounding constants.

Note that $\rho_{\Lambda 1}$ only depends on the diagonal elements $i+1$ to m of k_s due to the strictly upper triangular nature of \bar{T} . After using (6-31) and (6-32), the time derivative of Λ_ζ can be expressed as

$$\dot{\Lambda}_\zeta = N_{B1} + N_{B2}, \quad (6-34)$$

where

$$N_{B1} \triangleq - \sum_{j=i+1}^m \bar{T}_{ij} \sum_{k=1}^{p_1} \dot{Y}_{Ajk} \hat{\theta}_{Ak} \quad (6-35)$$

$$N_{B2} \triangleq - \sum_{j=i+1}^m \bar{T}_{ij} \sum_{k=1}^{p_1} Y_{Ajk} \dot{\hat{\theta}}_{Ak}. \quad (6-36)$$

After utilizing Property 1, (6-24), and (6-26), the following inequalities can be developed:

$$\|N_{B1}\| \leq \zeta_2 \quad \|N_{B2}\| \leq \zeta_3 \|r\|, \quad (6-37)$$

where $\zeta_2, \zeta_3 \in \mathbb{R}$ are known positive bounding constants.

Based on (6-29), the closed-loop error system can be expressed as

$$\begin{aligned} S^{-1} \dot{r} &= \tilde{N}_2 + N_{d2} + Y_A \tilde{\theta}_A - (k_s + I_{m \times m}) r \\ &\quad - T \dot{\mu}_1 - e, \end{aligned} \quad (6-38)$$

where

$$\tilde{N}_2 = \tilde{N}_1 + \begin{bmatrix} \Lambda_p \\ 0 \end{bmatrix} \quad N_{d2} = N_{d1} + \begin{bmatrix} \Lambda_\zeta \\ 0 \end{bmatrix}. \quad (6-39)$$

Based on (6-19), (6-33), and (6-39), the following inequalities can be developed:

$$\begin{aligned} \|\tilde{N}_2\| &\leq \rho_2 \|z\| & \|N_{d2}\| &\leq \zeta_{N_{d2}} \\ \|\dot{N}_{d2}\| &\leq \zeta_{\dot{N}_{d1}} + \zeta_2 + \zeta_3 \|r\|, \end{aligned} \quad (6-40)$$

where $\rho_2, \zeta_{N_{d2}} \in \mathbb{R}$ are known positive bounding constants, and $\zeta_{\dot{N}_{d1}}, \zeta_2$, and ζ_3 are introduced in (6-19) and (6-37).

6.4 Stability Analysis

Theorem 6-1: *The adaptive controller given in (6-14), (6-22)-(6-24) ensures that the output tracking error is regulated in the sense that*

$$\|e(t)\| \rightarrow 0 \quad \text{as} \quad t \rightarrow \infty, \quad (6-41)$$

provided the control gain matrix k_s introduced in (6-22) is selected sufficiently large (see the subsequent proof), α is selected to satisfy the sufficient condition

$$\alpha \geq \frac{1}{2}\beta_0, \quad (6-42)$$

and the control gains β and β_0 are selected to satisfy the following sufficient conditions:

$$\beta > \frac{1}{\varepsilon} \left(\zeta_{N_{d2}} + \frac{1}{\alpha} \zeta_{\dot{N}_{d1}} + \frac{1}{\alpha} \zeta_2 \right) \quad \beta_0 > \frac{1}{\varepsilon} \zeta_3, \quad (6-43)$$

where $\lambda_{\min}(\cdot)$ denotes the minimum eigenvalue of the argument, β is introduced in (6-23), $\beta_0 \in R$ is introduced in (6-45), $\rho_2, \zeta_{N_{d2}}, \zeta_{\dot{N}_{d1}}, \zeta_2$, and ζ_3 are introduced in (6-19), (6-37), and (6-39), and ε is introduced in (6-17).

Before proving Theorem 6-1, the following lemma will be set forth.

Lemma 6-1: *To facilitate the subsequent stability analysis, the auxiliary function*

$P(t) \in \mathbb{R}$ *is defined as*

$$P(t) \triangleq \beta Q |e(0)| - e(0)^T N_{d2}(0) - \int_0^t L(\tau) d\tau, \quad (6-44)$$

where $|\cdot|$ denotes the 1-norm of a vector, Q is defined in (6-17), and the auxiliary function $L(t) \in \mathbb{R}$ is defined as

$$L(t) \triangleq r^T (N_{d2}(t) - T\dot{\mu}_1) - \beta_0 \|e\| \|r\|. \quad (6-45)$$

Provided the sufficient conditions in (6-43) are satisfied, the following inequality can be obtained¹³ :

$$\int_0^t L(\tau) d\tau \leq \beta Q |e(0)| - e(0)^T N_{d2}(0). \quad (6-46)$$

Hence, (6-46) can be used to conclude that $P(t) \geq 0$.

Proof: (See Theorem 6-1) Let $D \subset \mathbb{R}^{2m+p_1+1}$ be a domain containing $w(t) = 0$, where $w(t) \in \mathbb{R}^{2m+p_1+1}$ is defined as

$$w(t) \triangleq \begin{bmatrix} z^T(t) & \tilde{\theta}_A^T(t) & \sqrt{P(t)} \end{bmatrix}^T. \quad (6-47)$$

Let $V(w, t) : \mathcal{D} \times [0, \infty) \rightarrow \mathbb{R}$ be a continuously differentiable, radially unbounded function defined as

$$V \triangleq \frac{1}{2} e^T e + \frac{1}{2} r^T S^{-1} r + \frac{1}{2} \tilde{\theta}_A^T \Gamma_A^{-1} \tilde{\theta}_A + P, \quad (6-48)$$

which is positive definite provided the sufficient condition in (6-43) is satisfied (see the appendix). After taking the time derivative of (6-48) and utilizing (6-6), (6-38), (6-44),

¹³ See Appendix for the details on the bound of $\int_0^t L(\tau) d\tau$.

and (6-45), $\dot{V}(w, t)$ can be expressed as

$$\begin{aligned}\dot{V}(w, t) &= -\alpha e^T e + r^T \tilde{N}_2 - r^T (k_s + I_{m \times m}) r \\ &\quad + \beta_0 \|e\| \|r\| - \tilde{\theta}_A^T \Gamma_A^{-1} \dot{\hat{\theta}}_A + r^T Y_A \tilde{\theta}_A.\end{aligned}\tag{6-49}$$

After utilizing (6-24) and (6-40), and using the fact that

$$\|e\| \|r\| \leq \frac{1}{2} \|e\|^2 + \frac{1}{2} \|r\|^2,\tag{6-50}$$

$\dot{V}(w, t)$ can be upper bounded as

$$\begin{aligned}\dot{V}(w, t) &\leq -\lambda_1 \|z\|^2 \\ &\quad - \left[\left(\lambda_{\min}(k_s) - \frac{1}{2} \beta_0 \right) \|r\|^2 - \rho_2 \|r\| \|z\| \right],\end{aligned}\tag{6-51}$$

where $\lambda_1 \triangleq \min \{ \alpha - \frac{1}{2} \beta_0, 1 \}$. Completing the squares for the bracketed terms in (6-51) yields

$$\dot{V}(w, t) \leq - \left(\lambda_1 - \frac{\rho_2^2}{4 \left(\lambda_{\min}(k_s) - \frac{1}{2} \beta_0 \right)} \right) \|z\|^2.\tag{6-52}$$

The inequality in (6-52) can be used to show that $V(w, t) \in \mathcal{L}_\infty$; hence, $e(t), r(t), \tilde{\theta}_A(t), P(t) \in \mathcal{L}_\infty$. Given that $e(t), r(t) \in \mathcal{L}_\infty$, standard linear analysis methods can be used to prove that $\dot{e}(t) \in \mathcal{L}_\infty$ from (6-6). Since $e(t), \dot{e}(t) \in \mathcal{L}_\infty$, (6-5) can be used along with the assumption that $y_m(t), \dot{y}_m(t) \in \mathcal{L}_\infty$ to prove that $y(t), \dot{y}(t) \in \mathcal{L}_\infty$. Since $\theta_A \in \mathcal{L}_\infty$, the assumption that $x_m(t), \dot{x}_m(t) \in \mathcal{L}_\infty$ can be used along with (6-21) to prove that $Y_A(t) \in \mathcal{L}_\infty$. Given that $r(t), \hat{\theta}_A(t), Y_A(t) \in \mathcal{L}_\infty$, the assumption that $(C\hat{B})^{-1} \in \mathcal{L}_\infty$ can be used along with the time derivative of (6-22) to show that $(C\hat{B})^{-1} \dot{\mu}_0(t) \in \mathcal{L}_\infty$. Since $(C\hat{B})^{-1} \dot{\mu}_0(t) \in \mathcal{L}_\infty$ and the time derivative of (6-23) can be used to show that $\dot{\mu}_1(t) \in \mathcal{L}_\infty$, Equation 2.78 of [80] can be used to show that $(C\hat{B})^{-1} (\dot{\mu}_0(t) - \dot{\mu}_1(t))$ can be upper bounded as $\left\| (C\hat{B})^{-1} (\dot{\mu}_0(t) - \dot{\mu}_1(t)) \right\| \leq R, \forall t \geq 0$, where $R \in \mathbb{R}^+$ is a bounding constant. Given that $\left\| (C\hat{B})^{-1} (\dot{\mu}_0(t) - \dot{\mu}_1(t)) \right\| \leq R$, the time derivative of (6-14) can be used to upper bound the elements $\dot{u}_i(t) \forall i = 1, \dots, m$ of $\dot{u}(t)$ as $\dot{u}_i(t) \leq -\alpha u_i(t) + R$.

Theorem 1.1 of [81] can then be utilized to prove that $u(t) \in \mathcal{L}_\infty$. Hence, (6-38) can be used to show that $\dot{r}(t) \in \mathcal{L}_\infty$. Since $\dot{e}(t), \dot{r}(t) \in \mathcal{L}_\infty$, (6-9) can be used to show that $z(t)$ is uniformly continuous. Since $z(t)$ is uniformly continuous, $V(w, t)$ is radially unbounded, and (6-48) and (6-52) can be used to show that $z(t) \in \mathcal{L}_\infty \cap \mathcal{L}_2$, Barbalat's Lemma [82] can be invoked to state that

$$\|z(t)\| \rightarrow 0 \quad \text{as} \quad t \rightarrow \infty \quad \forall w(0) \in \mathbb{R}^{2m+p_1+1}. \quad (6-53)$$

Based on the definition of $z(t)$, (6-53) can be used to show that

$$\|e(t)\| \rightarrow 0 \quad \text{as} \quad t \rightarrow \infty \quad \forall w(0) \in \mathbb{R}^{2m+p_1+1}. \quad (6-54)$$

6.5 Simulation Results

A numerical simulation was created, which illustrates the applicability and performance of the developed control law for an unmanned air vehicle (UAV). The simulation is based on the state-space system given in (6-1) and (6-2), where the state matrix A , input authority matrix B , and nonlinear disturbance function $f(x, t)$ are defined as in (6-1).

The reference model for the simulation is represented by the state space system given in (6-3)-(6-4), where the state matrix A_m and input matrix B_m are designed with the specific purpose of decoupling the longitudinal velocity and pitch rate as well as decoupling the lateral roll rate and yaw rate. In addition to this criterion, the design is intended to exhibit favorable transient response characteristics and to achieve zero steady-state error [35, 47]. Simultaneous and uncorrelated commands are input into each of the longitudinal and lateral model simulations to illustrate that each model behaves as two completely decoupled second order systems.

The output matrices C_{lon} and C_{lat} are selected as

$$C_{lon} = \begin{bmatrix} 0 & 0 & 1 & 0 \\ 1 & 0 & 0 & 0 \end{bmatrix} \quad C_{lat} = \begin{bmatrix} 0 & 1 & 0 & 0 \\ 0 & 0 & 1 & 0 \end{bmatrix}. \quad (6-55)$$

Based on the standard assumption that the longitudinal and lateral modes of the aircraft are decoupled, the state-space model can be represented using (6-1) and (6-2), where the state matrix $A \in \mathbb{R}^{8 \times 8}$ and input matrix $B \in \mathbb{R}^{8 \times 4}$ are given as

$$A = \begin{bmatrix} A_{lon} & 0_{4 \times 4} \\ 0_{4 \times 4} & A_{lat} \end{bmatrix} \quad B = \begin{bmatrix} B_{lon} & 0_{4 \times 2} \\ 0_{4 \times 2} & B_{lat} \end{bmatrix}, \quad (6-56)$$

and the output matrix $C \in \mathbb{R}^{4 \times 8}$ is designed as

$$C = \begin{bmatrix} C_{lon} & 0_{2 \times 4} \\ 0_{2 \times 4} & C_{lat} \end{bmatrix}. \quad (6-57)$$

In (6-56) and (6-57), $A_{lon}, A_{lat} \in \mathbb{R}^{4 \times 4}$, $B_{lon}, B_{lat} \in \mathbb{R}^{4 \times 2}$, and $C_{lon}, C_{lat} \in \mathbb{R}^{2 \times 4}$ denote the state matrices, input matrices, and output matrices, respectively, for the longitudinal and lateral subsystems, and the notation $0_{i \times j}$ denotes an $i \times j$ matrix of zeros. The state-vector $x(t) \in \mathbb{R}^8$ is given as

$$x = \begin{bmatrix} x_{lon}^T & x_{lat}^T \end{bmatrix}^T, \quad (6-58)$$

where $x_{lon}(t), x_{lat}(t) \in \mathbb{R}^4$ denote the longitudinal and lateral state vectors defined as

$$x_{lon} \triangleq \begin{bmatrix} V & \alpha & q & \theta \end{bmatrix}^T \quad (6-59)$$

$$x_{lat} \triangleq \begin{bmatrix} \beta & p & r & \phi \end{bmatrix}^T, \quad (6-60)$$

where the components of the state are defined as

$$\begin{aligned} V &= \text{velocity} & \alpha &= \text{angle of attack} \\ q &= \text{pitch rate} & \theta &= \text{pitch angle} \\ \beta &= \text{sideslip angle} & p &= \text{roll rate} \\ r &= \text{yaw rate} & \phi &= \text{bank angle} \end{aligned}$$

and the control input vector is defined as

$$\begin{aligned} u &\triangleq \begin{bmatrix} u_{lon}^T & u_{lat}^T \end{bmatrix}^T \\ &= \begin{bmatrix} \delta_{elev} & \delta_{thrust} & \delta_{ail} & \delta_{rud} \end{bmatrix}^T. \end{aligned} \quad (6-61)$$

In (6-61), $\delta_{elev}(t) \in \mathbb{R}$ denotes the elevator deflection angle, $\delta_{thrust}(t) \in \mathbb{R}$ is the control thrust, $\delta_{ail}(t) \in \mathbb{R}$ is the aileron deflection angle, and $\delta_{rud}(t) \in \mathbb{R}$ is the rudder deflection angle. The state and input matrices for the longitudinal and lateral dynamic models of the Osprey fixed-wing aircraft flying at 25 m/s at an altitude of 60 meters are given as [35, 47]

$$A_{lon} = \begin{bmatrix} -0.15 & 11.08 & 0.08 & 0 \\ -0.03 & -7.17 & 0.83 & 0 \\ 0 & -37.35 & -9.96 & 0 \\ 0 & 0 & 1.00 & 0 \end{bmatrix} \quad (6-62)$$

$$A_{lat} = \begin{bmatrix} -0.69 & -0.03 & -0.99 & 0 \\ -3.13 & -12.92 & 1.10 & 0 \\ 17.03 & -0.10 & -0.97 & 0 \\ 0 & 1.00 & -0.03 & 0 \end{bmatrix} \quad (6-63)$$

$$B_{lon} = \begin{bmatrix} 3E^{-3} & 0.06 \\ 1E^{-5} & 1E^{-4} \\ -0.98 & 0 \\ 0 & 0 \end{bmatrix} \quad B_{lat} = \begin{bmatrix} 0 & 0 \\ 1.50 & -0.02 \\ -0.09 & -0.17 \\ 0 & 0 \end{bmatrix}, \quad (6-64)$$

respectively. The nonlinear disturbance terms, denoted $f(x_{lon})$ and $f(x_{lat})$, are defined as

$$f(x_{lon}) = \begin{bmatrix} -9.81 \sin \theta + g(x) & 0 & 0 & 0 \end{bmatrix}^T \quad (6-65)$$

$$f(x_{lat}) = \begin{bmatrix} 0.39 \sin \phi & 0 & 0 & 0 \end{bmatrix}^T, \quad (6-66)$$

where $g(x)$ represents a disturbance due to a discrete vertical wind gust as defined in [73], and the trigonometric terms in $f(x_{lon})$ and $f(x_{lat})$ represent nonlinear dependence on gravity. All states, control inputs, and adaptive estimates were initialized to zero for the simulation.

The feedforward estimates \hat{B}_{lon} and \hat{B}_{lat} were selected as

$$\hat{B}_{lon} = \begin{bmatrix} 0 & 0.2 \\ 0.1 & 0 \\ -1.5 & 0 \\ 0 & 0 \end{bmatrix} \quad \hat{B}_{lat} = \begin{bmatrix} 0 & 0 \\ 1 & 0 \\ -0.5 & -0.25 \\ 0 & 0 \end{bmatrix}. \quad (6-67)$$

Remark 1. For the choices for \hat{B}_{lon} and \hat{B}_{lat} given in (6-67), Assumption 3 is satisfied. Specifically, the choice for \hat{B}_{lon} yields the following:

$$\min_{j \in (1, m-1)} \left\{ |T_{jj}| - \sum_{k=j+1}^m |T_{jk}| \right\} = 0.997 > \varepsilon > 0, \quad (6-68)$$

and the choice for \hat{B}_{lat} yields

$$\min_{j \in (1, m-1)} \left\{ |T_{jj}| - \sum_{k=j+1}^m |T_{jk}| \right\} = 0.890 > \varepsilon > 0. \quad (6-69)$$

In order to develop a realistic stepping stone to an actual experimental demonstration of the proposed controller, the simulation parameters were selected based on detailed data analyses and specifications. The sensor noise values are based on Cloud Cap Technology's Piccolo Autopilot and analysis of data logged during straight and level flight. These values are also corroborated with the specifications given for Cloud Cap Technology's Crista Inertial Measurement Unit (IMU). The simulation parameters are summarized in Table I.

The objectives for the longitudinal controller simulation are to track pitch rate and forward velocity commands. For the lateral controller simulation, the objectives are to track roll rate and yaw rate commands. Fig. 6-1 shows the simulation results of the closed-loop longitudinal system with control gains selected as follows (e.g., see (6-14),

Table 6-1. Parameters Used in the Controller Simulations.

Pitch Rate Sensor Noise	$\pm 1.7^\circ / \text{sec}$
Velocity Sensor Noise	$\pm 0.4 \text{ m} / \text{sec}$
Roll Rate Sensor Noise	$\pm 1.7^\circ / \text{sec}$
Yaw Rate Sensor Noise	$\pm 1.7^\circ / \text{sec}$
Control Thrust Saturation Limit	$\pm 200 \text{ N}$
Control Thrust Rate Limit	$\pm 200 \text{ N} / \text{sec}$
Elevator Saturation Limit	$\pm 30^\circ$
Elevator Rate Limit	$\pm 300^\circ / \text{sec}$
Aileron Saturation Limit	$\pm 30^\circ$
Aileron Rate Limit	$\pm 300^\circ / \text{sec}$
Rudder Saturation Limit	$\pm 30^\circ$
Rudder Rate Limit	$\pm 300^\circ / \text{sec}$

(6-22), and (6-24)):

$$\beta = \text{diag} \left\{ \begin{array}{cc} 0.3 & 10 \end{array} \right\} \quad k_s = \text{diag} \left\{ \begin{array}{cc} 0.1 & 34 \end{array} \right\}$$

$$\alpha = 1.2 \quad \Gamma_A = 10^{-5} I_{4 \times 4}$$

where the notation $I_{j \times j}$ denotes the $j \times j$ identity matrix. Fig. 6-1 also shows the simulation results of the closed-loop lateral system with control gains selected as

$$\beta = \text{diag} \left\{ \begin{array}{cc} 0.3 & 0.7 \end{array} \right\} \quad k_s = \text{diag} \left\{ \begin{array}{cc} 0.1 & 2.1 \end{array} \right\}$$

$$\alpha = 2.7 \quad \Gamma_A = 10^{-6} I_{4 \times 4}$$

Fig. 6-2 shows the control effort used during closed-loop operation. Specifically, Fig. 6-2 shows the elevator deflection angle and thrust used during closed-loop longitudinal controller operation and the aileron and rudder deflection angle used during closed-loop lateral controller operation.

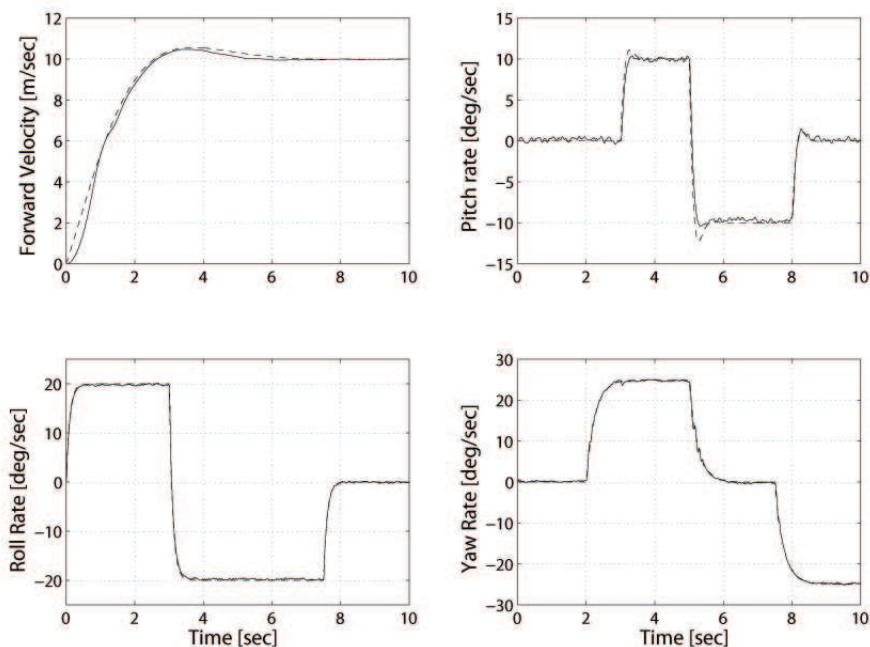


Figure 6-1. Reference and actual forward velocity (top left), pitch rate (top right), roll rate (bottom left), and yaw rate (bottom right) responses during closed-loop longitudinal and lateral controller operation.

6.6 Conclusion

A controller is presented, which achieves global asymptotic tracking of a model reference system, where the plant dynamics contain an uncertain input matrix and an unknown additive disturbance. This result represents application of a continuous control strategy in a robust ADI framework to a dynamic system with nonlinear, non-vanishing, non-LP disturbances, where the control input is multiplied by a non-square, column deficient matrix containing parametric uncertainty. By exploiting partial knowledge of the dynamic model, we are able to prove a global asymptotic tracking result while weakening some common restrictive assumptions concerning the system uncertainty. A Lyapunov-based stability analysis is provided to verify the theoretical result, and numerical simulation results are provided to demonstrate the performance of the proposed controller.

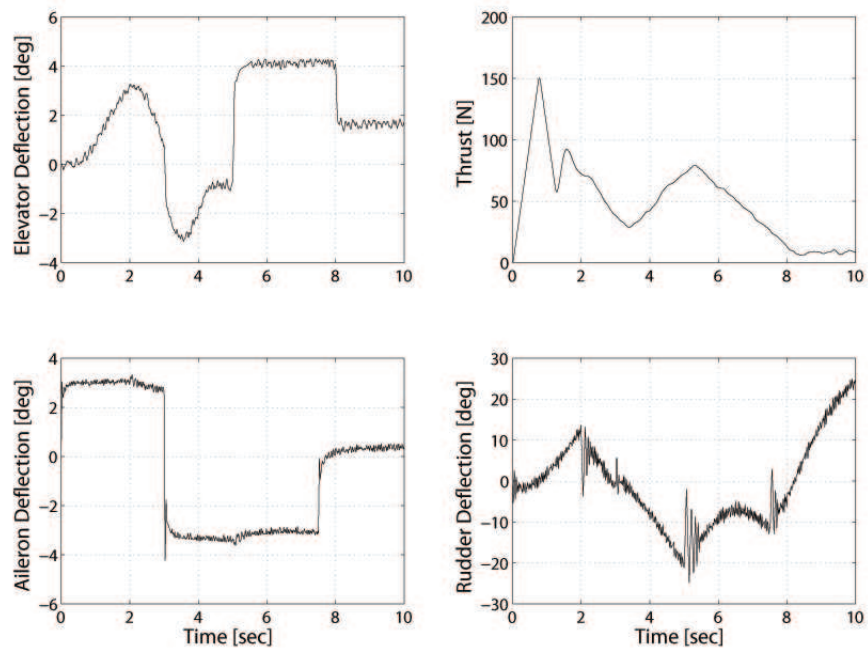


Figure 6-2. Control input elevator deflection (top left), thrust (top right), aileron deflection (bottom left), and rudder deflection (bottom right) used during closed-loop longitudinal and lateral controller operation.

CHAPTER 7 CONTRIBUTIONS AND FUTURE RESEARCH PLANS

7.1 Contributions of Previous Research

The contributions of the research in this dissertation up to this point are as follows:

- An singularity-robust attitude tracking controller for a rigid body satellite was developed, which adapts for parametric uncertainty in the satellite inertia matrix in addition to uncertainties in the input torque caused by static and dynamic CMG gimbal friction.
- A NN-based adaptive attitude tracking controller for a rigid body satellite was designed, which achieves UUB attitude tracking for a rigid-body satellite in the presence of general (i.e., non-LP) exogenous disturbances, parametric uncertainty in the satellite inertia matrix, and uncertainties in the input torque caused by static and dynamic CMG gimbal friction and electromechanical disturbances in the gimbal servo loops.
- The attitude controllers presented here are suitable for small-sats, for which significant disturbances resulting from the motion of the CMGs exist.
- An aircraft controller was developed, which achieves asymptotic tracking control of a model reference system where the plant dynamics contain input uncertainty and a non-LP disturbance. This result represents the first ever application of a continuous control strategy in a DI and MRAC framework to a nonlinear system with additive, non-LP disturbances, where the control input is multiplied by a non-square matrix containing parametric uncertainty.
- An aircraft controller was developed, which achieves asymptotic tracking control of a model reference system where the plant dynamics contain input uncertainty and a non-LP disturbance. This result represents application of a continuous control strategy in an ADI framework to a nonlinear system with additive, non-LP disturbances, where the control input is multiplied by a non-square matrix containing parametric uncertainty.

7.2 Limitations of Previous Research

- Attitude controller designs presented in Chapters 2 and 3 have only been able to achieve uniformly ultimately bounded tracking result (i.e., not asymptotic).
- All controllers proposed thus far have been designed to handle systems which are affine in the control input.

7.3 Proposed Research Plans

- Improve the CMG attitude control design to achieve an asymptotic tracking result (e.g., using RISE or a single network adaptive critic (SNAC) neural network).
- Design a controller capable of achieving asymptotic tracking for nonaffine-in-control dynamic systems (building on research by N. Hovakimyan, for example).
- Experimentally validate the NN-based adaptive attitude controller presented in Chapter 3.

APPENDIX: PROOF OF LEMMAS 4-1 AND 6-1

Lemma 4-1: Provided the sufficient condition in (4-37) is satisfied, the following inequality can be obtained :

$$\begin{aligned} \int_0^t L(\tau) d\tau &\leq \beta \|e(0)\| \|\Lambda\| - e(0)^T N_d(0) \\ &\quad + \sqrt{m} \int_0^t \beta \|\Delta\| \|r(\tau)\| d\tau. \end{aligned} \quad (\text{A-1})$$

Hence, (A-1) can be used to conclude that $P(t) \geq 0$.

Proof: Integrating both sides of (4-40) yields

$$\int_0^t L(\tau) d\tau = \int_0^t r(\tau)^T \left(N_d(\tau) - \beta \tilde{\Omega} \text{sgn}(e(\tau)) \right) d\tau. \quad (\text{A-2})$$

Substituting (4-20) into (A-2), utilizing (4-33), and rearranging yields

$$\begin{aligned} \int_0^t L(\tau) d\tau &= \int_0^t \left(\frac{\partial e(\tau)}{\partial \tau} \right)^T N_d(\tau) d\tau \\ &\quad - \int_0^t \left(\frac{\partial e(\tau)}{\partial \tau} \right)^T \beta \Lambda \text{sgn}(e(\tau)) d\tau \\ &\quad + \int_0^t \alpha e(\tau)^T (N_d(\tau) - \beta \Lambda \text{sgn}(e(\tau))) d\tau \\ &\quad - \int_0^t r(\tau)^T \beta \Delta \text{sgn}(e(\tau)) d\tau. \end{aligned} \quad (\text{A-3})$$

Integrating the first integral in (A-3) using integration by parts,

$$\begin{aligned} \int_0^t L(\tau) d\tau &= e(\tau)^T N_d(\tau) \Big|_0^t - \int_0^t e(\tau)^T \frac{\partial N_d(\tau)}{\partial \tau} d\tau \\ &\quad - \int_0^t \left(\frac{\partial e(\tau)}{\partial \tau} \right)^T \beta \Lambda \text{sgn}(e(\tau)) d\tau \\ &\quad + \int_0^t \alpha e(\tau)^T (N_d(\tau) - \beta \Lambda \text{sgn}(e(\tau))) d\tau \\ &\quad - \int_0^t r(\tau)^T \beta \Delta \text{sgn}(e(\tau)) d\tau. \end{aligned} \quad (\text{A-4})$$

From (A-4), the following bound can be obtained:

$$\begin{aligned}
\int_0^t L(\tau) d\tau &\leq \int_0^t \alpha \|e(\tau)\| (\|N_d(\tau)\| \\
&\quad + \frac{1}{\alpha} \left\| \frac{\partial N_d(\tau)}{\partial \tau} \right\| - \beta \lambda_{\min}(\Lambda)) d\tau \\
&\quad + \|e(t)\| (\|N_d(t)\| - \beta \lambda_{\min}(\Lambda)) \\
&\quad + \beta \|\Lambda\| \|e(0)\| - e(0)^T N_d(0) \\
&\quad + \sqrt{m} \int_0^t \beta \|\Delta\| \|r(\tau)\| d\tau,
\end{aligned} \tag{A-5}$$

where m was defined in (4-1). Thus, it is clear from (A-5) that if β satisfies (4-37), then (A-1) holds.

Lemma 6-1: Provided the control gains β and β_0 introduced in (6-23) and (6-45), respectively, are selected according to the sufficient conditions in (6-43), the following inequality can be obtained:

$$\int_0^t L(\tau) d\tau \leq \beta Q |e(0)| - e(0)^T N_{d2}(0). \tag{A-6}$$

Hence, (A-6) can be used to conclude that $P(t) \geq 0$, where $P(t)$ is defined in (6-44).

Proof: Integrating both sides of (6-45) yields

$$\begin{aligned}
\int_0^t L(\tau) d\tau &= \int_0^t \left(\sum_{i=1}^m r_i(\tau) \left(- \sum_{j=i}^m T_{ij} \dot{\mu}_{1j}(\tau) \right. \right. \\
&\quad \left. \left. N_{d2_i}(\tau) - \beta_0 \sum_{i=1}^m |e_i(\tau)| |r_i(\tau)| \right) \right) d\tau,
\end{aligned} \tag{A-7}$$

where $e_i(t), r_i(t), N_{d2_i}(t), \dot{\mu}_{1_i}(t) \in \mathbb{R}$ denote the i^{th} elements of $r(t), N_{d2}(t)$, and $\dot{\mu}_1(t)$, respectively, and T_{ij} is introduced in (6-17). Substituting (6-6) into (A-7), rearranging,

and performing integration by parts, (A-7) can be expressed as

$$\begin{aligned}
\int_0^t L(\tau) d\tau &= \sum_{i=1}^m e_i(\tau) N_{d_{2i}}(\tau) \Big|_0^t \\
&\quad - \int_0^t \sum_{i=1}^m e_i(\tau) \frac{\partial N_{d_{2i}}(\tau)}{\partial \tau} d\tau \\
&\quad - \int_0^t \sum_{i=1}^m \frac{\partial e_i(\tau)}{\partial \tau} \beta(\operatorname{sgn}(e_i(\tau))) \\
&\quad \quad + \sum_{j=i+1}^m \bar{T}_{ij} \operatorname{sgn}(e_j(\tau)) \Big) d\tau \\
&+ \int_0^t \sum_{i=1}^m \alpha e_i(\tau) (N_{d_{2i}}(\tau) - \beta(\operatorname{sgn}(e_i(\tau))) \\
&\quad \quad + \sum_{j=i+1}^m \bar{T}_{ij} \operatorname{sgn}(e_j(\tau))) \Big) d\tau \\
&\quad - \int_0^t \beta_0 \sum_{i=1}^m |e_i(\tau)| |r_i(\tau)| d\tau.
\end{aligned} \tag{A-8}$$

In (A-8), the fact that $\sum_{j=i}^m T_{ij} \dot{\mu}_{1_j}(t)$ is given by

$$\sum_{j=i}^m T_{ij} \dot{\mu}_{1_j}(t) = \beta \left(\operatorname{sgn}(e_i(t)) + \sum_{j=i+1}^m \bar{T}_{ij} \operatorname{sgn}(e_j(t)) \right) \tag{A-9}$$

$\forall i = 1, \dots, m-1$ was utilized (note that $\bar{T}_{mm} = 0$ since \bar{T} is strictly upper triangular).

Based on Assumption 3, the following equation holds $\forall i = 1, \dots, m-1$:

$$\operatorname{sgn}(e_i(t)) + \sum_{j=i+1}^m \bar{T}_{ij} \operatorname{sgn}(e_j(t)) = \phi \operatorname{sgn}(e_i(t)), \tag{A-10}$$

where $\phi \in \mathbb{R}^+$ is a parameter satisfying $\varepsilon \leq \phi \leq Q$, with ε and Q defined as in (6-17). By using (A-10) along with the fact that

$$\frac{\partial N_{d_2}(\tau)}{\partial \tau} = \frac{\partial N_{d_1}(\tau)}{\partial \tau} + N_{B_1}(\tau) + N_{B_2}(\tau), \tag{A-11}$$

the expression in (A-8) can be expressed as

$$\begin{aligned}
\int_0^t L(\tau) d\tau &= \sum_{i=1}^m e_i(\tau) N_{d2_i}(\tau)|_0^t \\
&- \int_0^t \sum_{i=1}^m e_i(\tau) \left(\frac{\partial N_{d1_i}(\tau)}{\partial \tau} + N_{B1}(\tau) \right) d\tau \\
&- \int_0^t \sum_{i=1}^m e_i(\tau) N_{B2}(\tau) d\tau \\
&- \int_0^t \sum_{i=1}^m \frac{\partial e_i(\tau)}{\partial \tau} \beta \operatorname{sgn}(e_i(\tau)) d\tau \\
&+ \int_0^t \sum_{i=1}^m \alpha e_i(\tau) (N_{d2_i}(\tau) - \beta \phi \operatorname{sgn}(e_i(\tau))) d\tau \\
&- \int_0^t \beta_0 \sum_{i=1}^m |e_i(\tau)| |r_i(\tau)| d\tau.
\end{aligned} \tag{A-12}$$

After exploiting the fact that

$$\int_0^t \frac{\partial e_i(\tau)}{\partial \tau} \beta \phi \operatorname{sgn}(e_i(\tau)) d\tau = \beta \phi |e_i(t)| - \beta \phi |e_i(0)| \tag{A-13}$$

and using (6-19), (6-37), and (6-40), (A-12) can be upper bounded as

$$\begin{aligned}
\int_0^t L(\tau) d\tau &\leq \int_0^t \sum_{i=1}^m \alpha |e_i(\tau)| (\zeta_{N_{d2}} \\
&+ \frac{1}{\alpha} \zeta_{\dot{N}_{d1}} + \frac{1}{\alpha} \zeta_2 - \varepsilon \beta) d\tau \\
&+ \int_0^t \zeta_3 \sum_{i=1}^m |e_i(\tau)| |r_i(\tau)| d\tau \\
&+ \sum_{i=1}^m |e_i(t)| (\zeta_{N_{d2}} - \varepsilon \beta) \\
&+ \sum_{i=1}^m (\beta Q |e_i(0)| - e_i(0) N_{d2_i}(0)) \\
&- \int_0^t \beta_0 \sum_{i=1}^m |e_i(\tau)| |r_i(\tau)| d\tau.
\end{aligned} \tag{A-14}$$

Thus, it is clear from (A-14) that if β and β_0 satisfy (6-43), then (A-6) holds.

REFERENCES

- [1] A. Cebrowski and J. Raymond, "Operationally responsive space: A new defense business model," *Parameters*, vol. Vol. 35, no. 2, pp. 67–77, 2005.
- [2] B. Costic, D. Dawson, M. de Queiroz, and V. Kapila, "A quaternion-based adaptive attitude tracking controller without velocity measurements," in *Proc. of the IEEE Conf. on Decision and Control*, vol. 3, Sydney, Australia, Dec. 2000, pp. 2424–2429.
- [3] J. Kim and J. Crassidis, "Robust spacecraft attitude control using model-error control synthesis," in *AIAA Guidance, Navigation, and Control Conf.*, Monterey, CA, Aug. 2002.
- [4] H. Pan, H. Wong, and V. Kapila, "Output feedback control for spacecraft with coupled translation and attitude dynamics," in *Proc. of IEEE Conf. on Decision and Control*, Paradise Island, Bahamas, Dec. 2004, pp. 4453–4458.
- [5] K. Subbarao and M. R. Akella, "Differentiator-free nonlinear proportional-integral controllers for rigid-body attitude stabilization," in *AAS/AIAA 14th Space Flight Mechanics Meeting*, vol. 27, no. 6, 2004, pp. 1092–1096.
- [6] V. Lappas, W. Steyn, and C. Underwood, "Design and testing of a control moment gyroscope cluster for small satellites," *Journal of Spacecraft and Rockets*, vol. 42, no. 4, pp. 729–739, 2005.
- [7] K. Omagari, T. Usuda, and S. Matunaga, "Research of control momentum gyros for micro-satellites and 3-DOF attitude dynamics simulator experiments," in *Proc. of the Int'l Symposium on Artificial Intelligence, Robotics and Automation in Space*, Munich, Germany, 2005.
- [8] D. M. Harland and R. D. Lorenz, *Space Systems Failures.*, J. Mason, Ed. Springer-Praxis, 2005.
- [9] K. KrishnaKumar, "Adaptive neuro-control for spacecraft attitude control," in *Proc. of the IEEE Conf. on Control Applications*, Aug. 1994.
- [10] Y. Liu, J. Cao, and N. Wang, "Attitude and vibration control of flexible spacecraft using adaptive inverse disturbance canceling," in *Int'l Joint Conf. on Neural Networks*, Vancouver, BC, Canada, July 2006.
- [11] M.-T. Choi and H. Flashner, "Neural-network-based spacecraft attitude control and momentum management," in *AIAA Guidance, Navigation, and Control Conf.*, Denver, CO, Aug. 2000.
- [12] —, "Neural-network-based spacecraft attitude control," in *AIAA Guidance, Navigation, and Control Conf.*, Denver, CO, Aug. 2000.
- [13] N. Sadati, A. Meghdari, and N. Dadkhah, "Optimal tracking neuro-controller in satellite attitude control," in *IEEE Int'l Conf. on Industrial Technology*, Dec. 2002.

- [14] N. Sadati, N. d. Tehrani, and H. R. Bolandhemmat, "Multivariable adaptive satellite attitude controller design using RBF neural network," in *Proc. of the IEEE Int'l Conf. on Networking, Sensing and Control*, Taipei, Taiwan, Mar. 2004.
- [15] N. Sivaprakash and J. Shanmugam, "Neural network based three axis satellite attitude control using only magnetic torquers," in *Digital Avionics Systems Conf.*, Nov. 2005.
- [16] C. W. Tan, S. Park, K. Mostov, and P. Varaiya, "Design of gyroscope-free navigation systems," in *IEEE Int'l Conf. on Intelligent Transportation Systems*, 2001, pp. 286–291.
- [17] N. Unnikrishnan, S. N. Balakrishnan, and R. Padhi, "Dynamic re-optimization of a spacecraft attitude controller in the presence of uncertainties," in *Proc. of IEEE Int'l Symposium on Intelligent Control*, Munich, Germany, Oct. 2006.
- [18] P. Singla, K. Subbarao, and J. L. Junkins, "Adaptive output feedback control for spacecraft rendezvous and docking under measurement uncertainty," *Journal of Guidance, Control, and Dynamics*, vol. 29, no. 4, pp. 892–902, 2006.
- [19] H. Wong, M. de Queiroz, and V. Kapila, "Adaptive tracking control using synthesized velocity from attitude measurements," in *Proc. of the American Control Conf.*, vol. 3, 2000, pp. 1572–1576.
- [20] K. A. Ford and C. D. Hall, "Singular direction avoidance steering for control-moment gyros," *Journal of Guidance, Control, and Dynamics*, vol. 23, no. 4, pp. 648–656, 2000.
- [21] Y. Nakamura and H. Hanafusa, "Inverse kinematic solutions with singularity robustness for robot manipulator control," *Journal of Dynamic Systems, Measurement, and Control*, vol. 108, no. 3, pp. 163–171, 1986.
- [22] N. Bedrossian, J. Paradiso, E. Bergmann, and D. Rowell, "Steering law designs for redundant SGCMG systems," *AIAA J. Guidance & Control*, vol. 13, no. 6, pp. 1083–1089, 1991.
- [23] W. MacKunis, K. Dupree, N. Fitz-Coy, and W. E. Dixon, "Adaptive satellite attitude control in the presence of inertia and CMG gimbal friction uncertainties," in *Proc. AIAA Guidance, Navigation, and Control Conf.*, Hilton Head, SC, Aug. 2007, AIAA-2007-6432.
- [24] A. Moutinho and J. R. Azinheira, "Stability and robustness analysis of the AURORA airship control system using dynamic inversion," in *Proc. of Int'l Conf. on Robotics and Automation*, Barcelona, Spain, April 2005, pp. 2265–2270.
- [25] M. W. Oppenheimer and D. B. Doman, "Control of an unstable, nonminimum phase hypersonic vehicle model," in *Proc. of the IEEE Aerospace Conf.*, Big Sky, MT, Mar. 2006, pp. 1–7.

- [26] S. Onori, P. Dorato, S. Galeani, and C. Abdallah, “Finite time stability design via feedback linearization,” in *Proc. of Conf. on Decision and Control, and the European Control Conf.*, Seville, Spain, Dec. 2005, pp. 4915–4920.
- [27] Z. Szabo, P. Gaspar, and J. Bokor, “Tracking design for Wiener systems based on dynamic inversion,” in *Proc. of Int’l Conf. on Control Applications*, Munich, Germany, Oct. 2006, pp. 1386–1391.
- [28] J. Chen, D. Li, X. Jiang, and X. Sun, “Adaptive feedback linearization control of a flexible spacecraft,” in *Proc. of Conf. on Intelligent Systems Design and Applications*, Jinan, China, Oct. 2006, pp. 225–230.
- [29] A. D. Ngo and D. B. Doman, “Dynamic inversion-based adaptive/reconfigurable control of the X-33 on ascent,” in *Proc. of IEEE Aerospace Conference*, Big Sky, MT, Mar. 2006, pp. 2683–2697.
- [30] M. D. Tandale and J. Valasek, “Adaptive dynamic inversion control of a linear scalar plant with constrained control inputs,” in *Proc. of American Control Conf.*, Portland, OR, June 2005, pp. 2064–2069.
- [31] N. Hovakimyan, E. Lavretsky, and A. Sasane, “Dynamic inversion for nonaffine-in-control systems via time-scale separation: Part I,” in *Proc. of American Control Conf.*, Portland, OR, June 2005, pp. 3542–3547.
- [32] N. Hovakimyan, E. Lavretsky, and C. Cao, “Dynamic inversion of multi-input nonaffine systems via time-scale separation,” in *Proc. of American Control Conf.*, Minneapolis, MN, June 2006, pp. 3594–3599.
- [33] E. Lavretsky and N. Hovakimyan, “Adaptive dynamic inversion for nonaffine-in-control systems via time-scale separation: part II,” in *Proc. of American Control Conf.*, Portland, OR, June 2005, pp. 3548–3553.
- [34] J. Buffington and A. Sparks, “Comparison of dynamic inversion and LPV tailless flight control law designs,” in *Proc. of American Control Conf.*, vol. 2, Philadelphia, PA, June 1998, pp. 1145–1149.
- [35] W. MacKunis, M. K. Kaiser, P. M. Patre, and W. E. Dixon, “Asymptotic tracking for aircraft via an uncertain dynamic inversion method,” in *Proc. American Control Conf.*, Seattle, WA, June 2008, pp. 3482–3487.
- [36] Q. Wang and R. F. Stengel, “Robust nonlinear flight control of a high-performance aircraft,” *IEEE Transactions on Control Systems Technology*, vol. 13, no. 1, pp. 15–26, Jan. 2005.
- [37] T. Yamasaki, H. Sakaida, K. Enomoto, H. Takano, and Y. Baba, “Robust trajectory-tracking method for UAV guidance using proportional navigation,” in *Int’l Conf. on Control, Automation and Systems*, Seoul, Korea, Oct. 2007, pp. 1404–1409.

- [38] Z. Liu, F. Zhou, and J. Zhou, "Flight control of unpowered flying vehicle based on robust dynamic inversion," in *Chinese Control Conference*, Heilongjiang, China, Aug. 2006, pp. 693–698.
- [39] J. Cheng, H. Li, and Y. Zhang, "Robust low-cost sliding mode overload control for uncertain agile missile model," in *Proc. of World Congress on Intelligent Control and Automation*, Dalian, China, June 2006, pp. 2185–2188.
- [40] X.-J. Liu, F. Lara-Rosano, and C. W. Chan, "Model-reference adaptive control based on neurofuzzy networks," *IEEE Transactions on Systems, Man, and Cybernetics C*, vol. 34, no. 3, pp. 302–309, Aug. 2004.
- [41] X. Zhang, D. Dawson, M. de Queiroz, and B. Xian, "Adaptive control for a class of MIMO nonlinear systems with non-symmetric input matrix," in *Proc. International Conf. on Control Applications*, Taipei, Taiwan, Sep. 2004, pp. 1324–1329.
- [42] A. S. Morse, "A gain matrix decomposition and some of its properties," *Systems and Control Letters*, vol. 21, no. 1, pp. 1–10, July 1993.
- [43] R. R. Costa, L. Hsu, A. K. Imai, and P. Kokotovic, "Lyapunov-based adaptive control of MIMO systems," *Automatica*, vol. 39, no. 7, pp. 1251–1257, July 2003.
- [44] A. Behal, V. M. Rao, and P. Marzocca, "Adaptive control for a nonlinear wing section with multiple flaps," *Journal of Guidance, Control, and Dynamics*, vol. 29, no. 3, pp. 744–748, 2006.
- [45] K. K. Reddy, J. Chen, A. Behal, and P. Marzocca, "Multi-input/multi-output adaptive output feedback control design for aeroelastic vibration suppression," *Journal of Guidance, Control, and Dynamics*, vol. 30, no. 4, pp. 1040–1048, 2007.
- [46] C. C. Cheah, C. Liu, and J. J. E. Slotine, "Adaptive Jacobian tracking control of robots with uncertainties in kinematic, dynamic and actuator models," *IEEE Transactions on Automatic Control*, vol. 51, no. 6, pp. 1024–1029, June 2006.
- [47] W. MacKunis, M. K. Kaiser, P. M. Patre, and W. E. Dixon, "Adaptive dynamic inversion for asymptotic tracking of an aircraft reference model," in *Proc. AIAA Guidance, Navigation, and Control Conf.*, Honolulu, HI, 2008, AIAA-2008-6792.
- [48] A. Calise and R. Rysdyk, "Nonlinear adaptive flight control using neural networks," *IEEE Control System Magazine*, vol. 18, no. 6, pp. 14–25, Dec. 1998.
- [49] J. Leitner, A. Calise, and J. V. R. Prasad, "Analysis of adaptive neural networks for helicopter flight controls," *Journal of Guidance, Control and Dynamics*, vol. 20, no. 5, pp. 972–979, Sept. 1997.
- [50] Y. Shin, "Neural network based adaptive control for nonlinear dynamic regimes," Ph.D. dissertation, Georgia Technical Institute, November 2005.

- [51] E. Lavretsky and N. Hovakimyan, “Adaptive compensation of control dependent modeling uncertainties using time-scale separation,” in *Proc. of Conf. on Decision and Control, and the European Control Conf.*, Seville, Spain, Dec. 2005, pp. 2230–2235.
- [52] B. Xian, D. M. Dawson, M. S. de Queiroz, and J. Chen, “A continuous asymptotic tracking control strategy for uncertain nonlinear systems,” *IEEE Transactions on Automatic Control*, vol. 49, no. 7, pp. 1206–1211, July 2004.
- [53] P. M. Patre, W. MacKunis, C. Makkar, and W. E. Dixon, “Asymptotic tracking for systems with structured and unstructured uncertainties,” in *Proc. of Conf. on Decision and Control*, San Diego, CA, Dec. 2006, pp. 441–446.
- [54] Z. Cai, M. S. de Queiroz, and D. M. Dawson, “Robust adaptive asymptotic tracking of nonlinear systems with additive disturbance,” *IEEE Transactions on Automatic Control*, vol. 51, no. 3, pp. 524–529, Mar. 2006.
- [55] B. Xian, M. S. de Queiroz, and D. M. Dawson, *A Continuous Control Mechanism for Uncertain Nonlinear Systems in Optimal Control, Stabilization, and Nonsmooth Analysis*. Heidelberg, Germany: Springer-Verlag, 2004.
- [56] X. Zhang, A. Behal, D. M. Dawson, and B. Xian, “Output feedback control for a class of uncertain MIMO nonlinear systems with non-symmetric input gain matrix,” in *Proc. Conf. on Decision and Control, and the European Control Conf.*, Seville, Spain, Dec. 2005, pp. 7762–7767.
- [57] M. L. McIntyre, W. E. Dixon, D. M. Dawson, and I. D. Walker, “Fault identification for robot manipulators,” *IEEE Transactions on Robotics and Automation*, vol. 21, no. 5, pp. 1028–1034, Oct. 2005.
- [58] S. Gupta, D. Aiken, G. Hu, and W. E. Dixon, “Lyapunov-based range and motion identification for a nonaffine perspective dynamic system,” in *Proc. American Control Conf.*, Minneapolis, MN, June 2006, pp. 4471–4476.
- [59] W. E. Dixon, Y. Fang, D. M. Dawson, and T. J. Flynn, “Range identification for perspective vision systems,” *IEEE Transactions on Automatic Control*, vol. 48, no. 12, pp. 2232–2238, Dec. 2003.
- [60] A. Behal, D. M. Dawson, W. E. Dixon, and Y. Fang, “Tracking and regulation control of an underactuated surface vessel with nonintegrable dynamics,” in *Proc. of Conf. on Decision and Control*, vol. 3, Sydney, Australia, Dec. 2000, pp. 2150–2155.
- [61] N. Hovakimyan, F. Nardi, A. Calise, and N. Kim, “Adaptive output feedback control of uncertain nonlinear systems using single-hidden-layer neural networks,” *IEEE Transactions on Neural Networks*, vol. 13, no. 6, pp. 1420–1431, Nov. 2002.
- [62] P. Hughes, *Spacecraft Attitude Dynamics*. New York: Wiley, 1994.

- [63] T. Kane, P. Likins, and D. Levinson, *Spacecraft Dynamics*. McGraw-Hill, New York, 1983.
- [64] F. Leve, A. Tatsch, and N. Fitz-Coy, “A scalable control moment gyro design for attitude control of micro-, nano-, and pico-class satellites,” in *AAS Guidance and Control Conf.*, Breckenridge, CO, 2007.
- [65] C. J. Heiberg, D. Bailey, and B. Wie, “Precision spacecraft pointing using single-gimbal control moment gyroscopes with disturbance,” *Journal of Guidance, Control, and Dynamics*, vol. 23, no. 1, Jan. 2000.
- [66] S. Di Gennaro, “Adaptive robust stabilization of rigid spacecraft in presence of disturbances,” in *Proc. of Conf. on Decision & Control*, New Orleans, LA, Dec. 1995, pp. 1147–1152.
- [67] W. E. Dixon, A. Behal, D. M. Dawson, and S. P. Nagarkatti, *Nonlinear Control of Engineering Systems: a Lyapunov-Based Approach*. Boston: Birkhuser, 2003.
- [68] F. L. Lewis, “Nonlinear network structures for feedback control,” *Asian Journal of Control*, vol. 1, no. 4, pp. 205–228, 1999.
- [69] F. L. Lewis, J. Campos, and R. Selmic, “Neuro-fuzzy control of industrial systems with actuator nonlinearities,” *SIAM*, 2002.
- [70] F. L. Lewis, A. Yesildirek, and K. Liu, “Multi-layer neural network controller with guaranteed tracking performance,” *IEEE Transactions on Neural Networks*, vol. 7, no. 2, Mar. 1996.
- [71] L. Duan, W. Lu, F. Mora-Camino, and T. Miquel, “Flight-path tracking control of a transportation aircraft: Comparison of two nonlinear design approaches,” in *Proc. of Digital Avionics Systems Conf.*, Portland, OR, Oct. 2006, pp. 1–9.
- [72] I. Szaszi, B. Kulcsar, G. J. Balas, and J. Bokor, “Design of FDI filter for an aircraft control system,” in *Proc. of Amer. Control Conf.*, Anchorage, AK, May 2002, pp. 4232–4237.
- [73] Department of Transportation, “Airworthiness Standards: Transport category airplanes,” in *Federal Aviation Regulations - Part 25*, Washington, DC, 1996.
- [74] F. L. Lewis, C. T. Abdallah, and D. M. Dawson, *Control of Robot Manipulators*. New York, NY: MacMillan, 1993.
- [75] B. S. Davis, T. Denison, and J. Kaung, “A monolithic high-g SOI-MEMS accelerometer for measuring projectile launch and flight accelerations,” in *Proc. of Conf. on Sensors*, Vienna, Austria, Oct. 2004, pp. 296–299.
- [76] V. Janardhan, D. Schmitz, and S. N. Balakrishnan, “Development and implementation of new nonlinear control concepts for a UA,” in *Proc. of Digital Avionics Systems Conf.*, Salt Lake City, UT, Oct. 2004, pp. 12.E.5–121–10.

- [77] T. Wagner and J. Valasek, “Digital autoland control laws using quantitative feedback theory and direct digital design,” *Journal of Guidance, Control and Dynamics*, vol. 30, no. 5, pp. 1399–1413, Sept. 2007.
- [78] M. Bodson, “Multivariable adaptive algorithms for reconfigurable flight control,” in *Proc. of Conf. on Decision and control*, Lake Buena Vista, FL, Dec. 1994, pp. 12.E.5–121–10.
- [79] B. J. Bacon, A. J. Ostroff, and S. M. Joshi, “Reconfigurable NDI controller using inertial sensor failure detection & isolation,” *IEEE Transactions on Aerospace and Electronic Systems*, vol. 37, no. 4, pp. 1373–1383, Oct. 2001.
- [80] G. Tao, *Adaptive Control Design and Analysis*, S. Haykin, Ed. Wiley-Interscience, 2003.
- [81] D. Dawson, M. Bridges, and Z. Qu, *Nonlinear Control of Robotic Systems for Environmental Waste and Restoration*. Englewood Cliffs, New Jersey: Prentice Hall PTR, 1995.
- [82] H. K. Khalil, *Nonlinear Systems*, 3rd ed. Upper Saddle River, NJ: Prentice Hall, 2002.
- [83] D. Enns and T. Keviczky, “Dynamic inversion based flight control for autonomous rmax helicopter,” in *Proc. of American Control Conf.*, Minneapolis, MN, June 2006, pp. 3916–3923.
- [84] P. M. Patre, W. MacKunis, C. Makkar, and W. E. Dixon, “Asymptotic tracking for systems with structured and unstructured uncertainties,” *IEEE Transactions on Control Systems Technology*, vol. 16, no. 2, pp. 373–379, 2008.
- [85] M. Bridges, D. M. Dawson, and C. Abdallah, “Control of rigid-link flexible-joint robots: A survey of backstepping approaches,” *Jnl. Robotic Systems*, vol. 12, pp. 199–216, 1995.
- [86] R. Lozano and B. Brogliato, “Adaptive control of robot manipulators with flexible joints,” *IEEE Transactions on Automatic Control*, vol. 37, no. 2, pp. 174–181, Feb. 1992.

BIOGRAPHICAL SKETCH

William MacKunis received his bachelor's degree in electrical engineering from Florida Atlantic University (FAU) in May of 2000. He then went on to finish his master's degree from FAU in 2003. Specializing in controls, his master's thesis research was based on autonomous, multi-agent control of mobile robots.

In May of 2009, William completed his Ph.D. in aerospace engineering in the Department of Mechanical and Aerospace Engineering at the University of Florida under the supervision of Dr. Warren Dixon.